FEMTOSECOND PULSE GENERATION IN FIBER OSCILLATORS AND PULSE PROPAGATION IN MULTIMODE FIBER

A Dissertation

Presented to the Faculty of the Graduate School

of Cornell University

in Partial Fulfillment of the Requirements for the Degree of

Doctor of Philosophy

by

Zhanwei Liu

August 2017

FEMTOSECOND PULSE GENERATION IN FIBER OSCILLATORS AND PULSE PROPAGATION IN MULTIMODE FIBER

Zhanwei Liu, Ph.D.

Cornell University 2017

Ultrafast optical pulses have been widely used in fundamental research, medical and industrial applications. For example, ultrafast lasers are used for chemistry, optical frequency metrology, terahertz generation, spectroscopy, multi-photon microscopy, optical coherence tomography, and micro-machining, etc.

Traditionally, solid-state lasers, which have been engineered for over 30 years, dominate the market. Fiber lasers, as their competitors, offer several advantages over the solid-state systems: compact size, excellent thermal management, high efficiency, diffraction-limited spatial quality and low cost. Therefore, fiber lasers are becoming more popular on the continuous-wave laser market. For pulsed operation, large net nonlinear effects due to the tight confinement of the light in the core and the long propagation distance have limited their performance. As a result, the performance of pulsed fiber lasers has lagged behind that of their solid-state counterparts. In addition, product-scale adoption of high-performance ultrafast fiber lasers in industrial application is hindered by the lack of environmental-stability.

This thesis focuses on the study of pulse propagation in fiber oscillators and multimode fibers, which aims to solve the above problems.

An environmentally-stable fiber laser source based on cascaded Mamyshev regeneration and the formation of parabolic pulses, which allows for at least an order of magnitude increase in peak power and 6-fold increase in nonlinear phase accumulation, is demonstrated experimentally. The outstanding performance, which is

$\sim$ 50 nJ and $\sim$ 40 fs, has also been boosted up to the comparable level as that of the Ti:sapphire lasers. In addition, The combination of excellent performance with the environmental stability make the Mamyshev oscillator extremely attractive for applications.

To further improve the laser performance, multimode fibers, which can offer much larger mode field diameter and complex spatio-temporal couplings, are studied. Remarkable phenomena such as beam clean-up and self-organized instability in graded-index multimode fibers are observed and explained. Understanding the pulse propagation in those complex systems provides a route to further energy scaling.

This thesis is not just limited to the generation of high-energy, short-duration, coherent pulses. It also covers interesting nonlinear dynamics such as extreme events in the all-normal dispersion fiber oscillators. This may attract attention from researchers in nonlinear systems and oceanography.

Finally, future directions are discussed.

BIOGRAPHICAL SKETCH

Zhanwei Liu was born in 1986 in a rural village, then raised in a small city, Qinhuangdao, Hebei, China. He was a difficult and disruptive student until enrolled in undergraduate school, so he and his parents never expected he would become a Ph.D. student and study in United States. His interests in math and physics dates from middle school. He became a member in the physics program at Nankai University after he graduated from high school. However, he lost this interest for nearly 3 years and was not passionate about studying during his undergraduate years. However, in his final year, he regained his interest and thought he should pursue Ph.D. studies in U.S. From this moment on, he worked hard on the required admission tests for graduate school.

Fortunately, despite this late resurgence (and not understanding some basic concepts such as eigensate, entropy and the Hamiltonian), he was accepted into the University of Florida (maybe his GPA and TOEFL score seemed not too bad?). His serious study of physics initiated from preparing for the qualify exam, which was taken before the graduate school began. He worked hard and tried to catch up, especially after he heard that all the previous Chinese students passed it without a second trial. Luckily, after 3 weeks of intensive study, Zhanwei didn't "make history".

The core courses in University of Florida were fantastic and he learned quite a lot from those brilliant professors. He also spent some extra time on self-studying and finally became a student who can get the highest scores in the class. Under the influence of Professor Charles Thorn, who was the instructor of electrodynamics, he chose optics as his research direction. He joined David Reitze's group and worked on the Laser Interferometer Gravitational-wave Observatory (LIGO) project. Zhanwei greatly enjoyed the time he spent in University of Florida and

the LIGO group.

Two years later, Zhanwei transferred to Cornell University after David Reitze became the director of LIGO and had no time to mentor any student. At Cornell, he joined Frank Wises group as a PhD candidate in 2013. For the next four years, he explored nonlinear fiber optics, in particular designing fiber lasers and understanding highly-coupled complex systems in multimode fibers. It is a wonderful experience to become a member in this group because of the collaborative and creative environment.

After completing his Ph.D., he will move to San Jose, CA to work on optical networking devices.

To my parents Zifang Wang and Wenzhou Liu and my wife Yunxi Guo.

ACKNOWLEDGEMENTS

I know it is impossible to explicitly thank all those who have supported me over my graduate school years, but I want to try.

First of all, I would like to thank to my PhD advisor Professor Frank Wise for his continued support during the past four years. Frank Wise is a frank and wise person and devotes a lot of energy on research and teaching. He has also been so willing to listen to the students' opinions and believe the students success is his success. Thus, we students have a lot of freedom to pursue various projects without objection. His knowledge and insightful advice are helpful. I learned from him not only the knowledge of physics and ways of thinking, but also the philosophy of how to make choices. I believe he is one of the best advisors at Cornell.

I will forever be thankful to my master degree advisor, Professor David Reitze, who gave me the opportunity to join his group despite knowing this honest young man knew nothing about optics, experiments, and programming. As his only student in Florida, I could learn a lot directly from him. I will always remember his smile and encouraging words. I will also remember the 6 rehearsals before my first conference talk and his expectations of me. I hope that I could be as lively, enthusiastic, and energetic as him.

I also owe my appreciation to Professor Jeffrey Moses and Professor Tsuhan Chen for serving as my committee members.

I would also like to give special appreciation to Professor Charles Thorn who had spent a large amount of his spare time helping the students who are eager to learn but lack a strong background.

The fiber laser group is a source of friendships, support, as well as good advice and collaboration. I express my sincere gratitude to Logan Wright, who has countless wisdom on physics and countless time from his busy days to offer help, and

for providing me countless support. Understanding physics becomes much easier after talking with him. Thanks also go to the other teammates who I worked with. To Williams Renninger, for his remarkable explanations on nonlinear optics and fiber oscillators. To Hui Liu, for patiently teaching me the skills of fiber laser experiments. To Erin Lamb, for giving me priceless suggestions on experiments and simulations. To Yuxing Tang, for kindly providing me help on fiber splicing and offering me help during my experiments. To Zimu Zhu and Walter Fu, for asking me great questions and giving me meaningful suggestions. To Lili Huang, for helping me do the beam clean-up experiments. To Xiaosheng Xiao, for discussing about experiments and telecommunication field. To Zachary Ziegler, for your helping me do the Mamyshev oscillator experiments. To Pavel Sidorenko, for willing to continue to work on my ideas. It is fortunate to work with all of these smart and kind people.

In particular, I thank Tianyu Wang, Yi Gu, Siyan Guo, Zhe Wang and Yuling Chen. I really appreciate the time when we had dinners, played video games and chatted together, sharing our happiness and annoyance. I also enjoyed the discussion on interesting physics and math with Tianyu Wang. I will remember our joke: "Million-photon microscopy, which can see deeper, for oil field locating".

I owe a great debt of gratitude to my wife Yunxi for her love, support, and sacrifices in all these years, who has been with me in Tianjin, Gainesville, Ithaca, Ames, and Sunnyvale.

Finally, I give special thanks to my parents for their unconditional love, encouragement and support for all these years. I guess they are the only people who are listening to my babbling about my experiments, life and hardness without complaining. It is impossible to thank them adequately for everything they have done for me.

TABLE OF CONTENTS

LIST OF TABLES

LIST OF FIGURES

BIBLIOGRAPHY

[1] C. Y. Chong, Ph.D. thesis (2008).

[2] F. Wise, A. Chong, and W. Renninger, Laser & Photonics Review **2**, 58 (2008).

[3] W. H. Renninger, A. Chong, and F. W. Wise, IEEE Journal on Selected Topics in Quantum Electronics **18**, 389 (2012).

[4] https://en.wikipedia.org/wiki/Opticalfiber .

[5] http://www.fiberlaser.fujikura.jp/eng/products/about-fiber-laser.html .

[6] E. S. Lamb, Ph.D. thesis (2015).

[7] S. Ngcobo, I. Litvin, L. Burger, and A. Forbes, Nature Communications **4**, 1 (2013).

CHAPTER 1

INTRODUCTION

Ultrafast optics becomes a relatively new and rapidly growing field after the invention of mode-locked lasers, which impacts over both fundamental research as well as industrial and medical applications. Major research areas include studies of ultrafast phenomena in molecules or atoms [1], terahertz generation [2], frequency comb [3], etc. Moreover, ultrashort pulses are also becoming more popular in industrial and medical applications like micro-machining [4], multiphoton imaging [5], coherent anti-Stoke Raman scattering (CARS) microscopy [6]. All the progress in these fields requires and benefits from the development of high-quality and low-cost ultrashort pulse sources.

The Ti:sapphire solid-state laser produces intense femtosecond pulses at ∼800nm wavelength with strong peak power and short pulse duration [7, 8]. Therefore, Ti:sapphire lasers can be found in many research laboratories worldwide and remain the workhorse of ultrafast science. While they have undeniably great output characteristics, these solid-state laser systems have many drawbacks such as high cost, high complexity, large size, cooling requirement, and lack of environmental stability. All of these factors prevent them from being widely used outside of specialized laboratories.

Over the past thirty years, fiber laser technology has advanced remarkably and laser sources in the near-IR spectral region based on ytterbium, erbium and thulium doped fibers have already replaced solid-state lasers in many applications, especially in the high average-power continuous-wave laser market. Compared with solid-state lasers, fiber lasers have the following advantages:

- Cost effective: A large number of components used in fiber lasers have been previously developed for telecommunications, thereby significantly reduce the cost.
- High efficiency: Using a doped-fiber as the gain medium, which works well for diode-pumping, gives a long interaction length between the pump and signal. This geometry results in high photon conversion efficiency, as well as a rugged and compact design.
- High stability: When the fiber components are spliced together, there are no discrete components to adjust or to align. The fiber laser/amplifier also requires no or minimal water cooling due to the fiber's large surface-to-volume ratio for efficient heat dissipation.
- High beam quality: Near Gaussian mode operation in single-mode fibers.
- Robustness and compact: Since the light propagates entirely inside the optical fiber, which can be coiled to very small volume, fiber laser systems are significantly more compact compared to solid-state lasers. Due to the nature of optical fiber, fiber lasers do not require beam alignment and maintenance.

Even though fiber lasers own numerous advantages, they still fall behind the solid-state lasers when they are used to generate pulses. The output performance of ultrafast fiber laser, such as pulse duration, pulse energy and peak power, is still below that of the mode-locked solid-state laser. The main challenges are large group velocity dispersion and high nonlinearity. To overcome these obstacles, several different fiber oscillators and fibers with larger mode field area (LMA) have been developed in the past three decades. Laser cavities such as soliton, dispersion-managed soliton, passive self-similar, dissipative soliton, active self-similar have been demonstrated experimentally and theoretically. LMA fibers like photonic

crystal fibers, chirally-coupled-core fibers, and higher-order mode fibers are invented and widely used in high power fiber lasers and amplifiers. As the result of so many research activities, the pulse peak power from fiber oscillators have increased by orders of magnitude.

Despite the significant progress in ultrafast fiber laser development, they still have their own problems. The peak power is still lower than solid-state lasers when single-mode fiber is used. And the lasers with LMA fibers are not as compact as single-mode fiber lasers. Additionally, the high-performance fiber lasers are still lack of environmental stability. All of these limits their applications.

Furthermore, the majority of fiber lasers/amplifiers and pulse propagation research rely on one spatial mode operation. As a result, only the temporal domain is studied. The multimode fiber did not draw enough attention in the past. With the increasing demand on higher power for fiber lasers and larger bandwidth for telecommunication, the multimode fibers are attracting more interests. Hence, understanding the spatial mode-coupling and spatio-temporal coupling becomes important.

The purpose of my research is trying to solve the above problems.

1.1 Organization of thesis

This thesis focuses on the study of generating high quality pulses from fiber lasers as well as the pulse propagation in multimode fibers. The thesis is organized as follows.

Chapter 1 introduces the basic concepts of pulse propagation in fibers. Different

fiber laser designs are summarized. At last, the important building blocks in fiber laser are presented.

Chapter 2 describes the study of an environmentally-stable Mamyshev oscillator. Based on cascaded Mamyshev regeneration principle and self-similar propagation physics, it can reach a peak power at least an order of magnitude higher than that of previous lasers with similar fiber mode area. The key idea is designing the oscillator to support parabolic pulse formation and taking the advantage the step-like saturable-absorbing property of Mamyshev regeneration. Unprecedented nonlinear phase can be managed. This is the first single-mode fiber laser that reaches megawatt-level peak power. In addition, it is environmentally stable, which is attractive for fabrication and industrial applications.

Chapter 3 explores the extreme statistics distribution of the pulse energy in a normal dispersion fiber laser.

In Chapter 4, the subject is changed from oscillators using single-mode fiber to pulse propagation in grade-index (GRIN) multimode fiber. A phenomenon called beam clean-up is studied experimentally and numerically. It may be used for beam cleaning/combining and saturable absorber.

Finally, future directions of these work will be discussed in Chapter 5.

1.2 Pulse propagation in passive single-mode fiber

Fundamentally, electromagnetic field propagation in medium is governed by Maxwells equations plus the corresponding boundary conditions. The starting point of the equation for describing pulse propagation in fiber is the electromag-

netic wave equation derives from Maxwell's equations with no source terms and under the assumption $\nabla \cdot \mathbf{E} = 0$:

$$\nabla^2 \mathbf{E(r,t)} - \frac{1}{c^2}\frac{\partial^2 \mathbf{E(r,t)}}{\partial t^2} = \mu_0 \frac{\partial^2 \mathbf{P(r,t)}}{\partial t^2}, \tag{1.1}$$

where $\mathbf{E(r,t)}$ is the electric field, c is the speed of light in vacuum. $\mathbf{P(r,t)}$ is the induced polarization and μ_0 is the magnetic permeability in free space. In linear media, the induced polarization is assumed to be proportional to the electric field. But in optical fibers, where the peak intensity of short pulses can be very high (>1 kW), this assumption is no longer valid, and higher order terms have to be included. The induced polarization is written as a sum of linear and nonlinear contributions:

$$\mathbf{P} = \mathbf{P}_L + \mathbf{P}_{NL} = \epsilon_0(\chi^{(1)} : \mathbf{E} + \chi^{(2)} : \mathbf{EE} + \chi^{(3)} : \mathbf{EEE} + \dots), \tag{1.2}$$

where $\mathbf{P}_L$ and $\mathbf{P}_{NL}$ are the linear and nonlinear portions of the polarizability, ϵ_0 is the permittivity in vacuum, $\chi^{(n)}$ is the linear ($n = 1$) and nonlinear ($n > 1$) susceptibilities tensors. Due to inversion symmetry in optical fiber, all even terms disappear, and hence $\chi^{(3)}$ is the only significant nonlinear term. $\chi^{(3)}$ relates to a variety of different nonlinear phenomena. In optical fibers, $\chi^{(3)}$ originates from the interaction of the light with the electrons of the medium (Kerr nonlinearity) and with the optical phonons (Raman scattering).

1.2.1 Generalized nonlinear Schrödinger equation

Under a series of approximations such as,

- The optical field maintains its polarization along the fiber.
- The optical field is quasi-monochromatic (slowly varying envelope approximation or narrow-band approximation), i.e., the envelope of the pulse changes on a time scale much slower than an optical cycle, which requires $\Delta\omega/\omega_0 \ll 1$.
- $\mathbf{P}_{NL}$ is a small perturbation to $\mathbf{P}_L$ (Usually, nonlinear changes in the refractive index are $< 10^{-5}$).
- The medium response is local.

, Equation 1.1 can be simplified to the generalized nonlinear Schrödinger equation (GNLSE). The pulse propagation in a single-mode optical fiber can be well described by the GNLSE. The derivation of the GNLSE equation from Equation 1.1 is well covered in numerous textbooks such as Ref. [9]. The final form of GNLSE obtained through the derivation is given by the following equation.

$$\frac{\partial A}{\partial z} + \frac{\alpha}{2}A - \sum_{n=2}^{\infty} i^{n+1}\frac{\beta_n}{n!}\frac{\partial^n A}{\partial t^n} = i\gamma\left(1 + \frac{i}{\omega_0}\frac{\partial}{\partial t}\right)\left(A(z,t)\int_{-\infty}^{t} R(t')|A(z,t-t')|^2 dt'\right), \tag{1.3}$$

where A is the slowly varying pulse envelope, z is the propagation distance, α is the linear loss, β_n are the n-th order of the fiber dispersion (β_2 and β_3 are often referred as the group velocity dispersion (GVD) and third-order dispersion (TOD) respectively), t is the time in the frame of the pulse, ω_0 is the center angular frequency, γ is the nonlinear coefficient which is defined as $\gamma = \frac{n_2\omega_0}{cA_{eff}}$ (n_2 is the nonlinear index coefficient and A_{eff} is the effective mode area), $R(t)$ is the nonlinear response function.

The nonlinear response function $R(t)$ incorporates both the electronic (instantaneous) and the vibrational (delayed) Raman contributions and takes the form:

$$R(t) = f_R h_R(t) + (1 - f_R)\delta(t) \tag{1.4}$$

where f_R represents the proportion of contribution from delayed Raman response, which is 0.18 for silica fibers [10]. The Raman response function $h_R(t)$ is responsible for the Raman gain and can be modeled in a useful form [11]:

$$h_R(t) = \frac{\tau_1^2 + \tau_2^2}{\tau_1 \tau_2^2} exp(-t/\tau_2) sin(t/\tau_1) \tag{1.5}$$

The parameters τ_1 and τ_2 are two parameters which are adjusted to match the actual Raman gain spectrum. For silica glasses, the appropriate valuses are $\tau_1 = 12.2$ fs, $\tau_2 = 32$ fs [11].

In this dissertation, we focus on the propagation of pulses with duration longer than ∼100 fs, so the effects from the fourth and higher-order dispersion are negligible in most cases. Therefore, we can even simplify the Equation 1.3 to:

$$\frac{\partial A}{\partial z} + \frac{\alpha}{2}A + \frac{i\beta_2}{2}\frac{\partial^2 A}{\partial t^2} - \frac{\beta_3}{6}\frac{\partial^3 A}{\partial t^3} = i\gamma(|A|^2 A + \frac{i}{\omega_0}\frac{\partial}{\partial t}(|A|^2 A) - T_R A\frac{\partial |A|^2}{\partial t}), \tag{1.6}$$

This equation models loss/gain, GVD, TOD, self-phase modulation ($i\gamma(|A|^2 A)$, self-steepening ($-\frac{\gamma}{\omega_0}\frac{\partial}{\partial t}(|A|^2 A)$), and stimulated Raman scattering ($-i\gamma T_R A\frac{\partial |A|^2}{\partial t}$).

When the loss and/or gain, higher-order dispersion, self-steepening, and the Raman response are negligible, which is the case for most of long duration (>300 fs) and low peak-power pulses propagating in a passive fiber, the GNLSE can be further reduced to the famous nonlinear Schrödinger equation (NLSE):

$$\frac{\partial A}{\partial z} = -\frac{i\beta_2}{2}\frac{\partial^2 A}{\partial t^2} + i\gamma|A|^2 A. \tag{1.7}$$

This well-studied equation is integrable and has analytical solutions called ***solitons***. The fundamental solitons are the result of balance between anomalous GVD and self-phase modulation (SPM). It is referred as the fundamental soliton since neither the pulse shape nor the pulse spectrum changes along the propagation direction and it can be described as

$$A(t,z) = \sqrt{P_0}\,\mathrm{sech}\left(\frac{t}{\tau}\right)e^{\frac{i\beta_2}{2\tau^2}z}, \tag{1.8}$$

where P_0 is the peak power of the soliton and the full-width at half-maximum (FWHM) pulse duration is 1.7627τ.

One important relation between the relevant parameters is the soliton area theorem [12]

$$E\tau = \frac{2|\beta_2|}{\gamma}, \tag{1.9}$$

where E is the pulse energy. For each pair of β_2 and γ, a family of soliton solutions, with different energy and the corresponding duration, can co-exist as long as they satisfy the soliton area theorem. The existence of solitons in an optical fiber was demonstrated by Mollenauer *et al.* [13].

1.3 Mode-locking and pulse generation from fiber lasers

Mode-locking refers to a process that the longitudinal modes of the laser resonant cavity can reach a fixed-phase relationship. A train of pulses separated by the round-trip time of the cavity can be generated by the constructive interference between these modes. In general, the relative phases between different modes are not fixed if there is no modulation in the laser cavity, and the output varies in an uncontrolled way. So, some approaches are needed to enforce coherence between these modes. In addition, the periodic boundary condition of the cavity is also needed to be satisfied by the pulsed field, which means the modulating period needs to be very close to the cavity round-trip time or its harmonics. Both active or passive methods have been studied extensively to generate high quality pulses.

Active mode-locking involves the periodic modulation of the resonator losses, achieved with an acousto-optic modulator (AOM) or electro-optic modulator (EOM). When the modulation period is matched with the laser cavity round-trip time, this can lead to the generation of short pulses. Output pulse duration from active mode-locked lasers are limited by the modulation speed and the typical values are picosecond or nanosecond. Passive mode-locking, which relies on self-amplitude modulation of the pulse (usually in picosecond time scale) through its interaction with a saturable absorber (detail will be given in the laser component section), allows the generation of much shorter (femtosecond) pulses. An excellent summary of all these mode-locking techniques can be found in a review paper from Herman Haus [14].

Although the first fiber laser was experimentally demonstrated in 1961 [15], the first mode-locked fiber laser did not appear until 1983. After that, several pulse-shaping mechanisms have been discovered to improve the fiber laser performance.

In the next few sections of the introduction, a brief review will be given on different classes of mode-locked fiber lasers. Their physical mechanisms, characteristic features, and typical output performances will be discussed.

1.3.1 Soliton lasers

Solitons are solutions of the NLSE, which is used to model the conservative system (no loss/gain) such as pulse propagation in a passive fiber. They can also exist in laser oscillators when the gain, loss, output coupling, saturable absorption acting as perturbations on the soliton. The laser is made up of anomalous dispersion fibers or normal dispersion fibers with anomalous dispersion segments such as grating pairs. The first soliton laser is demonstrated experimentally by Mollenauer in 1984 using anomalous dispersion fibers [16].

However, due to the periodic gain and loss, the soliton can develop side-bands in its spectrum, which can destabilize the soliton. The NLSE fundamental soliton has a wavevector $k_{sol} = \frac{\beta_2}{2\tau^2} = \frac{\pi}{4Z_0}$, while the linear wave have a dispersion relation $k_{lin} = -\omega^2\beta_2/2$, where $Z_0 = \pi/4k_{sol}$ is the soliton period. The periodic variation of the gain and loss (the period is the cavity length Z_c in this case) produces dispersive perturbations with wavevector $k_{pert} = 2\pi/Z_c$. The phase matching condition for providing efficient generation of dispersive waves is $|m|k_{pert} = k_{sol} - k_{lin}$, leading to the resonance frequency

$$\Omega_{res} = \frac{1}{\tau}\sqrt{\frac{8Z_0|m|}{Z_c} - 1}, \tag{1.10}$$

where m is an integer. The radiated energy can interfere constructively to form the characteristic Kelly sidebands on the soliton spectrum (Figure 1 in Ref. [17]).

These features on the output spectra are the signature of the soliton mode-locking.

The nonlinear phase shift per round-trip in a soliton fiber laser is inversely proportional to the pulse duration. Therefore, Kelly sidebands become much more pronounced as the pulse duration is decreased (the pulse energy is increased). When the laser is driven too far into this regime, the soliton pulses become unstable. Strong Kelly sidebands thus indicate that the pulse duration is near the minimum possible value [18]. Meanwhile, these sidebands set the limit on how high the solitons energy can be. In the physical cavity, length Z_c is bounded above by $8Z_0$. This relation restricts the possible outputs from a soliton laser, since for a certain cavity length, it imposes a lower bound pulse duration before instabilities arise ($Z_0 \propto \tau^2$).

In practice, while this mode-locking mechanism is simple and robust, its performance is limited by the onset of multiple-pulsing. Usually, the pulse energy is limited to 100-pJ level in single-mode fiber lasers. The corresponding pulse duration is in the picosecond or subpicosecond range.

1.3.2 Dispersion-managed soliton lasers

Dispersion-managed soliton lasers, also called stretched-pulse fiber lasers, are constructed with normal and anomalous dispersion fibers and the net dispersion is near to 0 (Figure 1.1 (upper row)). The stretched-pulse fiber laser gets its name from the fact that the pulses temporally stretch and compress twice as they circumnavigate the cavity (Figure 1.1 (bottom row)). The introduction of a dispersion map in the cavity can effectively decrease the nonlinear effect thus the output pulse carries roughly 10 times more energy than soliton [19]. The net cavity dispersion can be

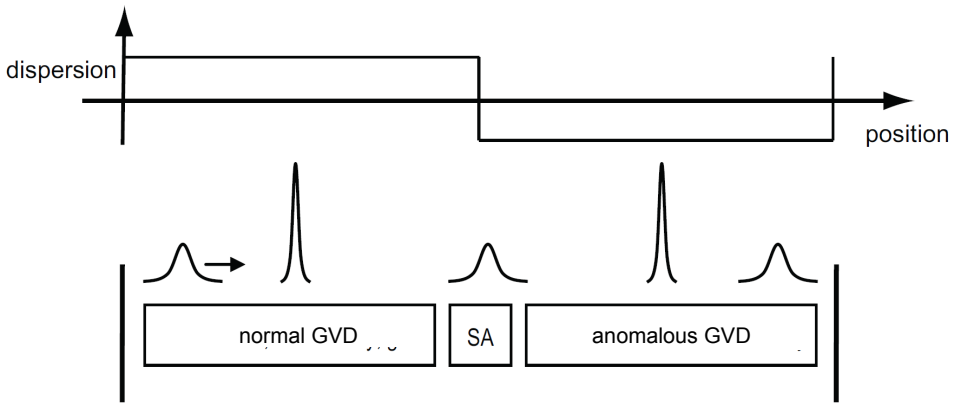

Figure 1.1: Schematic of the dispersion-managed soliton fiber laser. The dispersion map is shown in the upper row and the pulse evolution in temporal domain is shown in the bottom row. The pulse duration is maximized at the end of each segment of fiber, and compressed to minimum duration in the center of the segment. A saturable absorber is used to stabilize the cavity. Figure modified from Ref. [20].

slightly anomalous or normal. The output spectrum can be broader than the gain spectrum and no Kelly sidebands are observed (See Figure 10 in Ref. [14]).

A master equation was developed for the operation of the dispersion-managed soliton [21]. The pulses produced from dispersion-managed laser are the solution of the master equation and generally more consistent with a Gaussian shape. The typical performance is about 1 nJ and 40-100 fs and the maximum nonlinear phase for the dispersion-managed soliton is less than π. An excellent review of dispersion-managed solitons can be found in Ref. [14] and Ref. [22].

1.3.3 Passive self-similar lasers

Soliton fission and modulation instability are the fundamental constraints on the high-energy pulse generation from lasers using anomalous dispersion fiber. Hence, a natural question is whether it is possible to build a mode-locked fiber laser only with normal dispersion fiber. However, even in the normal-dispersion regime, high-

peak power pulses also subject to instability through the optical wave-breaking [23, 24].

In 1993, Anderson *et al.* studied the NLSE in normal dispersion regime and found the cause of optical wave-breaking. It is due to the overtaking of different parts of the pulse as a result of non-monotonic chirp. The nonlinear generation of new frequencies and sidelobes in temporal domain at the moment of overtaking break the pulse [25]. Furthermore, these researchers also found a wave-breaking-free solution, it has a parabolic temporal and phase profile (linear frequency chirp)

$$A(t,z) = A_0\sqrt{1-(t/\tau)^2}\,\exp(ib(z)t^2) \qquad (|t| \le \tau). \tag{1.11}$$

This is the asymptotic solutions of the NLSE. Besides the wave-breaking free property, another important feature is the pulse maintains the parabolic shape and the temporal profile is always a scaled version of itself during the propagation.

The physical insight of this evolution can be explained intuitively. The pulse is parabolic in both time and frequency domains (Fourier transform of a parabolic pulse with a parabolic phase profile in the time domain is parabolic spectrum with a parabolic phase profile in the frequency domain. It is no longer the truth if the phase is flat across the pulse). During propagation, SPM will add a parabolic shape to temporal domain because the temporal intensity is also parabolic and GVD will add parabolic phase in the spectral domain. Neither of these two effects is able to change the shape of the pulse or spectrum. Therefore, even though the pulse duration and spectrum width are increasing due to GVD and SPM, their shape remain parabolic. It is so-called self-similar propagation. Moreover, this self-similar propagation results in a linear frequency sweep, so the chirp of the parabolic pulse tends to remain linear, which can be compressed easily.

In 2004, Ilday *et al.* designed a laser that would support self-similar evolution in a passive fiber segment [26]. The laser includes a normal dispersion fiber and a dispersive delay line (DDL) (Fig. 1.2 bottom row). The pulse duration increases monotonically in the normal dispersion fiber and gets compressed in the DDL while the spectrum remains almost the same ((Fig. 1.2 top row)). The output chirped pulse is before the DDL and can be de-chirped close to the transform limit using a grating pair. The power spectrum exhibits a unique shape that is predicted numerically: parabolic near the peak, with a transition to a steep decay (Figure 2 and 4 in Ref. [26]). The approximately parabolic temporal profile, nearly linear chirp, shape of the output spectrum, and the evolution of the intensity profile are all signatures of passive self-similar mode-locked lasers.

We emphasize that this self-similar solution is the asymptotic solution of the nonlinear Schrödinger equation with only fiber nonlinearity and normal GVD, so the laser is called passive self-similar laser. It is distinct from the similariton that formed in the presence of gain [27]. This is the first self-similar laser. Pulse energies up to $\sim$ 10 nJ and pulse durations down to sub-100 fs can be generated from this laser.

1.3.4 Dissipative soliton lasers

In 2006, Chong *et al.* demonstrated a mode-locked fiber laser contained no components with anomalous GVD [29]. The pulse shaping is dominated by a spectral filter. The pulse circulates around the oscillator is highly-chirped and the filter shapes the pulse both in spectral and temporal domain. The output pulse is also highly-chirped but can be dechirped to $\sim$ 170 fs using grating compressor. The generated pulses from this all-normal-dispersion (ANDi) laser exhibit a unique

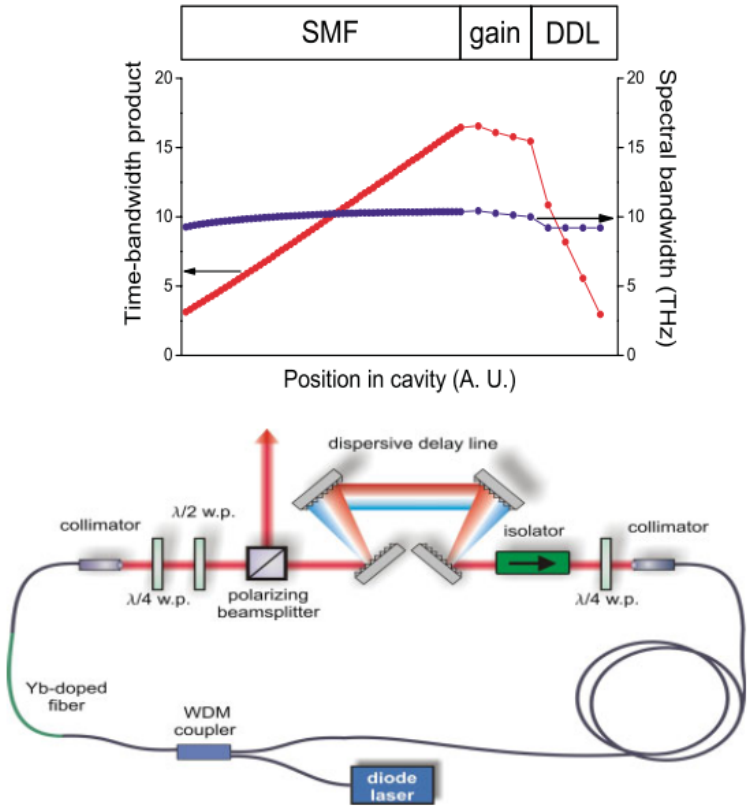

Figure 1.2: Top: the temporal and spectral evolution in the passive self-similar laser. Bottom: the main components of passive self-similar laser. Evolution is clockwise. Figure reproduced from Ref. [28].

steep-sided spectrum and acquire frequency chirps that can be several times larger than the net cavity dispersion [30]. This pulse evolution is distinguished from prior mode-locked fiber lasers such as soliton and stretched-pulse laser.

An typical example of ANDi laser is shown schematically in Figure 1.3. Nonlinear polarization evolution (detail is given in the fiber laser components section) is employed as the saturable absorber. A polarizing beam-splitter is used as the output coupler. A bandpass filter (6-20 nm bandwidth) centered at 1030 nm is placed after the beam splitter. Pulse energies up to around 10 nJ and pulse durations down to around 100 fs can be achieved. The peak power after compression is over two-orders of magnitude higher than soliton. And the maximum accumulated

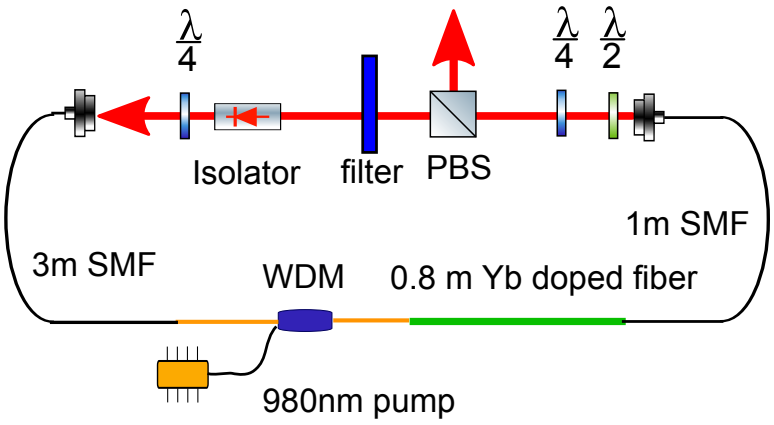

Figure 1.3: Schematic of the ANDi fiber laser. QWP: quarter waveplate; HWP: half waveplate; PBS: polarizing beam-splitter; WDM: wavelength-division multiplexer; SMF: single-mode fiber.

nonlinear phase is able to reach $\sim 10\pi$ [28].

There is a large degree of freedom in the cavity design by adjusting the passive fiber length (net GVD), filter bandwidth, and pump power. Pulses with different properties can be generated [30]. At repetition rates above 10 MHz, the output pulses can be de-chirped to close to the transform limit. At even lower repetition rates, longer chirped pulses are formed and the de-chirped pulses tend to acquire a larger deviation from the transform limit [31].

Energy scaling using 10 μm core SMFs was reported by Kieu *et al.* and they got 2.2W average power, 30-nJ pulse energy and sub 100-fs pulse duration [32]. These numbers are close to those from the commercial Ti:sapphire lasers on the markets. Further scaling has also been reported. Using photonic-crystal fiber (12W, 140-nJ, 115-fs) [33] and the large-pitch photonic-crystal fiber (66 W, 0.9 μJ, 90 fs) [34], megawatt-level peak power pulses are achieved.

Besides the outstanding performance, another exciting fact about ANDi laser is that it is an analytical solution of the cubic-quintic Ginzburg-Landau equation

(CQGLE) [35]. In general, the physical mechanisms that affect the pulse in a fiber laser are not uniformly distributed around the oscillator. For example, the filter is placed at one place rather than all over the cavity. However, on average, the pulse propagation can be modeled using CQGLE with constant coefficients:

$$\frac{\partial A}{\partial z} = gA + \left(\frac{1}{\Omega} - i\frac{D}{2}\right)\frac{\partial^2 A}{\partial t^2} + (\alpha + i\gamma)|A|^2|A| + \delta|A|^4 A, \tag{1.12}$$

where g models the gain or loss, D is GVD, α and δ together model the nonlinear loss from the SA. The spectral filter is introduced by the Ω term and γ is the Kerr nonlinear coefficient. The analytical solution of CQGLE matches with numerical simulation and experimental result very accurately [35].

The formation of pulse is the result of the balance between dispersion (normal), self-focusing nonlinearity, loss from the spectral filtering and SA and gain from the active fiber [35, 36, 37]. This type of soliton is referred as dissipative soltion because the gain and loss (dissipative process) also play a significant factor in the mode-locking. Moreover, dissipative solitons are also governed by an area theorem, but in a different form. The energy of dissipative soliton scales directly with the pulse duration and there is an upper limit for it [38].

1.3.5 Amplifier similariton lasers

When the pulse propagates in a doped fiber with normal dispersion and constant gain, it can be modeled using a simple equation

$$\frac{\partial A}{\partial z} = -\frac{i\beta_2}{2}\frac{\partial^2 A}{\partial t^2} + i\gamma|A|^2 A + \frac{g}{2}A. \tag{1.13}$$

A self-similar solution is derived by Fermann *et al.* [27]

$$A(z,t) = A_0(z)\sqrt{\left(1-\left(\frac{t}{\tau(z)}\right)^2\right)}e^{i\phi(z,t)} \quad (t \leq \tau). \tag{1.14}$$

The pulse phase $\phi(z,t)$, chirp $\delta\omega(t)$, amplitude $A_0(z)$ and duration $\tau(z)$ have the form of:

$$\phi(z,t) = \phi_0 + 3\gamma\left(\frac{1}{2g}\right)A_0^2(z) - g\left(\frac{1}{6\beta_2}\right)t^2. \tag{1.15}$$

$$\delta\omega(t) = -\frac{\partial\phi(z,t)}{\partial t} = g\left(\frac{1}{3\beta_2}\right)t, \tag{1.16}$$

$$A_0(z) = \frac{1}{2}(gE)^{1/3}(\frac{\gamma\beta_2}{2})^{-1/6}\exp(\frac{gz}{3}), \tag{1.17}$$

$$\tau(z) = 3g^{-2/3}(\frac{\gamma\beta_2}{2})^{1/3}\exp(\frac{gz}{3}). \tag{1.18}$$

Significantly, these results imply that the output is only determined by the energy of the initial pulse and fiber parameters. Any input pulse for the gain fiber eventually converge to the same parabola-shaped solutions and scale self-similarly along propagation as long as the input energy stays the same. Based on this self-similar attraction to parabolic pulses in the gain segment, different cavity designs have been reported. With the help of anomalous dispersion fiber (transform the pulses after the gain fiber into solitons) [39] or narrow bandpass filters (narrow down the spectrum and shorten the chirped-pulse duration) [40, 41], the amplified, wide-spectrum and highly chirped long-duration pulse returned to a low-energy,

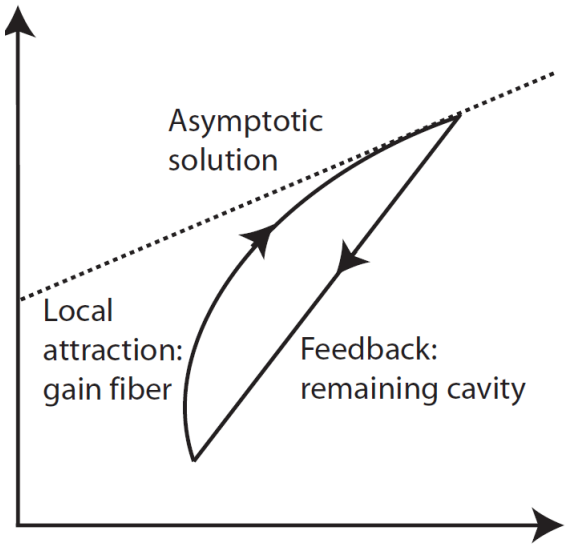

Figure 1.4: Illustration of the local attraction in an amplifier similariton fiber laser. Figure reproduced from Ref. [37].

narrow-spectrum and short-duration pulse (Figure 1.4) and formed a self-consistant condition. Mode-locked lasers have been demonstrated using doped-fiber [39, 40] or Raman gain as their gain medium. Because this self-similar solution is formed inside of the gain fiber, it is often referred as amplifier similariton (AS).

The demonstration of AS mode-locked fiber laser is remarkable as a feedback system with a local nonlinear attractor that is not a static solution, which is very different from soliton and dissipative solitions. Another remarkable feature of the AS laser is that it is subject to a local attractor rather than the design of the whole cavity, which allows for several practical advantages. For example, the output pulse parameters only change slightly as a function of the net GVD, which leaves a large room of freedom for the laser design [42].

Another important thing needed to know is the assumption of this model is that the gain medium has infinite gain bandwidth and does not have any other nonlinear terms except Kerr nonlinearity. In practice, this is not true. The gain

bandwidth of ytterbium and erbium doped fiber is $\sim$ 40-nm and other nonlinear effects such as stimulated Raman scattering exist. As a result, this ideal solution is experimentally limited due to these deleterious effects [43, 44, 45].

1.4 Fiber laser components

A summary of the important components that appear in a fiber laser is given in this section. This part introduces different kinds of components, such as fibers, spectral filters and saturable absorbers.

1.4.1 Optical Fibers

Single-mode fiber and multimode fibers

A fiber with core radius a and numerical aperture NA operates at λ_0 is a single-mode fiber if $V = 2\pi(a/\lambda_0)NA < 2.405$. Thus, when the fiber core radius is small, only one spatial mode can exist and this spatial profile of the optical field is invariant along the propagation path. And only the temporal domain effect is needed to be considered when studying the pulse evolution in a single-mode fiber (SMF). For instance, in the linear propagation case, the pulse duration broadens as a result of chromatic dispersion (Fig. 1.5(a): Pulse propagation). When the core size is getting larger, multiple spatial modes can be supported by the fiber and these modes have different group velocities. Thus pulse spreads faster in multimode fiber (MMF) than in SMF due to the extra contribution from modal dispersion (Fig. 1.5 (b): Pulse propagation). In most of the applications, the

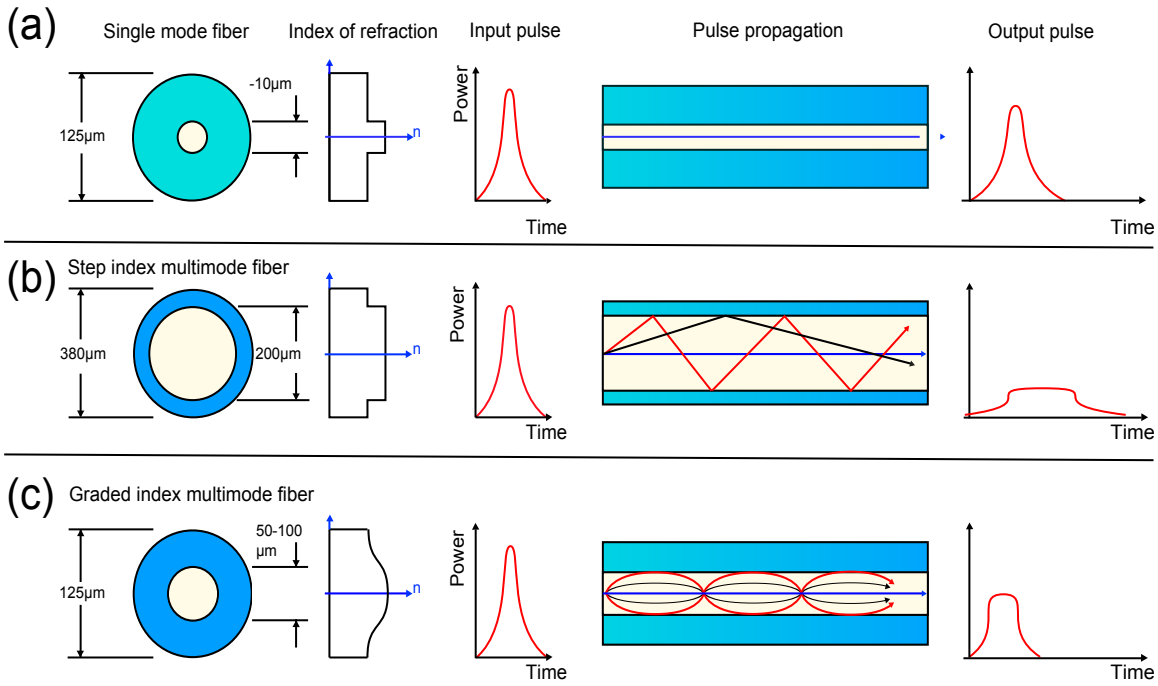

Figure 1.5: Cross-section, index of refraction and qualitative pulse propagation behavior for different types of fiber. (a) single-mode fiber, (b) step-index multimode fiber and (c) graded-index multimode fiber. Figure modified from Ref. [46].

modal dispersion is not desired. For example, in telecommunication area, it limits the transmission bandwidth; in high power laser and amplifier, it causes speckled output beam shape. Index grading is a remarkable way to reduce the differential modal delay. The refractive index decreases gradually from the core to the cladding (Fig. 1.5 (c): Index of refraction). Therefore, although higher order modes travel longer distance, they travel faster, so that the propagation times of the different rays are equalized (Fig. 1.5 (c): Pulse propagation).

SMF is one of the most important inventions in the past century. SMFs are widely used in optical fiber communication systems, fiber lasers (amplifiers), and scientific research areas due to the simplicity of their systems. In the nonlinear fiber optics field, even with the interplay between linear (dispersion) and nonlinear (gain, SPM, Raman, self-steepening) effects in temporal domain, there are tremendous

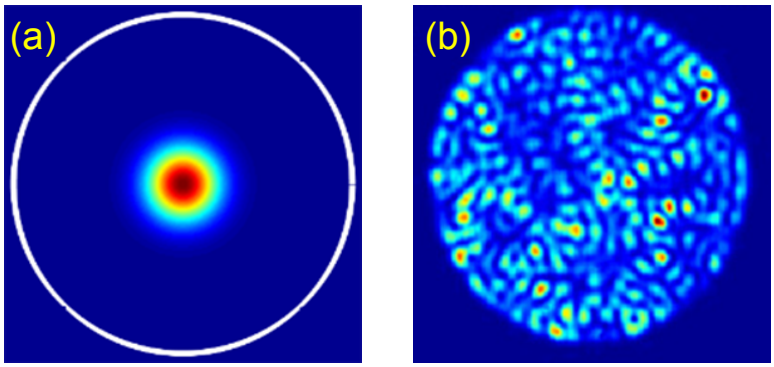

Figure 1.6: Typical output beam profiles from single-mode fiber (a) and multimode fiber(b).

nonlinear phenomena such as modulation instability, soliton, soliton fission, soliton self-frequency shift, super-continuum generation, spectrum compression and self-similar propagation have been discovered over the past few decades.

MMFs, which were invented even ahead of SMFs, were considered as low-price and low-quality waveguides for a long time. Their applications are limited to short-distance optical fiber communications and poor beam-quality, high-power light transportation due to the phenomena of intermodal dispersion and interference. The light experiences linear/nonlinear mode coupling when propagating along MMFs, whereby the high spatial quality input laser beams may fade into speckled output (Figure 1.6).

The view of MMFs starts changing since SMF-based communication systems and short-pulse lasers/amplifiers approach their fundamental limits and more and more researchers find different ways to control the light propagation in MMFs in the past few years. For example, there has been growing interest in fiber-optic communications using spatial-division multiplexing, imaging through MMFs, principle modes, etc.

When studying the pulse propagation in multimode fibers, GRIN MMFs are

often used because of low intermodal group delay. All the modes in GRIN MMFs propagate with nearly identical group velocities, therefore, nonlinear coupling among different modes for short pulses is maximally achieved.

The refractive index profile of a GRIN multimode fiber is given by

$$\begin{aligned} n^2(\rho) &= n_0^2\left[1-2\Delta(\frac{\rho}{R})^\alpha\right] \quad (\rho \le R) \\ &= n_0^2(1-2\Delta) \quad (\rho > R), \end{aligned} \tag{1.19}$$

where R is the core radius, n_0 is the maximum refractive index in the center of the core, Δ is the relative index step, and $\alpha \approx 2$ characterizes a near parabolic-index profile. Analytical solutions for the spatial mode and the propagation constant can be found in Ref. [47, 48].

Poletti and Horak [49] have shown that the GNLSE for pulse propagation in multimode fibers can be written as

$$\begin{aligned} &\partial_z A_p(z,t) = i\delta\beta_0^{(p)}A_p - \delta\beta_1^{(p)}\partial_t A_p + \hat{D}_p A_p + i\frac{n_2\omega_o}{c}(1+\frac{i}{\omega_o}\partial_t) \\ &\sum_{l,m,n}^{N}[(1-f_R)S^K_{plmn}A_l A_m A_n^* + f_R S^R_{plmn}A_l\int_\infty^t d\tau h_R(\tau)A_m(z,t-\tau)A_n^*(z,t-\tau)] \end{aligned} \tag{1.20}$$

where A_p is mode $p's$ temporal envelope, $\delta\beta_0^{(p)}$ ($\delta\beta_1^{(p)}$) are the differences relative to the fundamental mode of the 1^{st} (2^{nd}) coefficient in the Taylor series expansion of the wavenumber for the mode p about center angular frequency ω_o, $\hat{D}_p$ is the chromatic dispersion operator for mode p, and S^K_{plmn} and S^R_{plmn} are cubic nonlinear coupling coefficients for Kerr effect and SRS.

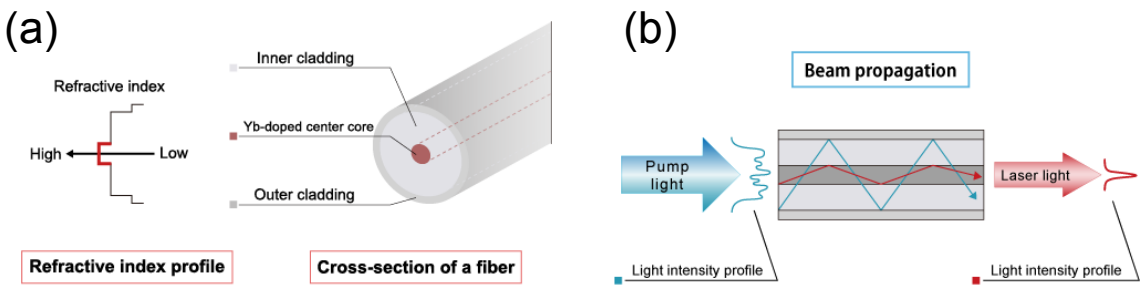

Figure 1.7: (a) Basic structure of double-cladding fiber and (b) pump and single light propagation in a double-clad fiber. Figure modified from Ref. [50].

Double-cladding fibers

Rare-earth-doped gain fibers are available with either a core-pumped or cladding-pumped design. Core-pumped gain fibers and pump laser diodes with a SMF pigtail are widely used for lower-power applications such as telecommunication and low-energy seed lasers. For high-power applications, cladding-pumped fibers with three layered structure are designed. The inner cladding with higher refraction index than the outer cladding acts as a waveguide for the pump light (Figure. 1.7 (a, left)). This double-clad fiber design typically has a high-NA, multimode cladding for the pump light and a single-mode or large-mode-area core for the signal light (Figure. 1.7 (a, right)). The large area of the multimode cladding-pump waveguide is able to handle large pump power whilst the signal is still carried through an active single-mode core. This allows high-power, low-brightness, multimode pump light to be efficiently converted to a high-power, high-brightness, high-spatial quality output as illustrated in Figure 1.7(b).

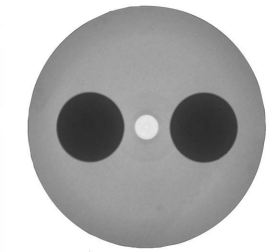

Figure 1.8: Ytterbium-doped, polarization maintaining, single-mode, double-clad fiber (YB1200-6/125DC-PM).

Polarization maintaining fibers

In an ordinary (non-polarization-maintaining) SMF, two degenerate orthogonal polarization modes (vertical and horizontal polarization) can exist. Under ideal conditions (perfect circular symmetry), the two modes have the same phase velocity and would not couple to each other. However, tiny amount of random birefringence caused by circular symmetry breaking during the manufacturing process or bending in the fiber, will result in the crosstalk between these two polarization modes.

Polarization maintaining (PM) fibers are optical fibers with a strong built-in birefringence, instead of a fiber without birefringence. The difference of propagation constants of the two polarization modes are much larger than ordinary SMF. The disturbances in the fiber, which are not fast enough to provide a Fourier component with a wavenumber that matches this propagation constant difference. Therefore, the mode coupling is mitigated. A linearly polarized light, if properly launched to one of the fiber axes, can preserve its polarization with little or no cross-coupling between the two polarization modes. The fiber structure is based on either introducing stress rods of different material into the cladding or via non-symmetrical cladding shapes (Figure. 1.8).

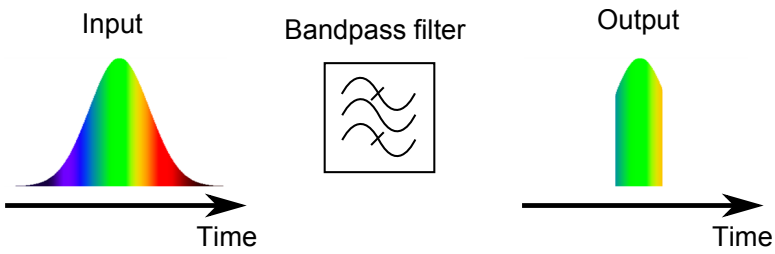

Figure 1.9: Pulse shaping by spectral filtering of a highly-chirped pulse.

1.4.2 Spectral filters

The spectral filter, which induces spectral loss, is also able to shape (shorten) the pulse in time domain when the pulse is highly chirped (Figure. 1.9). It is of particular importance for dissipative solitons [30, 35] and amplifier similariton [37] fiber lasers. Moreover, advanced temporal waveforms, such as bright and dark parabolic, triangular and saw-tooth-profile pulses can be generated by controlling the amplitude transfer function of the filter [51].

Spectral filters used in this thesis are interference fiber, birefringence fiber, and grating filter. Their mechanisms and characteristics are listed below.

Interference filters

Interference filters use the interference effect to preferably reflect or transmit particular part of the optical spectrum. In general, an interference filter consists of multiple thin layers of dielectric material with different refractive indices and/or thickness in order to cover a broad spectrum. In principle, through the constructive and destructive interference, the shape of transmittance curve can be arbitrary. However, in practice, it is difficult for interference filter to reach a smooth and low-loss transmission curve which matches well-known functions such as Gaussian, parabolic, etc. For example, Figure 1.10 shows a measured transmission curve of a

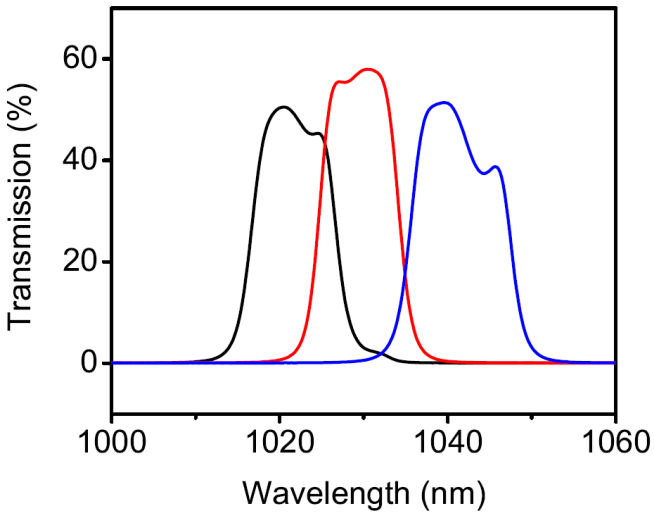

Figure 1.10: Measured transmittance of interference filters (the center wavelength of 1020, 1030, and 1040-nm with $\sim$ 10-nm BW. The peak transmission efficiency is $\sim$ 60%. Figure reproduced from Ref. [20]).

typical interference filter (λ_0=1030nm, BW=10 nm). It is hard to accurately model the laser cavity and predict the performance with numerical simulation because of this complex transmission curve.

Birefringent filters

A birefringent filter relies on the polarization evolution in a strong birefringent material, where the ordinary wave and extraordinary wave have different refraction index. This polarization evolution is a function wavelength. By adding a polarizer after this birefringent material, a wavelength-dependent loss will be created [52]. The transmission function of the birefringent filter is

$$T(\lambda) = \cos^2\left(\frac{\pi(n_e - n_o)d}{\lambda}\right), \tag{1.21}$$

where n_e and n_o are the extraordinary and ordinary refractive indices, d is the

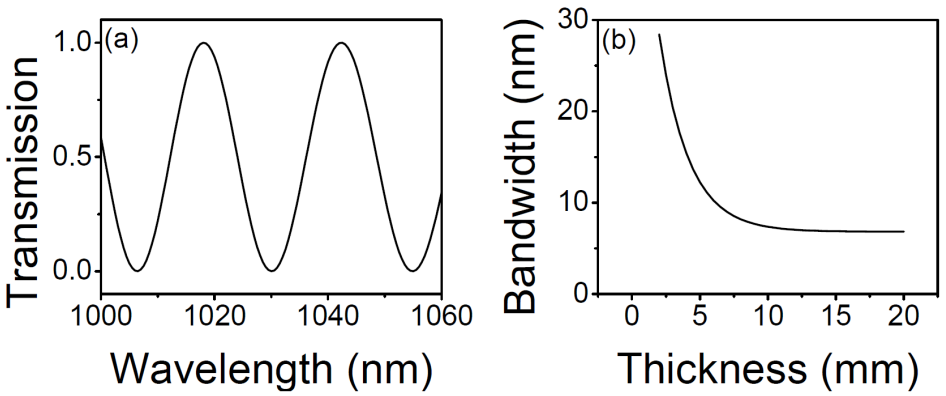

Figure 1.11: (a) Calculated filter profile for a 5-mm thick plate. (b) Filter bandwidth as a function of thickness. Figure reproduced from Ref. [54])

thickness of the birefringent plate. In this thesis, quartz birefringence plates are used ($n_0 = 1.53514, n_e = 1.54392$ at 1030 nm). The peak transmittance can be over 90% and the center wavelength of the passband can be tuned by rotating the quartz plate. The transmission curve is periodic and smooth (Fig. 1.11(a)). Moreover, different filter bandwidths can achieved by using plates with different thickness (Fig. 1.11 (b)). Experimental measurements confirm the correctness of this model (see Fig. 1.11 and Fig. 1.12 in Reference [20]).

Birefringent filters are widely used in dissipative soliton lasers [30, 53].

Grating filters

When some applications require single-peaked and narrow-band filters (<5 nm), birefringent filters cannot be good choices because of their multiple passband property (Fig. 1.11(a)), especially when the input spectrum is wide. Additionally, numerical simulations consistently show better performance are generated from the laser cavities with Gaussian-shape filters [55, 56]. A grating filter, which consists of a grating and a SMF, can accomplish the two goals simultaneously. The grating

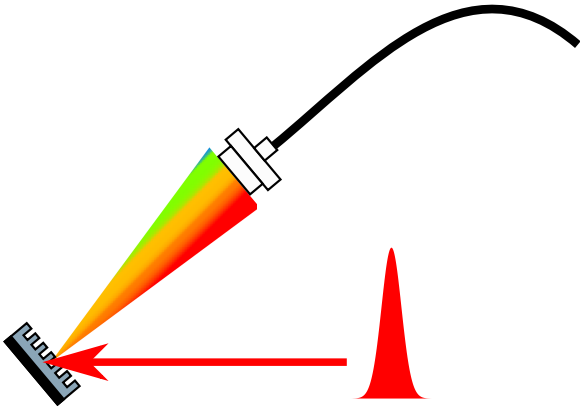

Figure 1.12: Schematic of a grating-based filter.

spatially disperses the spectrum of the incident pulse and a collimator collects the diffracted beam (Fig. 1.12). The fiber only picks up a portion of the spectrum because of the finite numerical aperture. The overlap of the linear spatially-chirped beam with the spatial mode of the SMF results in a spectral filter with a Gaussian transmission curve. When designing the filter bandwidth, the ABCDEF matrix is needed to choose which components to use [57]. It is a function of grating constant, input beam diameter, fiber mode field diameter and focal length of the collimator lens.

1.4.3 Saturable absorbers

Saturable absorbers (SA) are critically important for passively mode-locked lasers. An ideal fast saturable absorber, which is used in the simulations presented in this thesis, has a transmission curve of the form

$$T(t) = 1 - \frac{MD}{1 + P(t)/P_{sat}}, \tag{1.22}$$

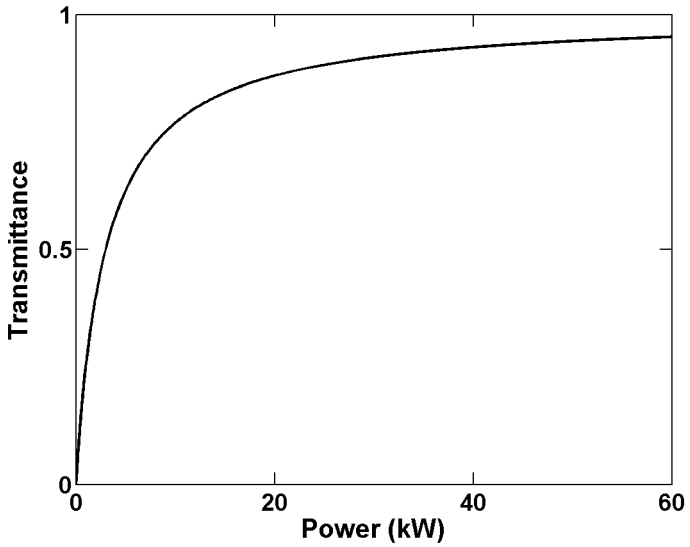

Figure 1.13: Transmission function of an ideal saturable absorber with $P_{sat} = 3$ kW and $MD = 1$.

where MD is the modulation depth, P_{sat} is the saturation power of the SA and the transmission $T(t)$ gets higher when the pulse peak power $P(t)$ increases (Figure 1.13).

SA promotes pulse formation by preferentially transmitting higher intensity light, enabling high intensity fluctuations to be boosted above the background noise level. Thus, a short pulse could produce a modulation of loss because the high intensity at the peak of the pulse saturates the absorber more strongly than its low intensity wings. The saturable absorber can shape the pulse and slightly reduce the pulse duration (Fig. 1.14).

There are two categories of SAs used in lasers, the material-based SAs and the artificial SAs. The former include semiconductor saturable absorber mirrors [58], carbon nanotubes [59] and some other 2-dimensional materials. The artificial SAs include Kerr-lens [7, 60], nonlinear polarization evolution [61, 62], nonlinear optical loop mirror [63] and nonlinear amplifying loop mirror [64].

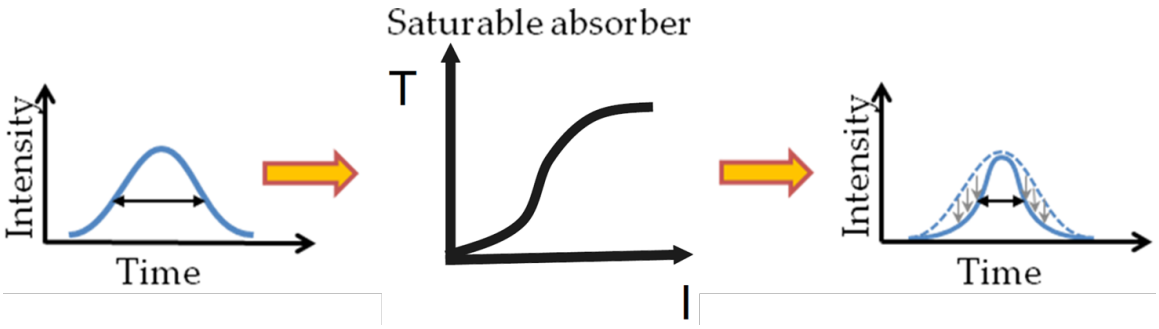

Figure 1.14: Pulse shaping through the saturable absorber.

Semiconductor saturable absorber mirror and nonlinear polarization evolution are discussed below.

Semiconductor saturable absorber mirrors

Semiconductor saturable absorber mirror (SESAM) is a mirror coated with a semiconductor material. The semiconductor material absorbs light when the input photon energy is sufficient to excite carriers from the valence band to the conduction band. The absorption is saturated under strong excitation conditions because the possible initial states of the transition are depleted.

SESAMs are widely used for passive mode-locking, particularly for solid-state bulk lasers. They work with a wide range of laser parameters and usually allow for reliable self-starting mode-locking. Another important application is passive Q-switching. SESAMs also have the advantage of being environmentally stable. However, they tend to be limited to low modulation depths (10%-40%). In addition, they are also easy to damage under high power circumstance and they degrade over time. All these impede their usages for high-performance fiber lasers.

A good summary of the SESAM can be found in Ref. [58].

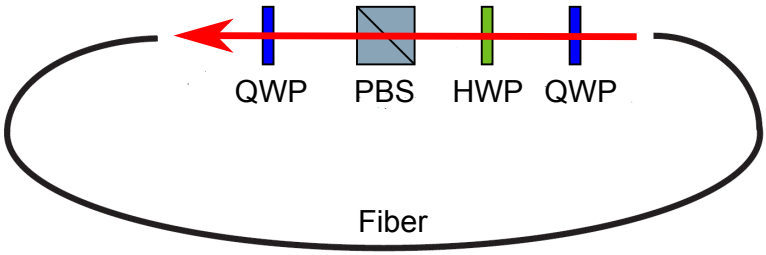

Figure 1.15: Schematic for NPE saturable absorber (PBS: polarizing beam splitter; HWP: half waveplate; QWP: quarter waveplate).

Nonlinear polarization evolution

Nonlinear polarization evolution (NPE) is an ultrafast passive artificial SA. It relies on the nonlinearity-induced polarization rotation in the fiber and can provide high-modulation depth (>90%) and tunable transmission curves. The typical implementation of NPE is illustrated in Fig. 1.15. The polarization state of light after the polarization beam splitter (PBS) is linear and is converted to elliptical through the quarter waveplate (QWP). Then, it propagates nonlinearly in the fiber. Due to cross-phase modulation, the polarization state of the elliptically polarized light will exhibit an intensity-dependent rotation. This rotation can be converted to an intensity-dependent loss after passing through the following QWP, HWP and PBS. If the waveplates are biased correctly, the transmission curve can be biased such that higher intensity has a higher transmission, thus allowing for a pulse to generate from noise. The rejection port of the polarizer can be used as the output coupler. NPE is prevalent in normal-dispersion fiber lasers. So far, their performance is better than fiber lasers using SESAMs or CNTs.

The major drawback for NPE is that it is very sensitive to the environmental perturbation. Changes from temperature, twisting or shaking can introduce changes to the fiber birefringence and in turn change the transmission curve of the NPE. Mode-locking state will be changed or even lost due to these perturbations.

BIBLIOGRAPHY

[1] M. J. Rosker, F. W. Wise, and C. L. Tang, Physical Review Letters **57**, 321 (1986).

[2] P. U. Jepsen, R. H. Jacobsen, and S. R. Keiding, Journal of the Optical Society of America B **13**, 2424 (1996).

[3] S. Diddams, D. Jones, J. Ye, S. Cundiff, J. Hall, J. Ranka, R. Windeler, R. Holzwarth, T. Udem, and T. Hänsch, Physical Review Letters **84**, 5102 (2000).

[4] D. Du, X. Liu, G. Korn, J. Squier, and G. Mourou, Applied Physics Letters **64**, 3071 (1994).

[5] W. W. W. W. Denk, J. H. Strickler, Science **248**, 73 (1990).

[6] A. Zumbusch, G. R. Holtom, and X. S. Xie, Physical Review Letters **82**, 4142 (1999).

[7] D. E. Spence, P. N. Kean, and W. Sibbett, Optics Letters **16**, 42 (1991).

[8] S. H. Cho, Y. Chen, H. A. Haus, J. G. Fujimoto, and E. P. Ippen, **24**, 411 (1999).

[9] G. P. Agrawal, *Nonlinear fiber optics* (Academic press, ADDRESS, 2007).

[10] R. H. Stolen, W. J. Tomlinson, H. a. Haus, and J. P. Gordon, Journal of the Optical Society of America B **6**, 1159 (1989).

[11] K. Blow and D. Wood, IEEE J. Quantum Electron. **25**, 2665 (1989).

[12] L. E. Nelson, D. J. Jones, K. Tamura, H. A. Haus, and E. P. Ippen, Appl. Phys. B **65**, 277 (1997).

[13] L. F. Mollenauer, R. H. Stolen, and J. P. Gordon, Physical Review Letters **45**, 1095 (1980).

[14] H. A. Haus, IEEE J. Sel. Top. Quantum Electron. **6**, 1173 (2000).

[15] E. Snitzer, Physical Review Letters **7**, 444 (1961).

[16] L. F. Mollenauer and R. H. Stolen, Optics letters **9**, 13 (1984).

[17] S. Kelly, Electronics Letters **28**, 806 (1992).

[18] M. L. Dennis and I. N. Duling, IEEE Journal of Quantum Electronics **30**, 1469 (1994).

[19] K. Tamura, E. P. Ippen, H. a. Haus, and L. E. Nelson, Opt. Lett. **18**, 1080 (1993).

[20] C. Y. Chong, Ph.D. thesis (2008).

[21] H. A. Haus, K. Tamura, L. E. Nelson, and E. P. Ippen, IEEE Journal of Quantum Electronics **31**, 591 (1995).

[22] S. K. Turitsyn, B. G. Bale, and M. P. Fedoruk, Phys. Rep. **521**, 135 (2012).

[23] W. J. Tomlinson, R. H. Stolen, and A. M. Johnson, Opt. Lett. **10**, 457 (1985).

[24] D. Anderson, M. Desaix, M. Lisak, and M. L. Quiroga-Teixeiro, J. Opt. Soc. Am. B **9**, 1358 (1992).

[25] D. Anderson, M. Desaix, M. Karlsson, M. Lisak, and M. L. Quiroga-Teixeiro, J. Opt. Soc. Am. B **10**, 1185 (1993).

[26] F. O. Ilday, J. R. Buckley, W. G. Clark, and F. W. Wise, Physical Review Letters **92**, 213902 (2004).

[27] M. Fermann, V. Kruglov, B. Thomsen, J. Dudley, and J. Harvey, Phys. Rev. Lett. **84**, 6010 (2000).

[28] F. Wise, A. Chong, and W. Renninger, Laser & Photonics Review **2**, 58 (2008).

[29] A. Chong, J. Buckley, W. Renninger, and F. Wise, Opt. Express **14**, 10095 (2006).

[30] A. Chong, W. H. Renninger, and F. W. Wise, J. Opt. Soc. Am. B **25**, 140 (2008).

[31] W. H. Renninger, A. Chong, and F. W. Wise, Opt. Lett. **33**, 3025 (2008).

[32] K. Kieu, W. H. Renninger, A. Chong, and F. W. Wise, Opt. Lett. **34**, 593 (2009).

[33] S. Lefrançois, K. Kieu, Y. Deng, J. D. Kafka, and F. W. Wise, Optics letters **35**, 1569 (2010).

[34] M. Baumgartl, C. Lecaplain, A. Hideur, J. Limpert, and A. Tünnermann, Optics Letters **37**, 1640 (2012).

[35] W. Renninger, A. Chong, and F. Wise, Phys. Rev. A **77**, 023814 (2008).

[36] P. Grelu, S. Chouli, J. M. Soto-Crespo, W. Chang, A. Ankiewicz, and N. Akhmediev, 2010 Photonics Glob. Conf. PGC 2010 **6**, 84 (2010).

[37] W. H. Renninger, A. Chong, and F. W. Wise, IEEE Journal on Selected Topics in Quantum Electronics **18**, 389 (2012).

[38] W. H. Renninger, A. Chong, and F. W. Wise, **27**, 1978 (2010).

[39] B. Oktem, C. Ülgüdür, and F. Ö. Ilday, Nat. Photonics **4**, 307 (2010).

[40] W. H. Renninger, A. Chong, and F. W. Wise, Phys. Rev. A **82**, 021805 (2010).

[41] C. Aguergaray, D. Méchin, V. Kruglov, and J. D. Harvey, Opt. Express **18**, 8680 (2010).

[42] W. H. Renninger, A. Chong, and F. W. Wise, Opt. Express **19**, 1 (2011).

[43] G. Chang, A. Galvanauskas, H. G. Winful, and T. B. Norris, Optics letters **29**, 2647 (2004).

[44] D. B. Soh, J. Nilsson, and A. B. Grudinin, J. Opt. Soc. Am. B **23**, 10 (2006).

[45] D. B. Soh, J. Nilsson, and A. B. Grudinin, J. Opt. Soc. Am. B **23**, 1 (2006).

[46] https://en.wikipedia.org/wiki/Opticalfiber .

[47] D. Gloge and E. A. J. Marcatili, Bell. Syst. Tech. J **52**, 1563 (1973).

[48] A. Mafi, Journal of Lightwave Technology **30**, 2803 (2012).

[49] F. Poletti and P. Horak, Journal of the Optical Society of America B **25**, 1645 (2008).

[50] http://www.fiberlaser.fujikura.jp/eng/products/about-fiber-laser.html .

[51] S. Boscolo, C. Finot, H. Karakuzu, and P. Petropoulos, Optics Letters **39**, 438 (2014).

[52] J. W. Evans, J. Opt. Soc. Am. **39**, 229 (1949).

[53] A. Chong, W. H. Renninger, and F. W. Wise, Optics Letters **32**, 2408 (2007).

[54] E. S. Lamb, Ph.D. thesis (2015).

[55] W. H. Rennigger, Ph.D. thesis (2012).

[56] Z. Liu, Z. M. Ziegler, L. G. Wright, and F. W. Wise, Optica **4**, 649 (2017).

[57] A. A. Tovar and L. W. Casperson, J. Opt. Soc. Am. A **12**, 1522 (1995).

[58] U. Keller, K. J. Weingarten, F. X. Kärtner, D. Kopf, B. Braun, I. D. Jung, R. Fluck, C. Hönninger, N. Matuschek, and J. Aus Der Au, IEEE J. Sel. Top. Quantum Electron. **2**, 435 (1996).

[59] S. Y. Set, H. Yaguchi, Y. Tanaka, and M. Jablonski, J. Light. Technol. **22**, 51 (2004).

[60] T. Brabec, C. Spielmann, P. F. Curley, and F. Krausz, Opt. Lett. **17**, 1292 (1992).

[61] M. E. Fermann, Opt. Lett. **18**, 894 (1993).

[62] R. H. Stolen, J. Botineau, and A. Ashkin, Opt. Lett. **7**, 512 (1982).

[63] N. J. Doran and D. Wood, Opt. Lett. **13**, 56 (1988).

[64] M. E. Fermann, F. Haberl, M. Hofer, and H. Hochreiter, Opt. Lett. **15**, 752 (1990).

CHAPTER 2

MEGAWATT PEAK POWER FROM A MAMYSHEV OSCILLATOR[1]

Fiber lasers that generate ultrashort light pulses can offer practical advantages over solid-state lasers for some applications. However, the achievement of high peak power with environmentally-stable designs remains a major challenge for fiber oscillators. We demonstrate that an environmentally-stable source based on cascaded Mamyshev regeneration can reach peak power at least an order of magnitude higher than that of previous lasers with similar fiber mode area. By designing the oscillator to support parabolic pulse formation and exploiting the step-like saturable absorber characteristic of Mamyshev regeneration, unprecedented nonlinear phase shifts can be managed. Numerical simulations reveal key aspects of the pulse evolution, and realistically suggest that (after external linear compression) peak powers that approach 10 MW are possible from ordinary single-mode fiber. Experiments with a ring-cavity oscillator based on ytterbium-doped fiber are limited by available pump power, but still yield 50-nJ and 40-fs pulses,for $\sim$ 1-megawatt peak power. The combination of environmental stability, established previously, with the performance described here should make the Mamyshev oscillator extremely attractive for applications.

2.1 Introduction

A consensus goal of research on ultrafast fiber lasers has been to develop an alternative to the solid-state mode-locked oscillator, with the purported benefits of the fiber platform: relatively low cost, simplicity, and robustness. Ultrafast lasers pro-

[1]Much of the work presented in this chapter was published in Optica [1].

vide precise and intense fields that have enabled many important advances, such as biomedical imaging and laser micromachining [2, 3]. Fiber ultrafast instruments could be transformative in enabling both widespread scientific and industrial applications of ultrafast pulses. However, for this they need to simultaneously reach sufficient performance and be amenable both to cost-effective manufacturing and use by non-experts. For a long time, the primary challenge to achieving high peak power was the management of nonlinearity in the waveguide medium. In the past decade, this challenge has been met with several developments. New pulse evolutions based in normal dispersion fiber now provide a means of tolerating high nonlinearity [4, 5, 6, 7, 8]. In laboratory prototypes that utilize nonlinear polarization evolution (NPE) as an effective saturable absorber, these sources rival solid-state oscillators. Their typical performance of $\sim$ 20-nJ and sub-100 fs pulses from standard single-mode fiber (SMF) represent order-of-magnitude higher peak power than early soliton [9] and stretched-pulse fiber oscillators [10]. However, for widespread use and commercialization, NPE is undesirable because it is highly sensitive to the random birefringence of the fiber, and consequently mode-locking is easily disrupted by environmental perturbations. This has become the impediment to the proliferation of fiber lasers in applications that employ femtosecond oscillators. It has stymied commercial instruments that reach beyond the scientific market.

Substantial effort has been devoted to solving this problem. Fiber lasers constructed with all polarization-maintaining (PM) fiber are robust against such environmental perturbations. To date, no work has been able to combine the high performance of NPE in standard SMFs with an all-PM design. Semiconductor saturable absorber mirrors (SESAMs) [11, 12] and nonlinear loop mirrors using PM fibers [13, 14, 15] have been employed as alternative saturable absorbers. Material-

based saturable absorbers, however, suffer from long-term reliability and poor power-handling capabilities. Nonlinear loop mirror (NOLM) and nonlinear amplifying loop mirror (NALM) based designs require precise control of the splitting ratio between loop directions, and their transmission cannot be easily and continuously tuned. Furthermore, although significant steps have been made, lasers based on SESAMs, NOLMs or NALMs still have not generated more than 5-nJ and sub-100 fs pulses.

Devices based on reamplification and reshaping have been considered as an alternative for the generation of short pulses [16, 17, 18, 19, 20]. This approach relies on self-phase-modulation (SPM) induced spectral broadening and offset spectral filtering, which leads to an effective self-amplitude modulation. Mamyshev proposed the use of the process for signal regeneration [21], and several studies focused mainly on pulse generation with telecommunication parameters [22]. The pulse energies and durations (usually picojoules and picoseconds) were limited by nonlinear phase accumulation in long fibers and narrow filter separation [18, 19, 20, 22]. Regelskis *et al.* first demonstrated a Mamyshev oscillator aimed at high-energy femtosecond pulses [23]. This environmentally-stable oscillator produced modest-energy (¡3-nJ) pulses with 2-ps duration. The measured spectral bandwidth could support $\sim$ 150-fs transform-limited pulses, but the compressed pulse duration was not measured. These researchers also reported that the oscillator could be started by reflecting light rejected by the filter back into the cavity [24]. Very recently, starting of a Mamyshev oscillator by modulation of the pump laser at 20 kHz to induce Q-switching was reported [25]. This oscillator featured an all-fiber construction and generated impressive 15-nJ pulses, which were dechirped to 150-fs duration.

The recent works by Regelskis *et al.* and Samartsev *et al.* nicely illustrate the potential practical advantages of Mamyshev oscillators over conventional mode-locked lasers. On the other hand, they do not address the nature of the intracavity pulse propagation beyond the self-amplitude modulation that arises from the offset filtering. As a result, important questions remain regarding fundamental aspects of their operation. Additionally, the peak power obtained with such devices still lags behind that of mode-locked lasers that employ NPE. If Mamyshev oscillators cannot reach high performance levels, the benefits they provide over alternative environmentally-stable designs will be limited. On the other hand, if the performance limits of the Mamyshev oscillator meet or even exceed those of previous designs, the combination of performance and practical advantages may allow it to find widespread applications. Clearly, there is ample motivation to understand pulse propagation and its performance limits. Finally, the mechanisms of self-starting are still unclear.

Here, we report results of a theoretical and experimental study of pulse propagation in a Mamyshev oscillator. Insight gained about the pulse propagation allows us to achieve record performance for a femtosecond fiber oscillator, and forecasts ultimate performance limits yielding nearly an order-of-magnitude higher peak power. Numerical simulations show that an oscillator comprised of ordinary SMF, when seeded by a low-energy short pulse (¡ 10-ps), can support mode-locked pulses with 190-nJ energy and ¡20-fs dechirped duration (Fourier transform limited). These parameters correspond to $\sim$ 8 MW peak power. The simulations reveal that this performance follows from the oscillator's remarkable capacity to manage nonlinear phase. In a suitably-designed cavity, the pulse evolves to a parabolic shape before it enters the gain fiber, which enables control of the nonlinear phase accumulated in the gain segment. Theoretically, the pulse can accumulate a round-trip non-

linear phase shift of 140π and still be stable. In experiments, $\sim$ 50-nJ and $\sim$ 40-fs pulses (after compression) at 17 MHz are generated, with the energy limited by the available pump power and/or damage to the PM fiber. Even so, the $\sim$ 1 MW peak power is about 10 times higher than that has been produced by a mode-locked fiber laser constructed with ordinary SMF [6]. The accumulated nonlinear phase shift is $\sim 60\pi$, which is $\sim$ 5 times larger than the largest reported for stable pulses with well-controlled phase from a mode-locked laser. We attribute this to the parabolic pulse propagation along with the step-like saturable-absorber behavior of the Mamyshev process, which will be elaborated on below. These results represent a significant step toward a high-energy, short-pulse fiber source that can be environmentally-stable. The outlook for self-starting Mamyshev oscillators, along with extensions to other wavelengths, will be discussed below. Finally, we consider fundamental aspects of the Mamyshev oscillator in the context of other driven nonlinear systems.

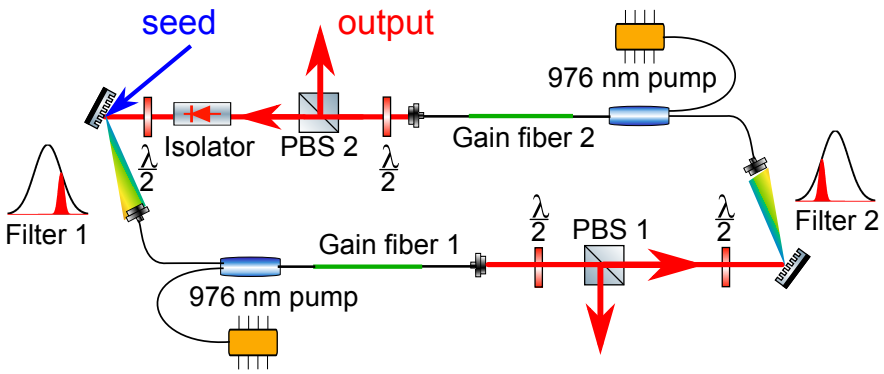

Figure 2.1: Schematic of the ring Mamyshev oscillator. Filter: The black curve shows the gain spectrum and the red curve indicates the passband of the filter; PBS: polarizing beam splitter.

2.2 Numerical and experimental results

The experimental configuration of the oscillator is schematically illustrated in Fig. 2.1. The laser operates in the all-normal-dispersion regime (as do all prior Mamyshev oscillators). A ring oscillator allows more design freedom to control the propagation compared to a linear oscillator. Ytterbium-doped fiber provides the gain, and all fibers are PM. The use of Gaussian spectral filters is important for maximizing the pulse quality and peak performance (see Supplement 1, section 3). To accomplish this, we use the overlap of the beam diffracted from a grating with the spatial mode of the fiber [26]. These filters inherit their Gaussian shape from the fundamental mode shape of the SMF, and were tuned to longer ($\sim$ 1040 nm) and shorter ($\sim$ 1030 nm) wavelengths than the $\sim$ 1035 nm peak of the gain spectrum. An isolator ensures unidirectional operation. Polarizing beam splitters are used as the output couplers. The steady-state operation cycle consists of amplification (gain fiber 1), spectral broadening (gain fiber 1 and the following passive SMF), pulse energy adjustment (PBS 1), filtering (filter 2), amplification (gain fiber 2), spectral broadening (gain fiber 2 and the following passive SMF), output (PBS 2) and spectral filtering (filter 1). The half-wave plates are used to adjust the polarization state of light going into the PM fiber and to optimize the output coupling ratio. To ignite pulsation in the cavity, a seed pulse is directed into the fiber via a grating.

We performed numerical simulations of the oscillator shown in Fig. 2.1 using the standard split-step method with accurate fiber parameters (the parameters are given in Supplement 1, Table S1). The simulation includes the Kerr nonlinearity, stimulated Raman scattering, and second and third order dispersion. The oscillator is seeded with different initial pulses (picosecond or femtosecond dura-

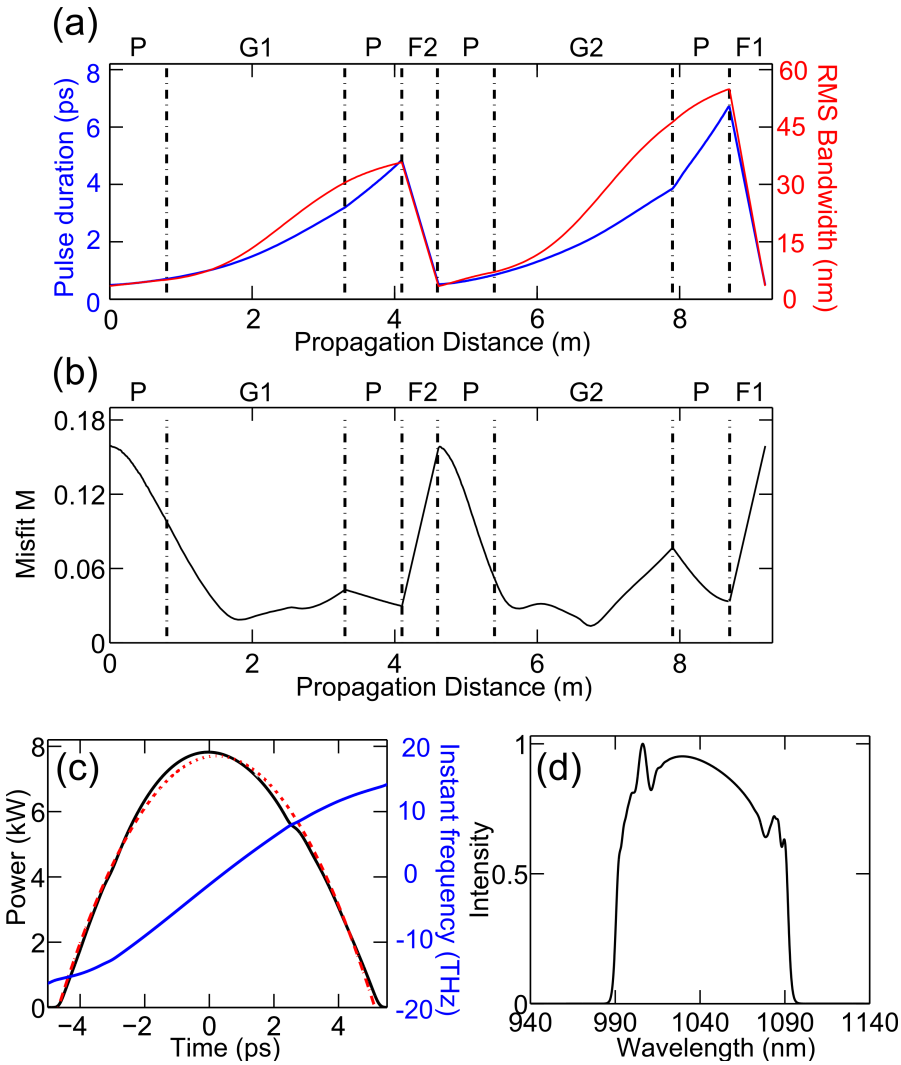

Figure 2.2: Numerical simulation results for $\sim$ 50 nJ output pulses. (a) Evolution of pulse duration (blue) and RMS bandwidth (red), P: passive fiber; G: gain fiber; F: filter; (b) evolution of misfit parameter M defined by $M^2 = \int (I - I_{fit})^2 dt / \int I^2 dt$, which indicates the difference between the pulse shape (I) and the best-fit parabolic profile I_{fit}; (c) temporal profile (black) with fitted parabolic curve (red) and instantaneous frequency across the chirped pulse (blue) and (d) simulated spectrum.

tion), but for given cavity parameters the simulations always converge to the same solution. The simplified gain dynamics and small temporal window of our simulations prevent our current numerical model from providing realistic insight into starting of pulse-formation from noise. Numerical simulations predict the cavity may generate up to 190-nJ pulses, which can be dechirped to below 20 fs. The

pulse energy is limited by deviations of the pulse from a parabolic shape, which causes wave breaking, and by stimulated Raman scattering (see Supplement 1, Fig. S1). Another example, for which 50-nJ pulses are produced, is shown in Fig. 2.2 for comparison to experimental results below. The pulse duration and bandwidth grow monotonically in the passive (80 cm), gain (2.5 m) and second passive fiber (80 cm) segments in both arms. The spectral filters (F1 and F2) shape the pulse to a narrow-band and short-duration pulse that seeds the propagation in the subsequent arm (Fig. 2.2 (a)). Over the course of its evolution, spectral breathing by a factor of 16 is observed. The pulse evolves quickly to a parabolic shape in the passive fiber (Fig. 2.2 (b)). This parabolic pulse is subsequently amplified in the gain fiber. The parabolic shape is maintained through this gain fiber and into the following passive fiber. This is in contrast to regenerative similariton lasers, where the self-similar evolution is localized to the gain fiber [27, 28]. The output in the time domain is a nearly linearly-chirped parabola (Fig. 2.2 (c)) with 110-nm bandwidth (Fig. 2.2 (d)), which corresponds to a $\sim$ 30-fs transform-limited pulse.

Experiments were performed with guidance from the simulations. Yb-doped, PM double-clad fiber with 6-μm core (YB1200-6/125DC-PM) is employed in the gain segments. The 2.5-m long gain segments support the parabolic evolution and absorb most of the pump light. All the passive fibers are standard PM-980. The oscillators repetition rate is $\sim$17 MHz. The separation of the two filters was adjusted to eliminate continuous-wave (CW) operation while allowing for the highest output pulse energy. With the seed pulses launched into the cavity, the optimal mode-locking conditions were found by adjusting the output coupling in each arm with the waveplates. The seed pulses can be quite weak and their duration is not important. For example, reliable starting was obtained with 80-pJ and 10-ps pulses, or with ¡10 pJ and 3-ps chirped pulses with 20-nm bandwidth. The band-

width of the seed pulse is a significant factor because it determines whether a seed can circulate and be amplified in the first roundtrip; if the bandwidth is not wide enough, larger seed energy or higher gain is needed to provide enough spectral broadening. Once pulsation is initiated, as indicated by a broad output spectrum, the seed pulse can be blocked and pulses will continue to circulate in the cavity. While the oscillator is running, physical perturbations such as twisting or shaking the fiber do not alter the operating state of the laser. Once the optimal conditions are found, oscillation can be extinguished by blocking the cavity or turning off the pump, and restarted to the same state by launching in seed pulses without any additional adjustment. Moreover, an isolated seed pulse is not necessary, as the pulsed operation is stable in the presence of continuous seeding (we tried different continuously-running pulsed lasers as seed sources, operating at 1 MHz and 40 MHz).

The oscillator generates 6-ps chirped pulses. The output spectra and autocorrelation traces of the dechirped pulses for a range of pulse energies are shown in Fig. 2.3. Here the output is taken from the output coupler directly before the isolator, and the energy is modified by changing the pump power. As the energy increases, the spectrum broadens due to stronger SPM (Fig. 2.3 (a)), and the dechirped duration decreases. We find that, using only a grating compressor (300 lines/mm), the dechirped pulses appear relatively clean without pedestals or structure (Fig. 2.3 (b)). For the energy range shown, the dechirped pulse duration is within 1.5 times the transform limit. This deviation can be accounted for by the third-order dispersion in the grating compressor. We estimate that the 50-nJ pulses accumulate a nonlinear phase of 60π. This shows that the huge nonlinear phase accumulation in the Mamyshev oscillator is well-controlled: it is converted into a nearly-linear chirp. Eventually, higher-order phase that cannot be compen-

sated by the grating pair becomes significant and the minimum dechirped duration grows despite increasing bandwidth (50-nJ trace). The ∼50-nJ pulses are limited by the maximum available pump power; we do not observe multi-pulsing, which commonly limits the pulse energy in mode-locked lasers.

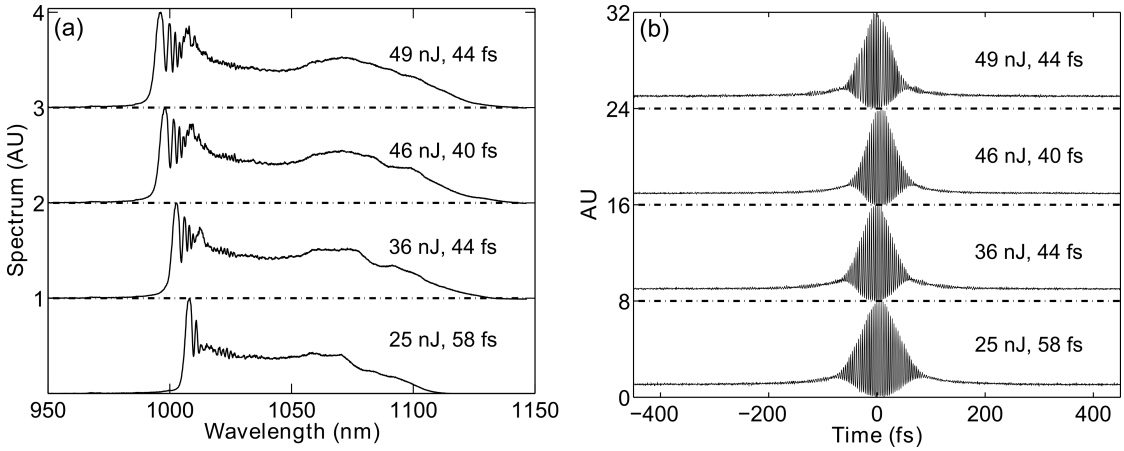

Figure 2.3: Measurements of pulses from the ring Mamyshev oscillator. (a) Measured output spectra and (b) autocorrelations for the indicated output energies.

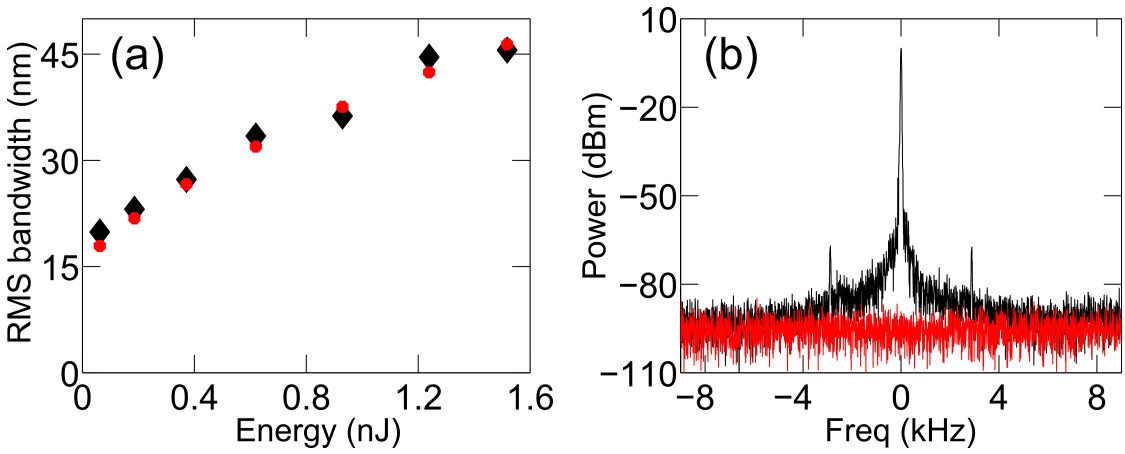

Figure 2.4: Pulse quality check. (a) Measured root-mean-square bandwidth after propagation through 2-m of SMF (black) compared to simulation (red). (b) Radio frequency spectrum with a resolution bandwidth of 30 Hz and a span range of 20 kHz. Noise floor is shown in red.

The pulse peak power is verified by launching the dechirped pulse into 2-m of SMF with a 6 μm core diameter (HI1060) and measuring the SPM-induced spectral broadening. The measurements are compared with results of numerical simulations

in Fig.2.4 (a)). In simulation, we launch a Gaussian pulse with the same energy and transform-limited duration, and with the residual third-order dispersion from the grating compressor, into a fiber with the parameters of 2-m of HI1060. The calculation accounts for fiber dispersion up to the third order, SPM, and intrapulse Raman scattering. The simulation reproduces the root-mean-square bandwidth observed for the experimental pulses accurately, which indicates the high quality of the output pulses.

The stability of the output pulse train was investigated using an RF spectrum analyzer. The resolution and dynamic range of the spectra are instrument-limited, but still confirm the stable mode locking and absence of sidebands and harmonic frequencies to at least 80 dB below the fundamental frequency (Fig.2.4 (b)). This is similar to the performance of mode-locked fiber oscillators.

For the conditions described above, the oscillator does not start from noise. Self-pulsation originating from amplified spontaneous emission (ASE) has been predicted [18] and demonstrated in long cavities (∼km) with highly nonlinear fibers (HNLF) [19, 20]. Starting is favorable in these cavities owing to the narrow filter separation, along with the possibility for sufficient nonlinear phase accumulation by even low-power fluctuations in the long HNLF. We speculate that the recently-described dissipative Faraday instability (DFI) can account for the self-starting in this case, since the small separation between the filters overlaps with the DFI gain spectrum [29, 30]. For broadband, high-energy pulses, the optimal filter separation is much broader than the DFI gain spectrum. In this regime, self-starting was proposed [24] and reported [31] by use of controlled feedback of amplified spontaneous emission in the linear cavity, through a so-far unexplained mechanism. We have recently confirmed self-starting operation of a linear cavity in our laboratory, at

Pulse evolution	Nonlinear phase	Typical performance	Best performance
Soliton [9]	~ 0	0.1 nJ, 300 fs	0.5 nJ, 100 fs
Stretched pulses [10]	0 to π	1 nJ, 100 fs	up to 3 nJ, down to 50 fs
Passive similariton [4]	2π - 10π	6 nJ, 150 fs	15 nJ, 100 fs
Dissipative soliton [5]	2π - 10π	6 nJ, 150 fs	up to 20 nJ, down to 70 fs
Amplifier similariton [26]	4π - 10π	3 nJ, 70 fs	up to 8 nJ, 40 fs
Ti:sapphire [32]	0 to π	30 nJ, 50-100 fs	200 nJ, 30 fs
Mamyshev oscillator	$>60\pi$ (in simulation: $>140\pi$)		experiment: 50 nJ, 40 fs (in simulation: >190 nJ, <20 fs)

Table 2.1: Performance Summary of SMF-based Ytterbium-doped Fiber Oscillators for Different Pulse Evolutions.

power levels lower than reached by the ring cavity (see Supplement 1, section 2). As will be discussed below, although the nature of the Mamyshev oscillator suggests that it is incompatible with self-starting, these initial results provide optimism regarding the near-future realization of a fully self-starting, environmentally-stable fiber oscillator with the high performance demonstrated here.

2.3 Discussion

The performance of mode-locked lasers is fundamentally limited by nonlinear effects. Solitons and dispersion-managed solitons are stable for at most a round-trip peak nonlinear phase shift of π. Experiments showed the passive similariton, dissipative soliton and amplifier similariton can support ¡100 fs and ¿10 nJ pulses, which corresponds to $\sim 10\pi$ nonlinear phase shift [33, 8]. Simulations of these evolutions, assuming ideal saturable absorbers, indicate that higher performance can be achieved with higher pump power. These high-energy pulses, *i.e.* larger nonlinear phase shift, require a very high modulation-depth saturable absorber to

suppress the CW background [33]. While NPE can be close to an ideal absorber, there is still a significant gap between simulations and experiments, and currently $\sim 10\pi$ represents an approximate limit for experiments. This value is consistent with the numerical prediction for dissipative soliton oscillators [33]. Table 2.1 summarizes the performance of representative Yb-doped mode-locked fiber lasers. (Actual pulse energies are scaled to the values that would be obtained with the same core size (6 μm).)

The Mamyshev oscillator overcomes these limitations. If the nonlinearity is correctly managed, high energy, wave-breaking-free pulses with good phase profile can be generated - apparently even well beyond the gain bandwidth limit. This performance follows from the step-like saturable absorber realized by the combination of two filters and the fiber. As pointed out by Pitois *et al.*, the cascaded frequency-broadening and offset filtering creates an effective transmission function that is step-like, with zero transmittance at low power and an abrupt transition to a constant value at high power [18]. This step-like saturable absorber means that the mode-locking pumping rate is below the continuous wave lasing threshold, so the Mamyshev oscillator only supports mode-locked operation. This eliminates the nonlinearity limit from the saturable absorber [33], and so allows for much higher energy. Already, the compressed pulse we obtain has a peak power roughly an order-of-magnitude above previous results. The performance is comparable that of the best commercial Ti:sapphire lasers, the current workhorses of ultrafast laser applications (Table 2.1).

Of course, the step-like saturable absorber property creates a challenge for starting a Mamyshev oscillator from noise. Despite this, two methods of starting similar cavities have recently been demonstrated: pump modulation [25] and

controlled feedback of amplified spontaneous emission [31]. Our own initial investigations confirm that the latter is, remarkably, a reliable and robust means of circumventing the starting problem (see Supplement 1, section 2). While the pump modulation scheme demonstrated by Samartsev et al. [25] is important, using a coupled cavity to start the Mamyshev oscillator has the practical benefit of being completely passive. It is surprising that any starting technique can be successful, because of the inevitable trade-off between starting and performance and the bias here towards performance due to the step-like saturable absorber property. That researchers have demonstrated such methods in similar cavities suggests that related techniques may be used for the ring cavity presented here. Future work will be focused on developing such techniques.

Prospects for further optimization and scaling of the Mamyshev oscillator are exciting. While simulations of ultrafast fiber sources have systematically suggested much higher performance than has been observed, we are more optimistic about our extrapolations for the Mamyshev oscillator. The discrepancy between experimental performance and anticipated results in conventional fiber lasers likely follows from uncertain starting conditions and overly-optimistic saturable absorber parameters. Starting the oscillator from a pulse systematically produces higher performance than starting from noise [34]. In contrast, our observations in the self-starting linear Mamyshev oscillator show that pulse-seeded and self-starting performance are similar. Meanwhile, standard numerical techniques for modeling ultrashort-pulse fiber lasers neglect gain relaxation dynamics and use a restricted temporal window. These fail to account for nanosecond laser spiking or other effects that may play an important role in starting, and ultimately the steady-state performance. In the Mamyshev oscillator, CW lasing is completely suppressed: the CW lasing threshold is much *higher* than the pulse threshold. Consequently, if

achieved, starting should be more deterministic, and the maximal nonlinear phase shift can be much higher than in a cavity where CW lasing needs to be constantly suppressed.

The approach described here can be extended in several directions. Scaling from the experimental results presented here, with large mode area (25 μm diameter) PM fiber we expect that Mamyshev oscillators will reach the microjoule level. Simulations also indicate that by changing the fiber length, the oscillator repetition rate can be tuned from hundreds of MHz to $\sim$ 1 MHz without sacrificing the performance (at lower repetition rates, additional dispersion compensation inside of the cavity is required). This will allow it to be a useful tool for both scientific and industrial applications. In addition, the linearly-chirped parabolic output pulses are attractive for applications such as highly-coherent continuum sources and optical signal processing, etc. [35]. High-performance Mamyshev oscillators at other wavelengths can be expected. If normal-dispersion gain fiber is available (as is the case at 1550 nm, e.g.), the design could be very similar to that presented here.

Given that it has taken more than a decade for the Mamyshev pulse generator to gain serious consideration as an alternative to conventional mode-locked fiber lasers, it is worthwhile to reconsider broader impacts of this system. Numerous works [22, 18] have explored optimization of the Mamyshev oscillator for signal regeneration. The results presented here explore the system in connection and contrast to mode-locked fiber lasers. Much work remains to optimize oscillator designs for this purpose. However, a crucial difference between the Mamyshev oscillator and a conventional mode-locked laser is that, in the Mamyshev oscillator, the pulsed state is bistable with amplified spontaneous emission. This kind of bistabil-

ity is also a key characteristic of systems supporting cavity solitons (where usually the pulsed-state is bistable with the continuous-wave field). Hence the Mamyshev oscillator should be compared and contrasted not only with mode-locked lasers, but also with systems that support cavity solitons, such as coherently-driven cavities, which have lately been explored extensively for producing mode-locked frequency combs [36, 37, 38, 39]. Two features of the pulse evolution we demonstrate here are worth noting. First, the Mamyshev oscillator can produce a stable pulse train even with extremely high roundtrip nonlinear phase shift and spectro-temporal breathing. This suggests that in a suitably-designed device, an octave-spanning frequency comb could be generated directly, possibly exceeding the bandwidth and certainly the power of microresonator combs. Second, as in fiber lasers, the roundtrip gain and loss are much higher than in coherently-driven cavities. This may allow more straightforward control over circulating pulses, at the point of minimum pulse energy by, for example, an intracavity electro-optic modulator or coupling to an external source of optical bits. Furthermore, following from the possibility for extreme nonlinear phase and pulse evolution, much more elaborate information processing schemes could be devised. Ultimately, these suggestions are only speculative examples of the more important message. Many questions remain about the Mamyshev oscillator, and its unique features suggest a wide variety of uses and phenomena which, to date, have been under-explored compared to conventional mode-locked laser cavities and coherently-driven high-Q optical resonators.

2.4 Conclusion

In conclusion, these results show that the Mamyshev oscillator allows a surprising and significant leap in the ongoing central challenge of high-power ultrafast fiber lasers: the management of nonlinearity. This is due to the formation and amplification of parabolic pulses and the step-like artificial saturable absorber formed by the Mamyshev regeneration mechanism. By making the continuous wave lasing threshold above the threshold for mode-locking, the Mamyshev oscillator supports stable mode-locking with huge nonlinear phase shifts. To harness this nonlinearity for the generation of clean, high-energy ultrashort pulses, we designed the oscillator to support parabolic pulse formation. Combined, these factors translate to unprecedented performance - our initial design already yields an order-of-magnitude higher peak power than any previous fiber oscillator with the same core size. As prior work has shown, the Mamyshev oscillator supports an environmentally-stable, fiber-format design which can be self-starting, thus solving a major practical impediment to the widespread use of ultrashort-pulse fiber sources in applications. Taken together, these features should make Mamyshev oscillator extremely attractive for applications in ultrafast science and technology.

Funding Information

Portions of this work were funded by the Office of Naval Research (N00014-13-1-0649) and the National Institutes of Health (EB002019). Z. Ziegler acknowledges support from an ELI undergraduate research award at Cornell University.

Acknowledgments

The authors gratefully acknowledge helpful discussions with J. Zeludevicius.

2.5 Supplementary 1

This document provides supplementary information to Megawatt peak power from a Mamyshev oscillator. We show numerical results on maximum performance of the experimental Mamsyshev oscillator design and discuss performance limits. We provide numerical results that show the importance of a Gaussian filter profile for obtaining high-quality, high-energy pulses. Finally, experiments on starting a linear cavity are described.

2.5.1 Simulation result for the highest energy pulses

Fig. 2.5 shows the simulation result for the highest pulse energy output (190 nJ) for the same cavity design as the experiment. The spectral breathing ratio is 26 (Fig. 2.5 (a)). Compared with the 50-nJ example, the pulse shape deviates more from the parabola during the whole roundtrip (Fig. 2.5 (b)). The chirp of the pulse is consequently not linear, and its deviation increases for higher pulse energy (Fig. 2.5 (c)). That said, the pulse is still coherent, and the 150-nm bandwidth (Fig. 2.5 (d)) corresponds to <20 fs transform-limited pulses, which could be obtained with a pulse compressor that controls higher-order dispersion. On a logarithmic scale, the spectrum shows the formation of a parasitic Raman peak (Fig. 2.5 (e)). Understanding these two factors - breakdown of the parabolic shape, and

formation of Raman and how to manage them will determine the ultimate limits of the Mamyshev oscillator.

2.5.2 Experiments on starting

To investigate the starting dynamics, we built a similar linear oscillator (Fig. 2.6 (a)). Two mirrors (M1 and M2), two bandpass filters (4-nm near super-Gaussian interference filters biased to longer and shorter wavelengths with respect to the gain spectrum) and the fiber segments form the Mamyshev cavity. The rejected beams from these filters are taken as the outputs. When seeded by short pulses as described in the main text, the linear oscillator behaves like the ring, but the maximum pulse energy is lower due to several practical problems. For example, simulations show that output performance is limited compared to the ring due to the super-Gaussian filter shape. Short-pulse generation can also be started by placing a mirror (M3) at one of the outputs to direct the rejected light back into the oscillator. This is consistent with previously reported work [31, 24]. Adding this mirror creates two coupled cavities: the Mamyshev cavity with two spectral filters, described above, and a cavity that can oscillate on a CW basis within the pass-band of filter 1. The Mamyshev cavity only oscillates for high peak power and does not support CW operation, while the opposite is true for the coupled CW cavity formed by M1 and M3. With the feedback cavity coupled, we observe that a pulse train in the Mamyshev typically starts after ~ 10 seconds of operation. The spectra recorded from the two outputs are shown in Fig. 2.6 (b), and are very similar to the spectra produced with seed pulses. The spectrum from output 2 (13 nJ) is wider than the spectrum from output 1 (6.5 nJ). The large bandwidth difference between the two outputs is a result of the filters not being symmetrically distant from the

peak of the gain spectrum. The measured autocorrelation for the dechirped output 1 (using a grating pair compressor) and the corresponding transform-limited pulses (125-fs duration) are shown in Fig. 2.6 (c). The close agreement implies that the chirp of the pulses exiting the cavity must be nearly linear. In contrast, the pulse from output 2 cannot be dechirped to the transform limit due to uncontrolled nonlinear phase accumulation. This is likely a consequence of the non-Gaussian filter profile.

By observing the cavity output prior to starting, we infer that self-starting in the coupled linear cavity Mamyshev oscillator is the result of spectral broadening of extreme lasing spikes that result from relaxation oscillations within the coupled cavity. We observe bunches of nanosecond-duration pulses from output 1, whose duration and $\sim$ hundred-μs temporal separation is consistent with relaxation oscillation in the CW cavity. These relaxation oscillations are only observed when the loss of the CW cavity is sufficiently large; when M3 is optimally-aligned, self-starting is not observed. When self-starting is observed, it is repeatable: if the cavity is blocked and unblocked, pulsation returns within $\sim$ 10 seconds. We attribute the self-starting to spectral broadening of the nanosecond-duration spikes. For rare extreme-amplitude spikes, relatively broad initial bandwidth and nonlinear spectral broadening are sufficient for them to couple into the Mamyshev cavity and initiate pulsation. Once the Mamyshev cavity has started, it is indefinitely stable in the continued presence of the coupled CW cavity, which is attractive for practical applications.

2.5.3 Effect of the filter shape

Using a Gaussian filter is evidently important for the peak performance and pulse quality because of its smoothness. For the ring cavity, when we replace the Gaussian filters (4-nm bandwidth) with super-Gaussian shape filters (4-nm bandwidth) in the simulation, the highest achieved pulse energy is $\sim$ 40 nJ (Fig. 2.7), which is much lower than the results using Gaussian filters (Fig. 2.5).

The simulations indicate that the use of filters that do not have Gaussian transmittance bands reduces the stable pulse energy and yields structure on the spectrum. Furthermore, the Gaussian filter's improvement of the output chirped pulses' smooth parabolic shape, and the smoothness of the spectra, is an important feature that should improve the pulses' use as a seed for low-distortion fiber amplifiers. Fig. 2.8 and Fig. 2.9 show the difference between the linear cavity output using Gaussian filter and super-Gaussian filter with similar bandwidth (4nm FWHM).

Component	Length (meter)	BW (nm)	WL (nm)	OC	A_{eff} (μm^2)	GVD (fs^2/mm)	TOD (fs^3/mm)	Loss	SE (nJ)
Filter 1		4	1040					30%	
Coupling Loss 1								25%	
Passive Fiber	0.8				37.8	22.2	63.8		
Gain Fiber 1	2.5	40	1035		29	24.9	59		9.15
Passive Fiber	0.8				37.8	22.2	63.8		
PBS 1				40%					
Filter 2		4	1030					30%	
Coupling Loss 2								25%	
Passive Fiber	0.8				37.8	22.2	63.8		
Gain Fiber 2	2.5	40	1035		29	24.9	59		36.6
Passive Fiber	0.8				37.8	22.2	63.8		
Output				88%					

Table 2.2: Parameters Used in the simulation. BW: bandwidth; WL: wavelegnth; OC: output coupling; SE: saturation energy.

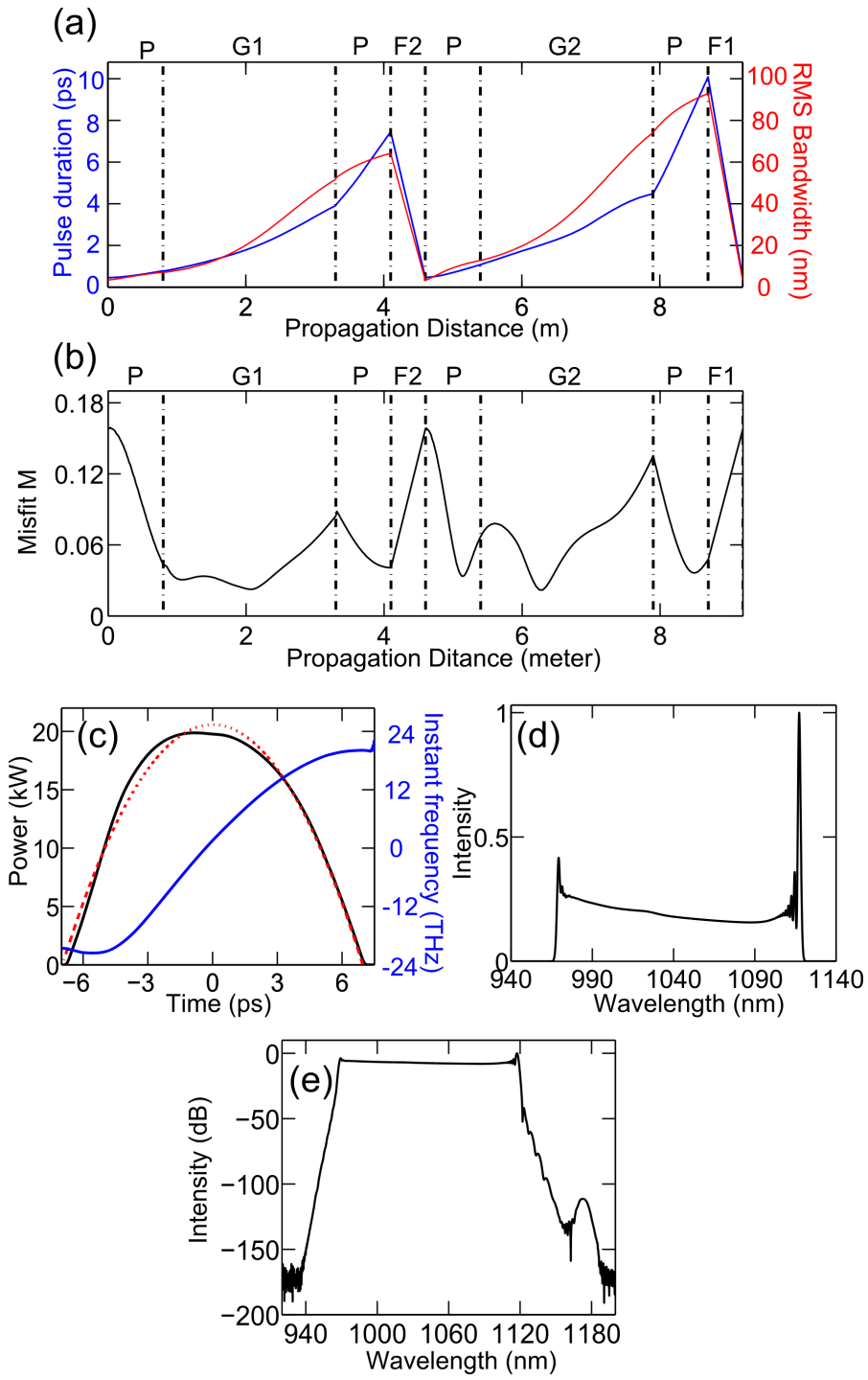

Figure 2.5: Numerical simulation results for 190 nJ pulses. (a) Evolution of pulse duration (blue) and RMS bandwidth (red), P: passive fiber; G: gain fiber; F: filter; (b) evolution of misfit parameter M, $M^2 = \int (I - I_{fit})^2 dt / \int I^2 dt$, which indicates the difference between the pulse shape (I) and its parabolic fitting profile I_{fit}; (c) temporal profile (black) with fitted parabolic curve (red) and instantaneous frequency across the chirped pulse (blue) and (d) (linear scale) and (e) (decibel scale) of the simulated spectrum.

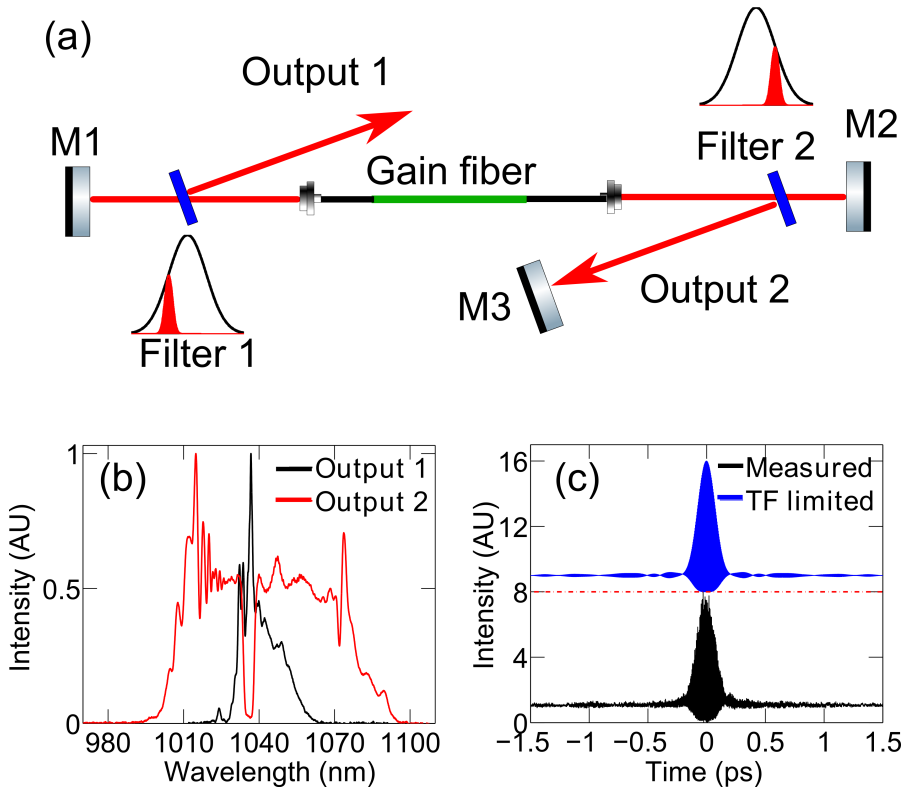

Figure 2.6: Linear Mamyshev oscillator used to study self-starting. (a) Schematic of the oscillator, (b) measured spectra of the outputs, and (c) transform limited and measured autocorrelation for output 1.

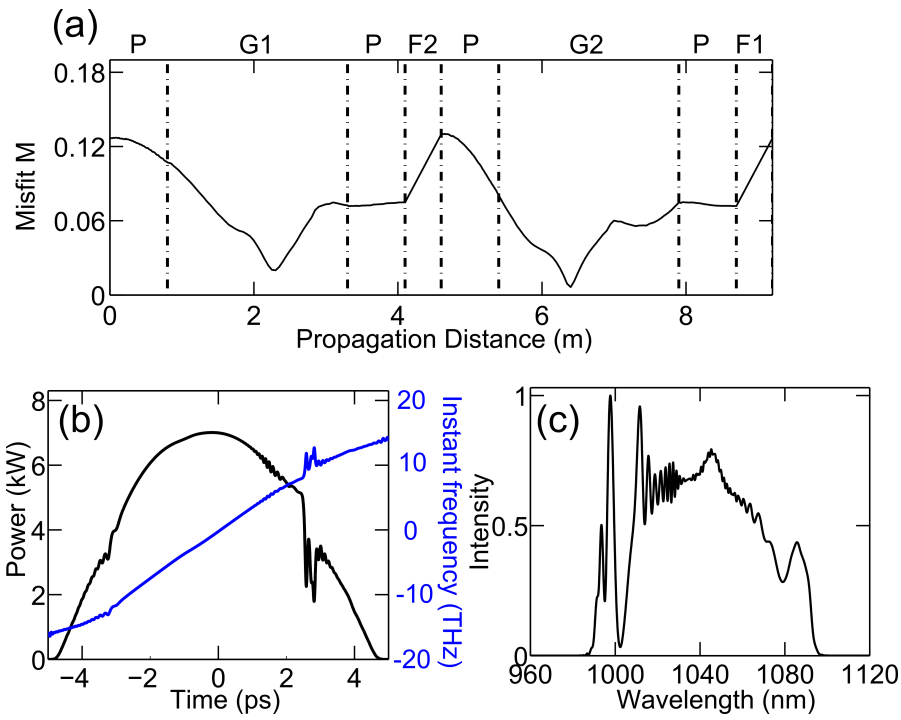

Figure 2.7: Simulated ring Mamyshev oscillator using super-Gaussian filters. The pulse energy is 42 nJ. (a) Evolution of misfit parameter M, (b) temporal profile (black) and instantaneous frequency across the chirped pulse (blue) and (c) the simulated spectrum.

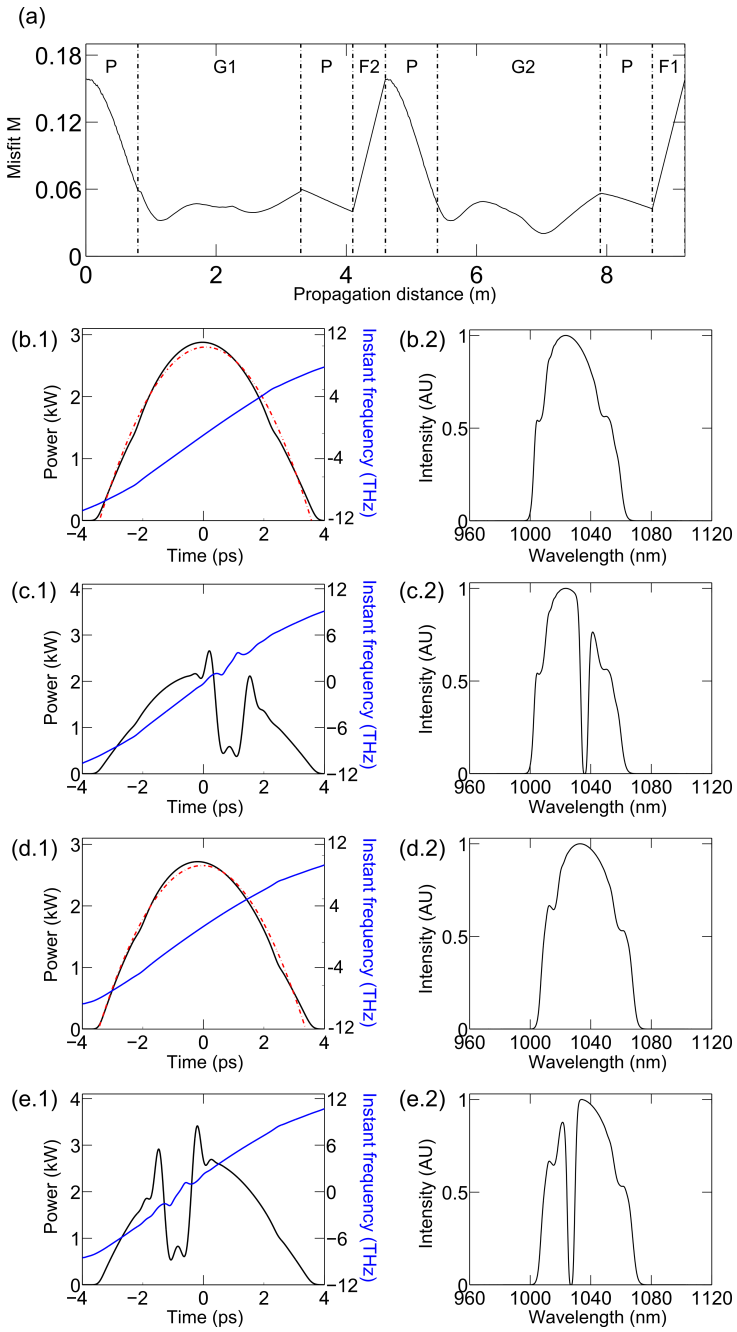

Figure 2.8: Simulated linear Mamyshev oscillator using Gaussian filters. (a) Evolution of misfit parameter, (b.1, b.2) temporal profile (black) with fitted parabolic curve (red) and instantaneous frequency across the chirped pulse (blue) and spectrum before output 1, (c.1, c.2) temporal profile (black) and instantaneous frequency across the chirped pulse (blue) and spectrum from filter 1, (d.1, d.2) temporal profile (black) with fitted parabolic curve (red) and instantaneous frequency across the chirped pulse (blue) and spectrum before output 2, (e.1, e.2) temporal profile (black) and instantaneous frequency across the chirped pulse (blue) and spectrum from filter 2.

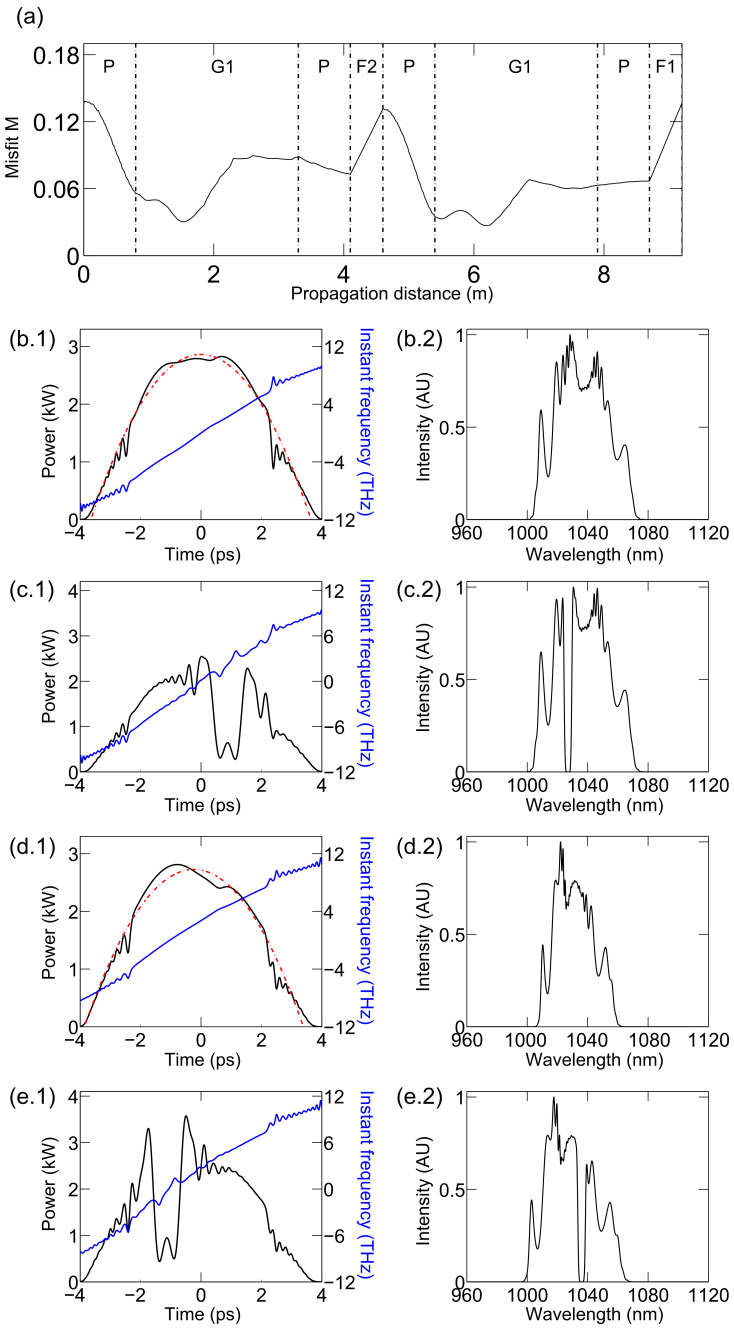

Figure 2.9: Simulated linear Mamyshev oscillator using super-Gaussian filters. (a) Evolution of misfit parameter, (b.1, b.2) temporal profile (black) with fitted parabolic curve (red) and instantaneous frequency across the chirped pulse (blue) and spectrum before output 1, (c.1, c.2) temporal profile (black) and instantaneous frequency across the chirped pulse (blue) and spectrum from filter 1, (d.1, d.2) temporal profile (black) with fitted parabolic curve (red) and instantaneous frequency across the chirped pulse (blue) and spectrum before output 2, (e.1, e.2) temporal profile (black) and instantaneous frequency across the chirped pulse (blue) and spectrum from filter 2.

BIBLIOGRAPHY

[1] Z. Liu, Z. M. Ziegler, L. G. Wright, and F. W. Wise, Optica **4**, 649 (2017).

[2] W. R. Zipfel, R. M. Williams, and W. W. Webb, Nature Biotechnology **21**, 1369 (2003).

[3] R. R. Gattass and E. Mazur, Nature Photonics **2**, 219 (2008).

[4] F. O. Ilday, J. R. Buckley, W. G. Clark, and F. W. Wise, Physical Review Letters **92**, 213902 (2004).

[5] A. Chong, J. Buckley, W. Renninger, and F. Wise, Opt. Express **14**, 10095 (2006).

[6] A. Chong, W. H. Renninger, and F. W. Wise, Optics Letters **32**, 2408 (2007).

[7] B. Nie, D. Pestov, F. W. Wise, and M. Dantus, Opt. Express **19**, 12074 (2011).

[8] A. Chong, L. G. Wright, and F. W. Wise, Reports on Progress in Physics **78**, 113901 (2015).

[9] L. F. Mollenauer and R. H. Stolen, Optics letters **9**, 13 (1984).

[10] K. Tamura, E. P. Ippen, H. a. Haus, and L. E. Nelson, Opt. Lett. **18**, 1080 (1993).

[11] A. Chong, W. H. Renninger, and F. W. Wise, Optics letters **33**, 1071 (2008).

[12] U. Keller, K. J. Weingarten, F. X. Kärtner, D. Kopf, B. Braun, I. D. Jung, R. Fluck, C. Hönninger, N. Matuschek, and J. Aus Der Au, IEEE J. Sel. Top. Quantum Electron. **2**, 435 (1996).

[13] C. Aguergaray, N. G. R. Broderick, M. Erkintalo, J. S. Y. Chen, and V. Kruglov, Optics Express **20**, 10545 (2012).

[14] C. Aguergaray, R. Hawker, A. F. J. Runge, M. Erkintalo, and N. G. R. Broderick, Applied Physics Letters **103**, (2013).

[15] J. Szczepanek, T. M. Kardaś, M. Michalska, C. Radzewicz, and Y. Stepanenko, Optics Letters **40**, 3500 (2015).

[16] U. Keller, T. H. Chiu, and J. F. Ferguson, Optics Letters **18**, 1077 (1993).

[17] M. Piche, Proc. SPIE **2041**, 358 (1994).

[18] S. Pitois, C. Finot, L. Provost, and D. J. Richardson, Journal of the Optical Society of America B **25**, 1537 (2008).

[19] K. Sun, M. Rochette, and L. R. Chen, Optics express **17**, 736 (2009).

[20] T. North and M. Rochette, Optics letters **39**, 174 (2014).

[21] P. V. Mamyshev, in Proceedings of 24th European Conference on Optical Communication, Madrid, Spain 475 (1998).

[22] L. A. Provost, C. Finot, P. Petropoulos, K. Mukasa, and D. J. Richardson, Optics Express **15**, 5100 (2007).

[23] K. Regelskis, J. Želudevičius, K. Viskontas, and G. Račiukaitis, Optics letters **40**, 5255 (2015).

[24] K. Regelskis and G. Račiukaitis, WO2016020188 A1 5255 .

[25] I. Samartsev, A. Bordenyuk, and V. Gapontsev, Proc. SPIE **10085**, 100850S (2017).

[26] W. H. Renninger, A. Chong, and F. W. Wise, Physical Review A - Atomic, Molecular, and Optical Physics **82**, 3 (2010).

[27] C. Finot, S. Pitois, and G. Millot, Opt. Lett. **30**, 1776 (2005).

[28] T. North and C.-S. Brès, APL Photonics **1**, 021302 (2016).

[29] A. M. Perego, N. Tarasov, D. V. Churkin, S. K. Turitsyn, and K. Staliunas, Physical Review Letters **116**, 1 (2016).

[30] N. Tarasov, A. M. Perego, D. V. Churkin, K. Staliunas, and S. K. Turitsyn, Nature Communications **7**, 12441 (2016).

[31] J. Želudevičius, Personal communication (2015).

[32] A. Fernandez, T. Fuji, A. Poppe, A. Fürbach, F. Krausz, and A. Apolonski, Optics Letters **29**, 1366 (2004).

[33] W. H. Renninger and F. W. Wise, IEEE Journal on Selected Topics in Quantum Electronics **21**, (2015).

[34] V. G. Bucklew, W. H. Renninger, P. S. Edwards, and Z. Liu, Opt. Express **25**, 13481 (2017).

[35] C. Finot, J.-M. Dudley, D. Richardson, and G. Millot, 2009 IEEE/LEOS Winter Topicals Meeting Series **45**, 1482 (2009).

[36] F. Leo, S. Coen, P. Kockaert, S.-P. Gorza, P. Emplit, and M. Haelterman, Nature Photonics **4**, 471 (2010).

[37] T. Herr, V. Brasch, J. D. Jost, C. Y. Wang, N. M. Kondratiev, M. L. Gorodetsky, and T. J. Kippenberg, Nature Photonics **8**, 145 (2014).

[38] Y. K. Chembo and C. R. Menyuk, Physical Review A - Atomic, Molecular, and Optical Physics **87**, 1 (2013).

[39] S. Coen and M. Erkintalo, **38**, 1790 (2013).

CHAPTER 3

ROGUE WAVES IN A NORMAL-DISPERSION FIBER LASER[1]

Experimental evidence of rogue wave formation in a normal-dispersion ytterbium fiber laser is reported. Spectral filtering is a primary component of pulse-shaping in normal-dispersion lasers, and we find that the choice of filter dramatically influences the distribution of noise-pulse energies produced by these lasers. With an interference filter in the cavity, non-Gaussian distributions with pulses as large as 6 times the significant wave height are observed. These correspond to pulse energies as high as $\sim$ 50 nJ. To our knowledge, the results presented are not accounted for by existing theoretical models of rogue-wave formation.

3.1 Introduction

High-amplitude waves that occur unexpectedly and rarely, known as rogue waves (RWs), were first reported in the study of water waves [2, 3]. Solli *et al.* observed extreme waves in supercontinuum generation, and referred to them as "optical rogue waves" [4]. Optics provides a convenient platform for the study of RWs, with its fast field evolution and ease of parameter control. These systems include linear light propagation in multimode fiber [5], optically-injected semiconductor lasers [6], supercontinuum generation [7], mode-locked Ti:sapphire lasers [8], and fiber lasers [9, 10, 11, 12], among others. Across this range of physical settings, non-Gaussian distributions of wave amplitudes have been observed. A variety of mechanisms have been proposed to account for RW formation. Perhaps the most-developed theoretical understanding is in the context of nonlinear and dispersive wave propagation. With a positive nonlinear index and anomalous dispersion,

[1]Much of the work presented in this chapter was published in Optics Letters [1].

modulation instability and soliton and breather formation are thought to underlie the formation of RWs [9, 13, 14].

Fiber lasers can be valuable for studies of nonlinear dynamics. Different operating regimes are identified by the net dispersion of the laser cavity. Pulses in lasers with anomalous dispersion can be described approximately but quite well as solitons of the conservative nonlinear Schrödinger equation. These pulses are allowed to have different speeds, amplitudes and phases, which make strong interactions between them possible. Soto-Crespo *et al.* numerically predicted and Lecaplain *et al.* experimentally observed RWs in this type of oscillator. Chaotic collisions of multiple pulses has been identified as the underlying mechanism in the formation of RWs in soliton lasers [9, 10]. In lasers with net normal dispersion, dissipative processes contribute significantly to pulse shaping; both amplitude and phase modulations balance to create stable pulses. The simplest forms of modulation instability, multisoliton collisions and breather excitations do not exist at normal dispersion. Thus, it is interesting and important to determine if RWs can exist in normal-dispersion lasers. Zaviyalov *et al.* observed RWs in numerical simulations of a normal dispersion oscillator [12]. These authors showed that gain saturation plays a crucial role in a nonlinear focusing process that produces the RWs. However, the gain saturation energy, as well as the saturable absorber parameters, in the simulation are difficult to realize experimentally. Broderick *et al.* found that the appearance of this type of RWs depends critically upon which numerical model is used [15]. Runge *et al.* observed parasitic Raman-shifted pulses in an all-normal dispersion laser operated to produce noise bursts. These Raman pulses, but not the primary noise-like pulses, exhibited long-tailed pulse energy statistics [11]. It is known that rogue statistics are observed in the unsaturated regime of stimulated Raman scattering [16]. To date, experimental studies of normal-dispersion lasers

have found no evidence of RWs in the primary pulse statistics [17, 18]. Thus, experimental results have been consistent with the picture of RWs arising from multiple-pulsing collisions in short-pulse lasers.

In this letter we report an investigation of pulse-energy distributions in an all-normal dispersion fiber laser that is designed to generate dissipative solitons (DSs) [19]. With certain choices of filters in the cavity, non-Gaussian distributions of noise bursts with a large fraction of extreme-energy pulses are observed. Measured single-shot spectra confirm that these extreme-energy pulses have high peak power. These RWs cannot be understood in terms of soliton formation, and in fact we are not aware of any detailed theoretical explanation for them. The results therefore challenge our understanding of RW formation in short-pulse propagation.

3.2 Experiments

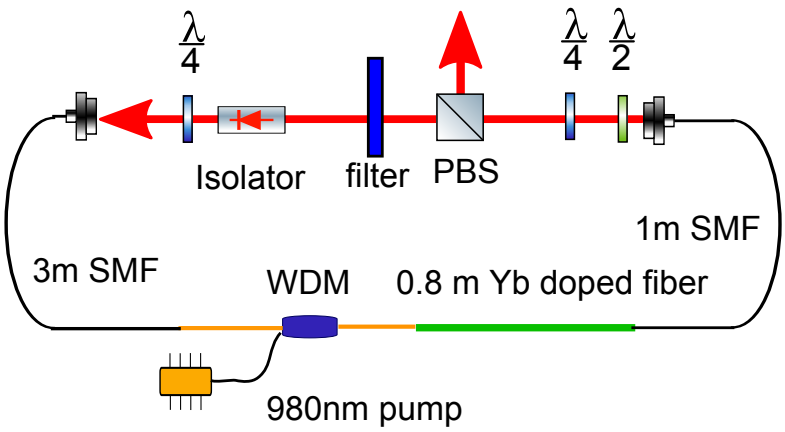

Figure 3.1: Schematic of the all normal dispersion fiber laser.

The laser used in our experiments is a unidirectional ring-cavity DS laser, as shown in Fig.3.1. The fiber section consists of 3 m of single-mode fiber (SMF) followed by 80 cm of Yb-doped gain fiber and another 1 m of SMF. After traversing

the fiber set, light propagates through a filter and bulk components that implement nonlinear polarization evolution (NPE) based saturable absorber, and then back into the fiber. The total dispersion is about 0.09 ps^2, and the repetition rate is 35 MHz. Results obtained with birefringent filters (BRFs) and interference filters (IFs) placed in the cavity alternatively will be described. The output is sent to a 45-GHz photodetector and recorded by a 25 GHz, 100 GSa/s oscilloscope, which provides $\sim$ 40 ps temporal resolution. For all of the results described below, the combination of the high-speed oscilloscope and long-range autocorrelator were used to confirm that only a single pulse circulates in the cavity. Typically, $\sim$ 3 million pulses are recorded to create a pulse-energy distribution. Single-shot spectra for consecutive roundtrips of the laser cavity are measured by the dispersive Fourier-transform technique. Pulses from the laser are stretched in 2.1 km of fiber with dispersion $\beta_2 = 20.1$ ps^2 km^{-1}. The spectral resolution is about 1 nm [20].

As a control experiment, we operated the laser in the DS regime, with a 13-nm BRF in the cavity. With 300 mW pump power, the laser generates stable pulses with 3-nJ energy and 170-fs dechirped duration. The pulse-energy distribution reflects small apparent fluctuations that are an artifact of aliasing in the oscilloscope sampling process (Fig. 3.2(a)). Single-shot spectra recorded over 1000 cavity traversals (Fig. 3.2(b)) are barely distinguishable and reflect the sharp peaks at the edges of the spectrum of DS lasers [19].

By tuning the waveplates and the orientation of the BRF, the laser can be made to generate noise bursts [21]. When pumped with $\sim$ 750 mW, the output power is $\sim$ 180 mW, for an average pulse energy of $\sim$ 5 nJ. The optical spectrum again exhibits the characteristic "cat-ear" peaks of a dissipative soliton but is somewhat smoother and less-structured (Fig. 3.3(a)) than a mode-locked spec-

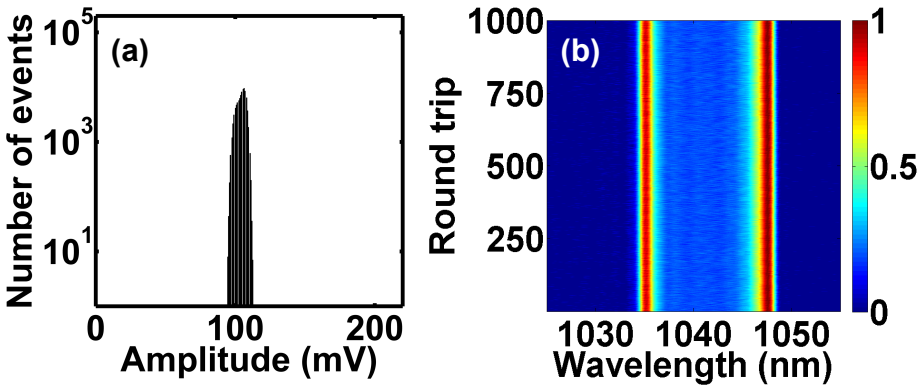

Figure 3.2: DS regime with 13-nm BRF: (a) pulse-energy histogram (log scale). (b) 1000 consecutive single shot spectra.

trum. The pulse autocorrelation (not shown) exhibits a narrow coherence spike on a background of duration $\sim$ 30 ps, with a contrast ratio of 2:1, which is expected theoretically for a Gaussian random field [22]. The energy and spectrum fluctuate significantly, but nonetheless the pulse energy statistics (Fig. 3.3(b)) remain Gaussian. The consecutive spectra (Fig. 3.3(c)) indicate the fluctuations from burst to burst.

BRFs with bandwidths of 8, 10, 12, and 13 nm yield numerous mode-locked and noise-burst states, but the pulse-energy distribution is always Gaussian. However, replacement of the BRF with an IF with similar parameters causes dramatic changes in the pulse-energy distribution, despite what appear to be minor differences between the filter characteristics in their main pass-band (Fig. 3.4). (Another difference is that the interference filter only has one pass-band while the transmittance of the BRF is periodic, with a free spectral range of 15 to 23 nm depending on the transmission bandwidth.) Large fluctuations in the noise-pulse energy are readily apparent on the pulse train, and these can be used as real-time feedback to enhance the frequency of the high-energy events by adjustments of the waveplates and filter. In contrast to the RWs observed in anomalous-dispersion

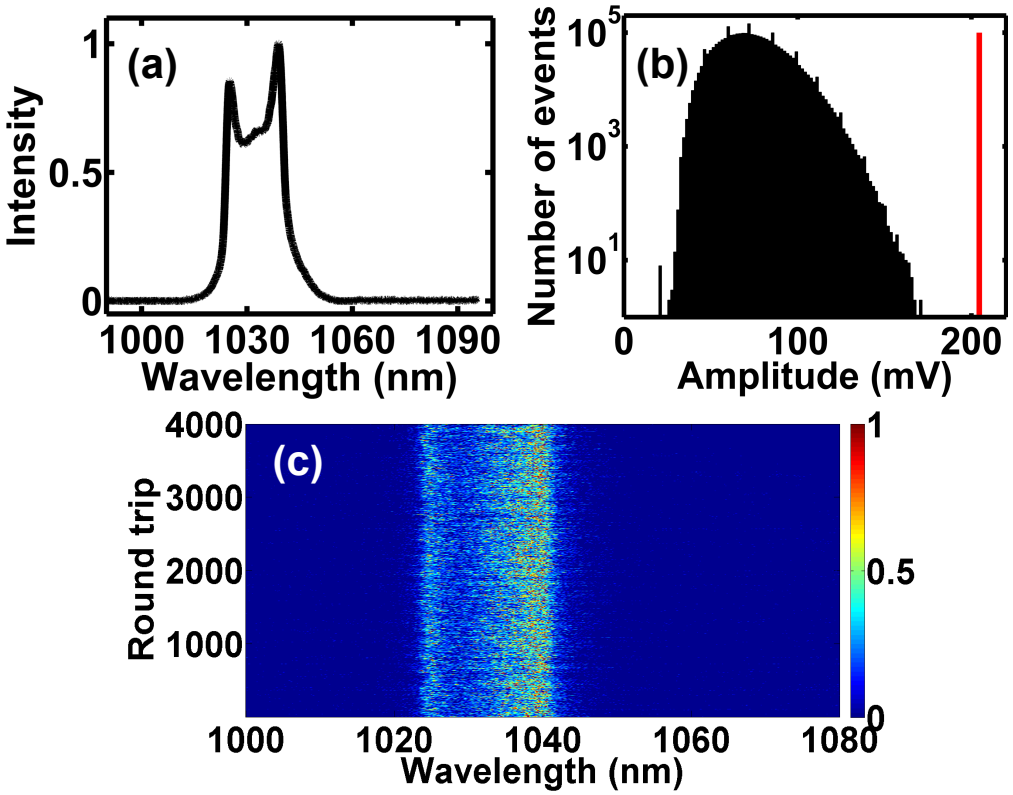

Figure 3.3: Noise bursts observed with a 13-nm BRF in the laser: (a) Output spectrum. (b) Pulse-energy histogram (log scale); vertical red bar is the RW threshold (2.2 times the significant wave height). (c) 4000 consecutive single-shot spectra.

cavities, which correspond to energy redistribution between multiple picosecond pulses within the nanosecond-duration bursts [10], here we observe fluctuations in the total burst energy from roundtrip to roundtrip. With a 10-nm IF, a long-tailed pulse-energy distribution (Fig. 3.5(b)) is readily observed. About 0.1% of the pulses exceed a standard definition of the RW threshold (2.2 times the significant-wave height), and the pulse energy reaches 6 to 7 times the significant-wave height. The fraction of rogue events in the distribution is somewhat higher than that in experiments at anomalous dispersion [10]. The distribution is also remarkable in terms of the actual pulse energies. The average noise-pulse energy is 5.3 nJ, and the most extreme pulses reach more than 50 nJ.

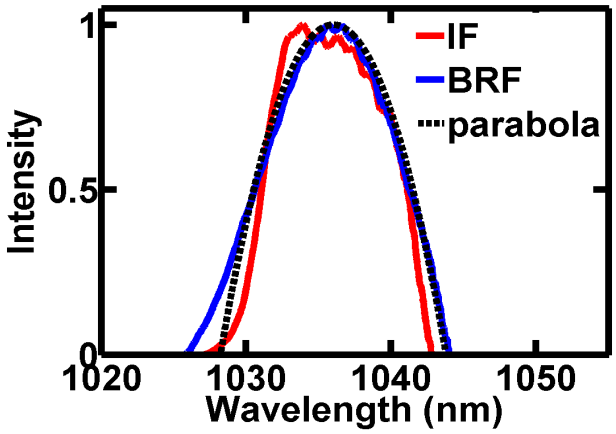

Figure 3.4: Comparison of two filter shapes. The dashed line is the fitted parabolic shape.

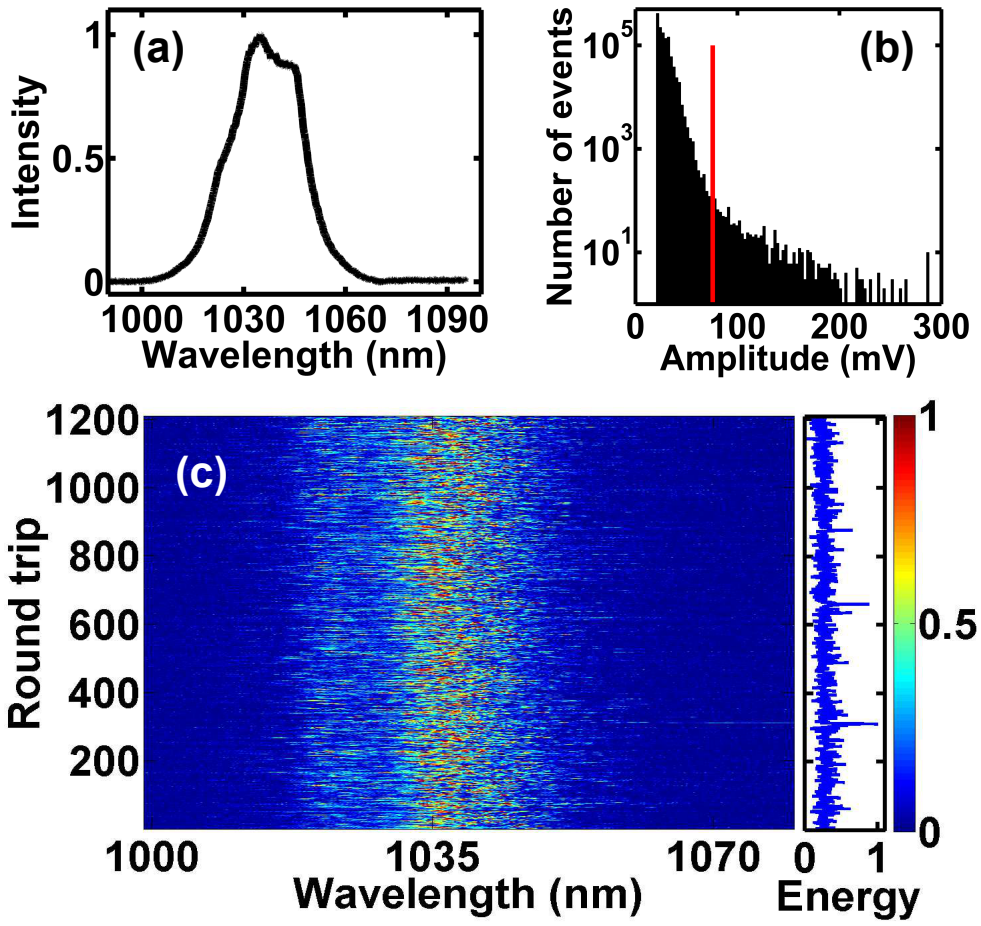

Figure 3.5: RWs observed with 10 nm IF: (a) Output spectrum. (b) Pulse-energy histogram (log scale); vertical red bar is the RW threshold. (c) 1200 consecutive single-shot spectra.

The spectrum (Fig. 3.5(c)) exhibits much larger fluctuations than the spectra of ordinary noise bursts. By integrating each single-shot spectrum (the dispersive temporal data), we can also capture the total energy of each shot (Parseval's theorem). The corresponding normalized integrated energy is plotted in the right panel of Fig. 3.5(c). For example, extreme events are observed at round trips number 311 and 661. The single-shot spectra reveal some properties of the extreme events. Fig. 3.6 is an expanded view of the spectra near the events shown in Fig. 3.5(c). We find that the highest-energy pulses are always accompanied by Raman peaks in the spectral domain (Fig. 3.6(a)). For pulses closer to the RW threshold, however, the spectra are broadened with no observable Raman peaks (Fig. 3.6(b)). The appearance of the Raman peak is consistent with a rough estimate of the minimum peak power in the burst (10 kW). [23]

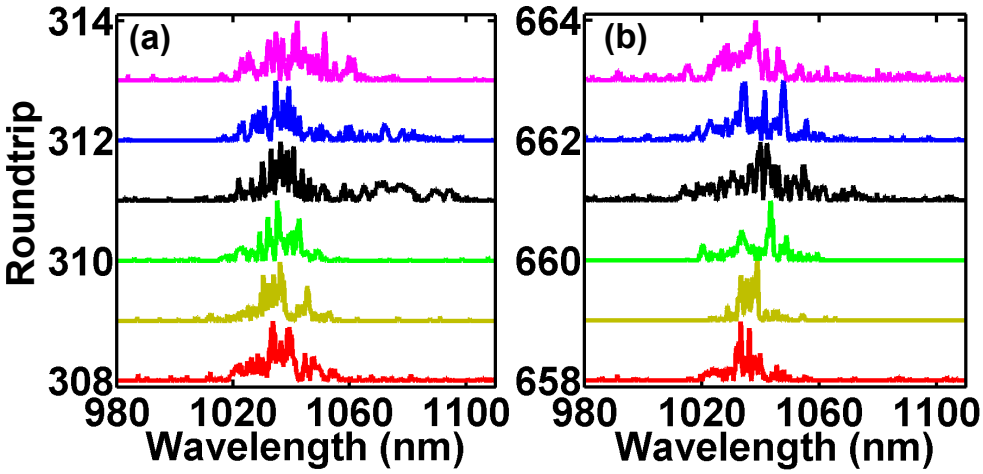

Figure 3.6: Spectra around the extreme events: (a) event at roundtrip 311, (b) event at roundtrip 661.

The autocorrelation trace for the conditions that generate RWs (Fig. 3.7) exhibits differences from the noise bursts obtained with the BRF in the cavity. The reduced contrast ratio is an indication of the non-Gaussian nature of the fluctuations. The narrow central coherent peak sitting on a 7-ps pedestal indicates

that the RW pulses are $\sim$ 5-ps wave packets with irregular femtosecond structure, which is $\sim$ 4 times shorter than the regular noise bursts (20 ps). The autocorrelator with 100 ps delay range in combination with the fast detector confirm single-burst operation in this regime.

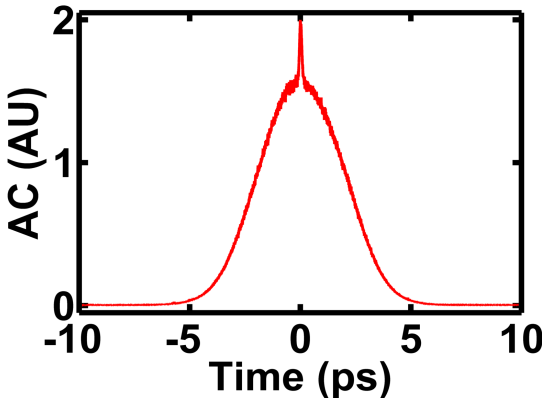

Figure 3.7: Autocorrelation trace of RW state.

With an IF in the cavity, pulse-energy distributions with substantial occurrences of RWs are observed for filter bandwidths of 9 and 10 nm, center wavelengths between 1025 and 1035 nm, and pump power between 500 and 750 mW. For pump powers below 500 mW, mode-locked pulses and noise bursts can be generated with the IF, but no RWs are observed. Distributions observed with the 9-nm filter and two different pump powers are shown as examples in Fig. 3.8. The peak transmittance of the IFs is much lower than that of BRFs. To address whether the loss plays a major role in the generation of RWs, we replaced the IF with a combination of BRF and neutral-density filter with the same loss. No RWs are observed in that case, which implies that the shape of the filter passband is the critical issue, not the overall transmittance.

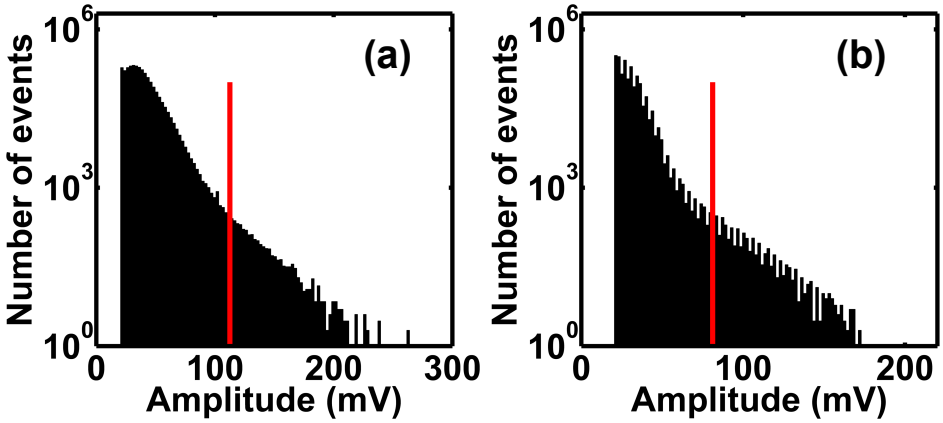

Figure 3.8: RWs state pulse-energy histogram (log scale) with 9-nm IF for pump powers (a) 600 mW, (b) 750 mW. The vertical red bars are RW thresholds.
.

3.3 Discussion

We attempted to model the experiments described above through simulations. Zaviyalov *et al.* found that a temporal focusing process starting from a random field can produce extreme peak powers in a normal-dispersion laser operated at very low pulse energy [12]. These numerical results suggest a possible mechanism for RW formation, but it is not clear that it is pertinent to the experiments described here. We observe stable DS solutions and noise bursts in simulations with parameters close to the experimental values, but we do not observe any RWs. This is true for both a single-field model and a model that solves coupled generalized nonlinear Schrödinger equations to account for two polarizations and NPE. The simulations include stimulated Raman scattering. Of course, we cannot reach a conclusion based on failing to observe the RWs numerically. Work in this direction will continue. A practical challenge is the desire to monitor many thousands of cavity round trips for each of numerous wave-plate settings in the simulation.

In a DS oscillator, pulse formation is based on nonlinear gain and loss, disper-

sion, and nonlinear phase accumulation. When these effects are balanced precisely, the pulse parameters are rigidly determined by the cubic-quintic Ginzburg-Landau equation (CQGLE) [19]. DS of the CQGLE have identical velocities and should not interact. When the balance constraints are loosened, for example, by tuning the waveplates to adjust the net gain, noise bursts (without the extreme events) occur and we view these pulses as having greater freedom in their dynamics. The best mode-locked performance is obtained with a BRF filter in a DS laser. The sinusoidal characteristic of a BRF is a good approximation to the parabolic filter assumed in the CQGLE (Fig. 3.4). With an IF in the cavity instead, the experiment does not approximate the CQGLE as well, and we conjecture that fluctuating pulses may be more common in the resulting system.

3.4 Conclusion

To conclude, we have observed rogue statistics in the noise bursts from a dissipative-soliton laser. With a filter that is not optimal for mode-locking, we observe a large fraction of extremely-high energy pulses: the amplitude can be 6 times the significant wave height, and in actual terms the energy can be 50 nJ. The results challenge the current understanding of RW formation in dispersive pulse propagation. We hope that the experimental results presented here motivate further theoretical study.

Portions of this work were supported by the Office of Naval Research under grant N00014-13-1-0649 and National Natural Science Foundation of China under grant No. 11374089. The authors thank Logan Wright for valuable discussions.

BIBLIOGRAPHY

[1] Z. Liu, S. Zhang, and F. W. Wise, Optics Letters **40**, 1366 (2015).

[2] C. Kharif and E. Pelinovsky, European Journal of Mechanics, B/Fluids **22**, 603 (2003).

[3] a. Chabchoub, N. P. Hoffmann, and N. Akhmediev, Physical Review Letters **106**, 204502 (2011).

[4] D. R. Solli, C. Ropers, P. Koonath, and B. Jalali, Nature **450**, 1054 (2007).

[5] F. T. Arecchi, U. Bortolozzo, a. Montina, and S. Residori, Physical Review Letters **106**, 153901 (2011).

[6] C. Bonatto, M. Feyereisen, S. Barland, M. Giudici, C. Masoller, J. R. R. Leite, and J. R. Tredicce, Physical Review Letters **107**, 1 (2011).

[7] D. R. Solli, C. Ropers, and B. Jalali, Physical Review Letters **101**, 233902 (2008).

[8] M. G. Kovalsky, A. a. Hnilo, and J. R. Tredicce, Optics letters **36**, 4449 (2011).

[9] J. M. Soto-Crespo, P. Grelu, and N. Akhmediev, Physical Review E - Statistical, Nonlinear, and Soft Matter Physics **84**, 1 (2011).

[10] C. Lecaplain, P. Grelu, J. M. Soto-Crespo, and N. Akhmediev, Physical Review Letters **108**, 233901 (2012).

[11] A. F. J. Runge, C. Aguergaray, N. G. R. Broderick, and M. Erkintalo, Optics letters **39**, 319 (2014).

[12] A. Zaviyalov, O. Egorov, R. Iliew, and F. Lederer, Physical Review A **85**, 013828 (2012).

[13] J. M. Dudley, G. Genty, F. Dias, B. Kibler, and N. Akhmediev, Opt. Express **17**, 21497 (2009).

[14] B. Kibler, J. Fatome, C. Finot, G. Millot, F. Dias, G. Genty, N. Akhmediev, and J. M. Dudley, Nature Physics **6**, 790 (2010).

[15] N. Broderick, M. Erkintalo, and G. Donovan, in *Advanced Photonics* (Optical Society of America, ADDRESS, 2014), p. NTH1A.6.

[16] A. Aalto, G. Genty, and J. Toivonen, Opt. Express **18**, 1234 (2010).

[17] C. Lecaplain, P. Grelu, J. M. Soto-Crespo, and N. Akhmediev, Journal of Optics **15**, 064005 (2013).

[18] C. Lecaplain and P. Grelu, Physical Review A - Atomic, Molecular, and Optical Physics **90**, 1 (2014).

[19] W. H. Renninger, A. Chong, and F. W. Wise, Physical Review A - Atomic, Molecular, and Optical Physics **77**, 1 (2008).

[20] Y. C. Tong, L. Y. Chan, and H. K. Tsang, Electronics Letters **33**, 983 (1997).

[21] M. Horowitz, Y. Barad, and Y. Silberberg, Optics Letters **22**, 799 (1997).

[22] A. Weiner, *Ultrafast Optics*, *Wiley Series in Pure and Applied Optics* (Wiley, ADDRESS, 2011).

[23] R. Stolen and A. Johnson, IEEE Journal of Quantum Electronics **22**, 2154 (1986).

CHAPTER 4

KERR SELF-CLEANING OF FEMTOSECOND-PULSED BEAMS IN GRADED-INDEX MULTIMODE FIBER[1]

We observe a nonlinear spatial self-cleaning process for femtosecond pulses in graded-index (GRIN) multimode fiber (MMF). Pulses with $\sim$ 80 femtosecond duration at 1030 nm are launched into GRIN MMF with 62.5 μm core. The near-field beam profile at the output end of the fiber evolves from a speckled pattern to a centered, bell-shaped transverse structure with increasing pulse energy. The experimental observations agree well with numerical simulations, which show that the Kerr nonlinearity underlies the process. This self-cleaning process may find applications in ultrafast pulse generation and beam-combining.

4.1 Introduction

Single-mode optical fibers (SMFs) provide a convenient environment for studies of a wide range of nonlinear phenomena [2], and are the basis of technologies such as optical communication systems [3] and mode-locked lasers [4, 5, 6]. Accordingly, propagation of light in SMFs has been studied extensively. The capabilities of communication systems [7] and short-pulse lasers [8] are reaching what appear to be fundamental limits, so researchers have begun to consider the use of MMF in these and other applications. MMFs offer larger mode areas, which reduces nonlinear effects directly, along with new degrees of freedom for controlling optical fields. As examples, principle-mode analysis, [9, 10], imaging through MMFs [11, 12], and space-division multiplexing [13] currently generate substantial research activity.

[1]Much of the work presented in this chapter was published in Optics Letters [1].

Although nonlinear effects in SMFs [2] and linear propagation in MMFs [9, 10, 11, 12, 13] have been intensely investigated, it is only recently that nonlinear propagation in MMFs has attracted major interest [14, 15, 16, 17, 18]. In the nonlinear regime, intermodal cross-phase modulation, four-wave mixing, and stimulated Raman scattering can all play important roles, leading to complex dynamics. MMFs allow studies of fundamental nonlinear phenomena such as multimode soliton formation [17, 19], multimode dispersive waves [20], spatiotemporal instabilities [21], and classical wave condensation [22], and may yield future improvements to high-power fiber devices.

So-called beam cleanup effects in MMFs have been studied in the past two decades. Stimulated Brillouin scattering (SBS) [23] and stimulated Raman scattering (SRS) [24, 25] have been recognized as the mechanisms that underlie beam-cleanup effects in their respective optical parameter regimes. In particular, Terry *et al.* analyzed the overlap of different transverse modes with the pump to provide an explanation of Raman beam cleanup in GRIN fibers [25].

Additionally, beam-cleanup effects that do not arise from Raman or Brillouin processes have been reported very recently. Krupa *et al.* studied propagation of picosecond and nanosecond pulses in normal-dispersion GRIN fiber and observed clear beam cleanup with increasing power, which they attributed to the combination of index guiding and the nonlinear Kerr effect [26]. Here, we present observations of a similar beam cleanup in experiments performed with femtosecond-duration pulses in the normal-dispersion regime. Short pulses with high peak power (500-600 kW at the input) propagating in GRIN MMF self-organize spatially from speckled patterns to a centered and bell-shaped beam profile as a result of intermodal interactions mediated by the Kerr nonlinearity. The use of short

pulses with peak powers that are high but still well below the critical power for self-focusing, along with short fibers, enables suppression of SBS and SRS beam-cleanup effects. Near-field beam profiles and spatially- and spectrally-resolved imaging [27] measurements are employed to characterize this phenomenon. The results of coupled-mode theory simulations are consistent with experiments, and show a transfer of energy from higher-order modes (HOMs) to the fundamental mode through the electronic Kerr nonlinearity. The results presented here complement and extend those reported by Krupa *et al.* Although a complete explanation is still needed, our experiments and modeling of the femtosecond-pulse regime support indications that the effect is primarily spatial, driven by the Kerr nonlinearity, and that SRS and random mode-coupling are of negligible importance. Moreover, observation of nonlinear self-cleaning in another distinct parameter regime supports a now-significant body of work suggesting that nonlinear attraction towards low-order modes is a universal feature of propagation in GRIN MMFs [25, 17, 16, 26, 28, 29]. Finally, beam-cleaning presents exciting opportunities for practical ultrashort-pulse fiber sources, which will be discussed.

4.2 Experimental results

In experiments, we launched 60-80 fs pulses (corresponding to a dispersion length of $L_{DS} \sim 7$ cm) at 1030 nm into 20 cm of GRIN fiber with 0.275 NA and 62.5 μm core diameter (the fiber supports $\sim$ 300 modes at 1030 nm). The calculated variation in group delay across the modes used in our experiment and simulation is less than $\sim$ 20 fs for this fiber. A lens, polarizing beamsplitter, wave plates, and three-axis translation stage are used to adjust the initial energy, modal excitation content, and polarization. Multiple modes are excited by the use of an imperfect input

beam that is not matched to the fundamental mode, tilting the input wavefront, and mode coupling caused by stress from a clamp that holds the fiber in place. The fiber is laid straight and without any other stress, to mitigate inter-mode coupling and losses through higher-order modes (HOMs) after the field is launched. The near-field profile and the beam quality are measured at the output.

At low pulse energy (0.44 nJ), a speckled near-field profile is observed (Fig. 4.1 (a)), and the output beam exhibits different interference patterns at different locations (Fig. 4.2 (a)). The beam quality parameter $M^2 \approx 2.3$ provides an estimate of the multimode content (We estimate that the fundamental mode content is typically $\sim 30\%$). As the energy increases to a maximum of 47 nJ (corresponding to an averaged nonlinear length $L_{NL} \sim 8$ mm), energy flows toward the center of the waveguide and forms a centered, bell-shaped beam profile (Fig. 4.1 (b)-(f)). M^2 decreases to ~ 1.8 (Fig. 4.2 (b)), and we estimate the fundamental mode content is about 70 %.

The beam cleanup originates from the increase of fundamental mode content, and is not a result of a particular interference pattern at the fiber output. We observe similar cleanup effects with a variety of different modal excitations and polarizations. However, cleanup does not occur for arbitrary initial modal excitations, even at the highest pulse energy we launched; it only happens when the majority of energy is distributed in the lower-order modes, *i.e.*, near the center of the waveguide. In addition, we measured the beam profile at each wavelength, which provides some insight into the cleanup behavior. For low-energy pulses, the energy is distributed over a large area for different wavelengths (see Visualization 1). When the energy is higher, cleanup is observed more or less for all wavelengths (see Visualization 2). Thus, this beam cleanup is not just the result of averaging

speckle patterns over a broadband spectrum, and the beam is self-cleaned over most of its spectrum.

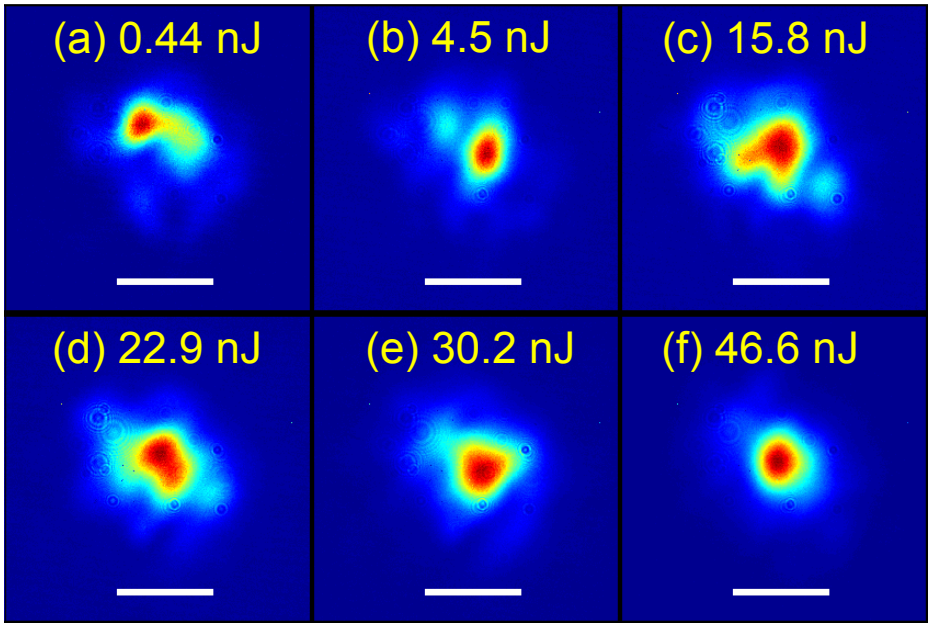

Figure 4.1: Near-field beam profiles for different input pulse energies (Intensity in linear scale. Scale bar: fundamental mode diameter of GRIN-625 MMF (13 μm)). Near-field beam profile for each wavelength in linear and nonlinear regimes using 100 cm fiber are shown in Visualization 1 and 2.

The spectra for different input energies are shown in Fig. 4.3 (a). There is an approximately symmetric spectral broadening from self-phase modulation when the pulse energy is below 25 nJ. At the highest energy, a slight asymmetry due to SRS is present. However, cleanup is observable before this asymmetry appears (Fig. 4.1 (c) and (d)). Furthermore, we do not observe strong, discrete SRS peaks, which would indicate Raman-induced beam cleanup [30]. This is because dispersion broadens the pulses quickly and most of the nonlinear phase is accumulated within a short fiber length ($\sim$ 20 cm). The strong linear dispersion and 20 cm total propagation length ensure that the threshold for SRS is not reached.

Pulse autocorrelations were measured with the whole output beam focused on the detector [17]. The output pulse widths for different energies (Fig. 4.3 (b))

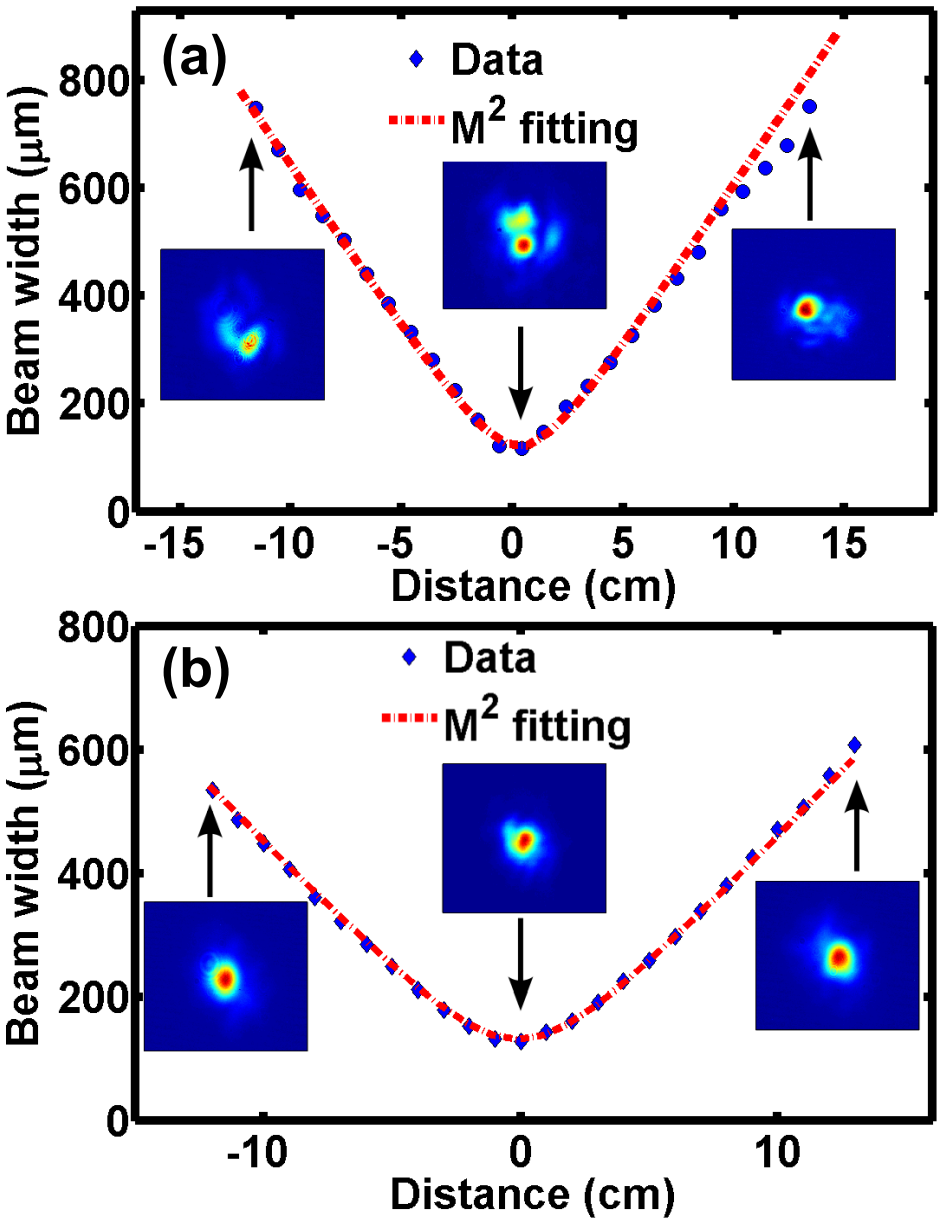

Figure 4.2: Beam quality measurements for 0.44 nJ (a) and 46.6 nJ (b). The inferred values of M^2 are 2.3 and 1.8 respectively.

agree well with the pulse broadening due to nonlinearity and chromatic dispersion. The 8 : 1 contrast ratio shows that the output field is temporally coherent. This is further supported by the fact that the output pulses can be dechirped to equal or below the input pulse duration, to as short as 34 fs when the input pulse energy is 47 nJ. (Fig. 4.3 (c)).

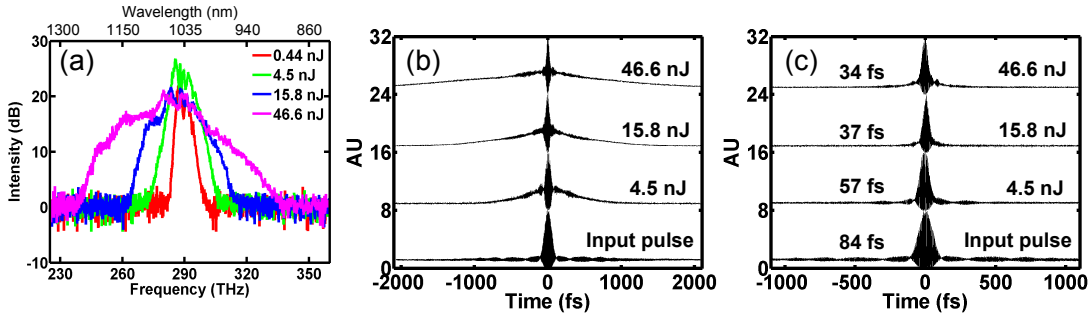

Figure 4.3: Spectral and temporal measurements of the output field. (a) Spectra corresponding to beam profiles in Fig. 4.1. The input pulse spectrum is almost the same as the 0.44 nJ curve. (b) Autocorrelation of the input pulse and output pulse from the fiber for different input pulse energies. (c) Autocorrelation of the input pulse and dechirped output pulse from the fiber.

4.3 Numerical simulation

To model the beam cleanup, we employ the generalized multimode nonlinear Schrödinger equation (GMM-NLSE) [14]. The eigenmodes of the MMF are coupled *via* the cubic nonlinearity. The nonlinear Kerr coefficient used in all the simulations is $n_2 = 2.3 \times 10^{-20} m^2/W$. SRS is turned off at first by setting $f_R = 0$.

For simplicity and to ensure reasonable computational time, we considered only the first 10 modes of the fiber. This is a reasonable approximation to the experiments, in which lower-order modes were excited. For the excitation we assume equal energy in the lowest 5 modes, and only noise in the next 5 modes. A limited number of simulations with 30 modes produce similar results. In numerical

simulations we launched 60-fs, Gaussian pulses into 100 cm of fiber with the experimental parameters. The simulated transverse spatial profiles at 20 cm are given in Fig. 4.4. The multi-lobed shape of the input beam (Fig. 4.4 (a)) is caused by interference among the first 5 modes. In linear propagation, different spatial modes pick up different phases. The beam profiles along the propagation direction are speckled and vary substantially because of this (Fig. 4.4 (b)). When the input pulse energy is increased to 38 nJ, as shown above, a considerable amount of energy transfers to the fundamental mode in 20 cm (Fig. 4.4 (c)). After that, the beam profile breathes with propagation but retains a bell-shaped structure without appreciable speckles. In addition, speckled patterns are observed during the linear propagation while centered and bell-shaped profiles form in nonlinear propagation for each wavelength. These results agree reasonably with the experiments using 20 cm and 100 cm fibers.

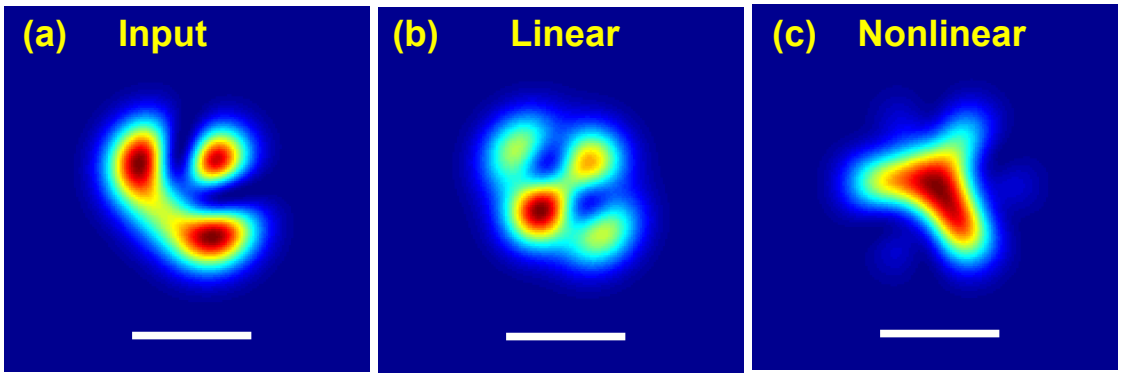

Figure 4.4: Numerical results for spatial evolution. (a) Input beam; (b) 0.38 nJ after 20 cm (see also Visualization 3); (c) 38 nJ after 20 cm (see also Visualization 4).

During nonlinear propagation, energy transfers from the launched modes into the fundamental mode in less than 10 cm, and a steady state is reached after $\sim$ 20 cm, with more than 40% of the energy in the fundamental mode (Fig. 4.5 (a)). Moreover, the remaining energy is distributed roughly equally among the HOMs. These resemble important features predicted for classical wave condensation [22].

The overall energy transfer process is shown in Visualization 5.

The variation of fundamental mode content with input energy is shown in Fig. 4.5 (b). We observe that there is strong energy transfer from HOMs to the fundamental mode (LP_{01}) as the input pulse energy increases (red curve in Fig. 4.5 (b)). In the linear propagation regime (pulse energy less than 1 nJ), there is almost no nonlinear coupling and the energy in each mode maintains the launched value. Therefore, the LP_{01} mode content remains at 20%. As the pulse energy increases, more energy transfers from HOMs to the fundamental mode. About 45% of the total energy is concentrated in the LP_{01} mode when the launched energy reaches 40 nJ . This is consistent with the observations in Fig. 4.1. Surprisingly, when SRS is included in the simulation (black dashed curve in Fig. 4.5 (b)), the fundamental mode content at each energy level is less than the result without SRS. This is because SRS reduces Kerr nonlinear effects in the fiber. However, it is not strong enough to cause significant SRS-induced beam cleanup.

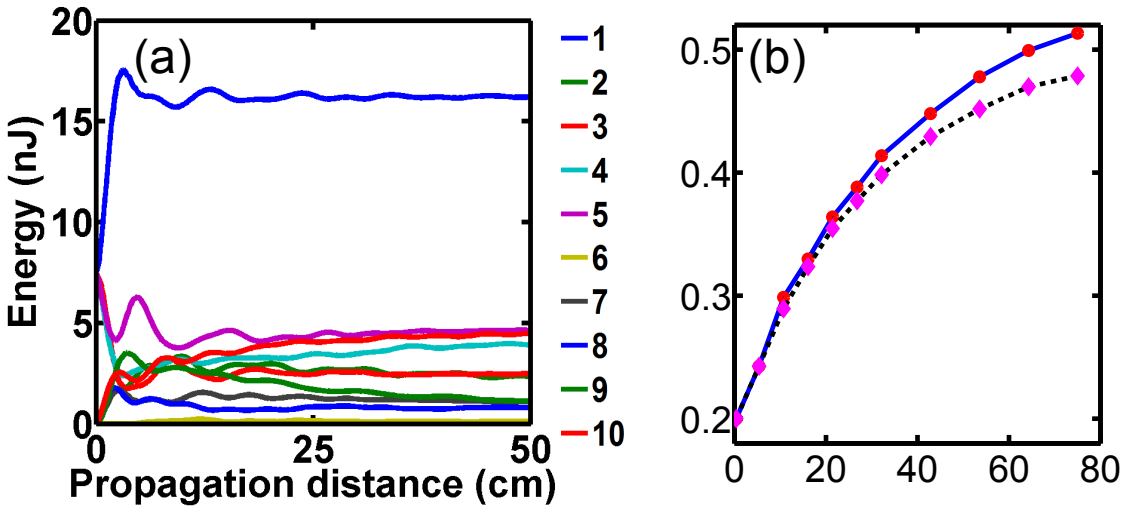

Figure 4.5: Numerical results for modal energy evolution. (a) Evolution of the modal energy distribution along the propagation distance for 60 fs, 38 nJ pulses (see also Visualization 5). (b) Fundamental mode content at the output end of the fiber with SRS (black dots) and without SRS (red dots) for varying input energy. The lines connect the points.

Of particular interest is whether temporal effects exert strong influence on the cleanup behavior. We simulated the propagation for several input pulse durations between 50 and 400 fs. In order to keep the accumulated nonlinear phase approximately constant, we adjusted the pulse energy to maintain constant peak power at the input of the fiber. The fundamental mode content exhibits qualitatively the same evolution along the propagation direction for all pulse durations in this range (Fig. 4.6 (a)). In all of these examples, fundamental mode energies increase by a factor of 2 and reach a steady state after propagating $\sim$ 20 cm. This indicates that the cleanup is caused primarily by spatial nonlinear effects.

We repeated the simulations with SRS included, by setting $f_R = 0.18$ in the GMM-NLSE model. The LP_{01} mode content for different pulse durations are shown in Fig. 4.6 (b). Comparing each curve in Fig. 4.6 (b) to its corresponding curve in Fig. 4.6 (a), we can only observe small differences. These results further indicate that the Kerr effect, rather than SRS, is the origin of the beam cleanup.

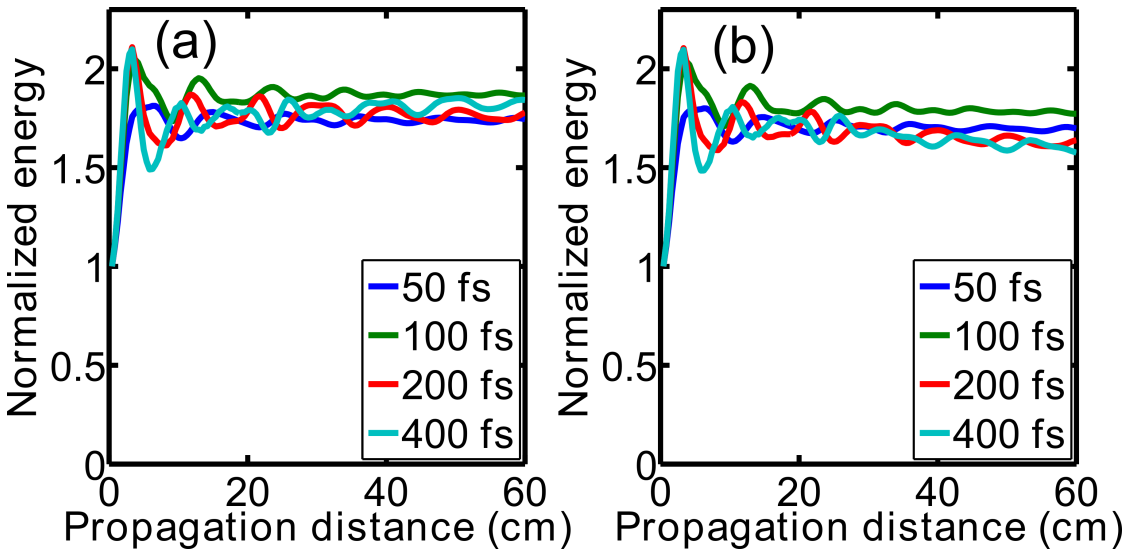

Figure 4.6: LP_{01} mode energy evolution along the propagation direction for different pulse durations. The energy is normalized to the initial energy in the LP_{01} mode. (a) Evolution without SRS and (b) evolution with SRS.

Ongoing simulations suggest that the origin of the self-cleaning is the nonlinear instability of higher-order modes in GRIN fiber. In the presence of strong nonlinearity, different modes exchange energy through four-wave mixing, and all modes are unstable except for the fundamental mode [28]. Because of this, on average, high-order modes transfer energy to the fundamental mode irreversibly. Although this hypothesis is so far supported by simulations, further work is required for a detailed physical understanding of the process, including the connection between this cleanup and classical wave condensation.

4.4 Discussion

We now briefly summarize the relation of the work presented here to that of Krupa *et al.* [26]. The experimental studies were performed in different parameter regimes: we employed femtosecond pulses and short fibers (20 cm) with weak linear coupling, while Krupa *et al.* used longer pulses (30 picoseconds and 1 nanosecond) and longer fibers ($\sim$ 10 meters) with stronger linear coupling. The net nonlinear phase accumulation for beam cleanup in our experiments ($\sim \pi$) is comparable to that in Ref. [26] ($\sim 2\pi$). As a minor point, we use different numerical methods: we employed the GMM-NLSE while Krupa *et al.* used a full-field model. Nevertheless, we reach similar conclusions regarding the origin of the effect in the Kerr nonlinearity.

Finally, although potential applications of this effect are implied by earlier work, this potential is most significant for broadband and/or ultrashort pulses. Therefore, our demonstration of Kerr beam cleanup with femtosecond, high-power pulses is a critical step for these applications. Since the larger energy capacity of

multimode fibers may allow higher-power femtosecond lasers, it is interesting that self-cleaning may provide a multimode-fiber-compatible saturable absorber [31], similar to the Kerr lens in solid-state systems. Self-cleaning in GRIN waveguides may also facilitate or inspire approaches to passive beam combining. Finally, maintaining spatial beam quality when performing multiphoton imaging through MMFs is a critical concern. Therefore, the demonstration of ultrashort-pulsed self-cleaning may lead to new approaches for endoscopic nonlinear imaging.

4.5 Conclusion

To conclude, we experimentally and numerically demonstrate self-induced, Raman-free cleanup of femtosecond-pulsed beams in GRIN MMF. Nonlinear coupling of modes causes the field to evolve from a specked beam to a bell-shaped one dominated by the fundamental mode. This work contributes to understanding of fundamental topics such as spatiotemporal multimode nonlinear systems, and perhaps classical wave condensation. Furthermore, the results should be valuable for applications such as passive beam combining, saturable absorbers, high-power fiber lasers and amplifiers, and multiphoton imaging.

Funding Information

Portions of this work was supported by the Office of Naval Research under grant N00014-13-1-0649. L.G. Wright acknowledges support from NSERC.

Acknowledgments

We thank K. Krupa, A. Tonello, A. Barthélémy, V. Couderc, G. Millot, and S. Wabnitz for discussions.

BIBLIOGRAPHY

[1] Z. Liu, L. G. Wright, D. N. Christodoulides, and F. W. Wise, Optics Letters **41**, 3675 (2016).

[2] G. Agrawal, *Nonlinear Fiber Optics (Fifth Edition)*, *Optics and Photonics* (Academic Press, ADDRESS, 2013).

[3] G. Agrawal, *Fiber-Optic Communication Systems*, *Wiley Series in Microwave and Optical Engineering* (Wiley, ADDRESS, 2012).

[4] L. F. Mollenauer and R. H. Stolen, Optics letters **9**, 13 (1984).

[5] K. Tamura, E. P. Ippen, H. a. Haus, and L. E. Nelson, Opt. Lett. **18**, 1080 (1993).

[6] A. Chong, J. Buckley, W. Renninger, and F. Wise, Opt. Express **14**, 10095 (2006).

[7] R. J. Essiambre and R. W. Tkach, Proceedings of the IEEE **100**, 1035 (2012).

[8] K. Kieu, W. H. Renninger, A. Chong, and F. W. Wise, Opt. Lett. **34**, 593 (2009).

[9] S. Fan and J. M. Kahn, Opt. Lett. **30**, 135 (2005).

[10] J. Carpenter, B. J. Eggleton, and J. Schroder, Nature Photonics **9**, 751 (2015).

[11] A. M. Caravaca-Aguirre, E. Niv, D. B. Conkey, and R. Piestun, Opt. Express **21**, 12881 (2013).

[12] R. N. Mahalati, R. Y. Gu, and J. M. Kahn, Opt. Express **21**, 1656 (2013).

[13] K. P. Ho and J. M. Kahn, *Optical Fiber Telecommunications VIB: Systems and Networks: Sixth Edition*, sixth edition ed. (Elsevier Inc., ADDRESS, 2013), pp. 491–568.

[14] F. Poletti and P. Horak, Journal of the Optical Society of America B **25**, 1645 (2008).

[15] A. Mafi, Journal of Lightwave Technology **30**, 2803 (2012).

[16] L. G. Wright, D. N. Christodoulides, and F. W. Wise, Nature Photonics **9**, 306 (2015).

[17] L. G. Wright, W. H. Renninger, D. N. Christodoulides, and F. W. Wise, Opt. Express **23**, 3492 (2015).

[18] G. Lopez-Galmiche, Z. S. Eznaveh, M. A. Eftekhar, J. A. Lopez, L. G. Wright, F. Wise, D. Christodoulides, and R. A. Correa, Opt. Lett. **41**, 2553 (2016).

[19] S. Buch and G. P. Agrawal, Opt. Lett. **40**, 225 (2015).

[20] L. G. Wright, S. Wabnitz, D. N. Christodoulides, and F. W. Wise, Physical Review Letters **115**, 1 (2015).

[21] K. Krupa, A. Tonello, A. Barthelemy, V. Couderc, B. M. Shalaby, A. Bendahmane, G. Millot, and S. Wabnitz, Physical Review Letters **116**, 1 (2016).

[22] P. Aschieri, J. Garnier, C. Michel, V. Doya, and A. Picozzi, Physical Review A - Atomic, Molecular, and Optical Physics **83**, 1 (2011).

[23] B. C. Rodgers, T. H. Russell, and W. B. Roh, Opt. Lett. **24**, 1124 (1999).

[24] S. H. Baek and W. B. Roh, Optics Letters **29**, 153 (2004).

[25] N. B. Terry, T. G. Alley, T. H. Russell, and K. T. Engel, Optics Express **15**, 17509 (2007).

[26] K. Krupa, A. Tonello, B. M. Shalaby, M. Fabert, A. Barthélémy, G. Millot, S. Wabnitz, and V. Couderc, Nature Photonics **11**, 237 (2017).

[27] J. W. Nicholson, a. D. Yablon, S. Ramachandran, and S. Ghalmi, Optics express **16**, 7233 (2008).

[28] S. Longhi and D. Janner, Journal of Optics B: Quantum and Semiclassical Optics **6**, S303 (2004).

[29] L. G. Wright, Z. Liu, D. A. Nolan, M.-J. Li, D. N. Christodoulides, and F. W. Wise, Nature Photonics **10**, 771 (2016).

[30] A. B. Grudinin, E. M. Dianov, D. V. Korbkin, A. M. Prokhorov, and D. V. Khaĭdarov, ZhETF Pisma Redaktsiiu **47**, 297 (1988).

[31] E. Nazemosadat and A. Mafi, Journal of the Optical Society of America B **30**, 1357 (2013).

CHAPTER 5

FUTURE DIRECTIONS

5.1 Continue research of Mamyshev oscillator

The Mamyshev oscillator for generating high energy pulses is a new field, and a more systematic description of the pulse evolution physics in the Mamyshev oscillator and the design guidance for different parameters (pulse durations and energies) are needed to be studied. Here, I list a few examples.

5.1.1 Mamyshev oscillator at different wavelength

The Mamyshev oscillator mechanism can be applied to the other wavelength whenever normal dispersion fiber is available. For example, simulations also show some excellent performance can be reached at 1550 nm, using the similar experiment setup as 1030 nm. The gain fiber is Er20-4/125 ($\beta_2 = 19fs^2/mm$) and the passive fiber is Corning Vascade S1000 ($\beta_2 = 47fs^2/mm$). One simulation example shows the pulse energy can be $\sim$ 45 nJ with linear chirp. However, its temporal shape is not parabolic (Fig. 5.1 (a)). The transform-limited pulse duration is $\sim$ 30 fs (Fig. 5.1 (b)). Using a gain fiber with $\beta_2 = 47fs^2/mm$ (the gain fiber with this dispersion value is not available, and this example is used to show the importance of the dispersion value. The closest available fiber dispersion is $\beta_2 = 37fs^2/mm$), the output pulse shape can be much closer to parabola and the pulse energy is higher. Fig. 5.1 (c, d) shows a $\sim$ 100 nJ example. We can see the pulse shape is almost parabolic. With the increment of the fiber dispersion, the pulse energy can be even higher (>200 nJ). Thus, the fiber dispersion is another significant factor

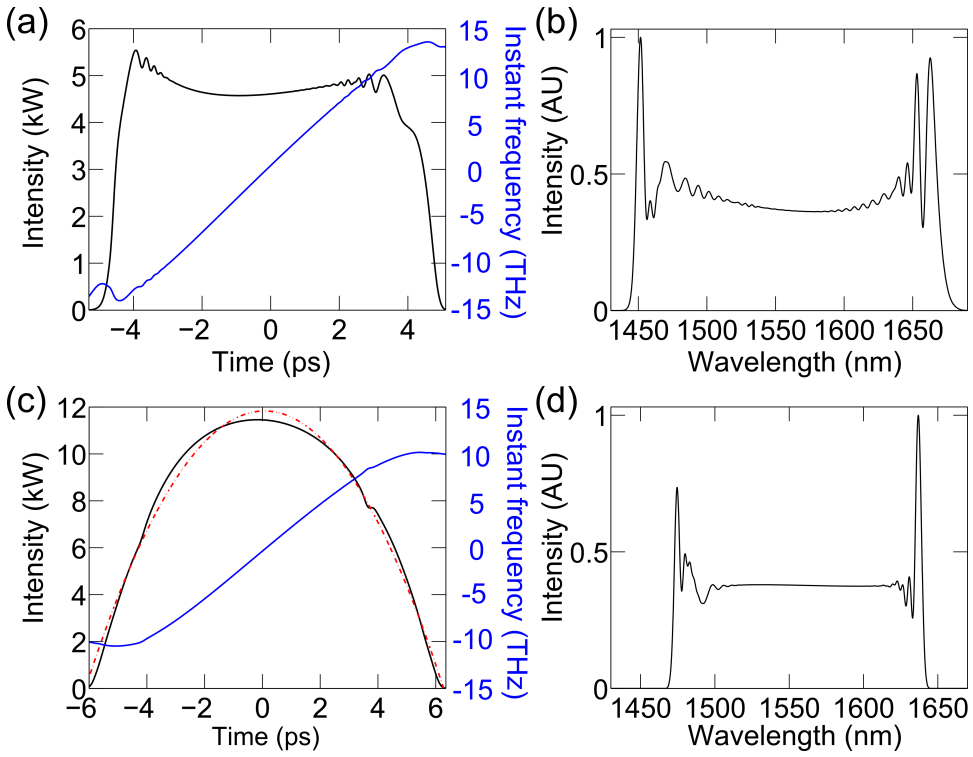

Figure 5.1: (a, b) Simulation results for a Mamyshev oscillator using Er20-4/125 as the gain fiber. (c, d) Simulation results for a Mamyshev oscillator using a gain fiber with $\beta_2 = 47 fs^2/mm$.

to achieve higher pulse energy for Mamyshev. We can see that there are several factors that can affect the Mamyshev oscillators performance. So more study on the pulse evolution is needed.

5.1.2 Mamyshev oscillator at low repetition rate

Since the above oscillators repetition rate is too high for most of the applications, a long cavity ($\sim$ 1.8 MHz) is designed as Fig. 5.2. 100-m passive fiber is used to lower the repetition rate and a dispersion delay line (DDL) is used to compress the highly-chirped pulse inside of the cavity. The mode-locking can be reached by choosing the appropriate DDL value. The output bandwidth is $\sim$ 80 nm (Fig. 5.3

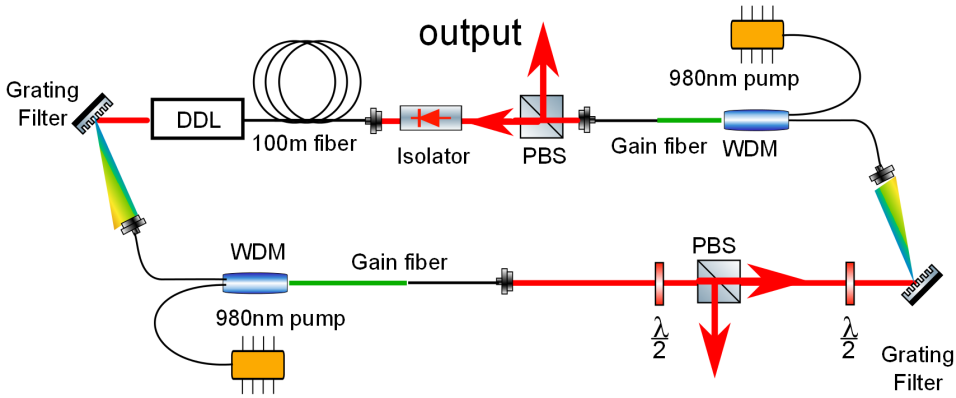

Figure 5.2: Experimental setup for low repetition-rate Mamyshev oscillator. DDL: dispersion delay line, which compensates 98-m fiber GVD. Filters use 600 lines/mm gratings.

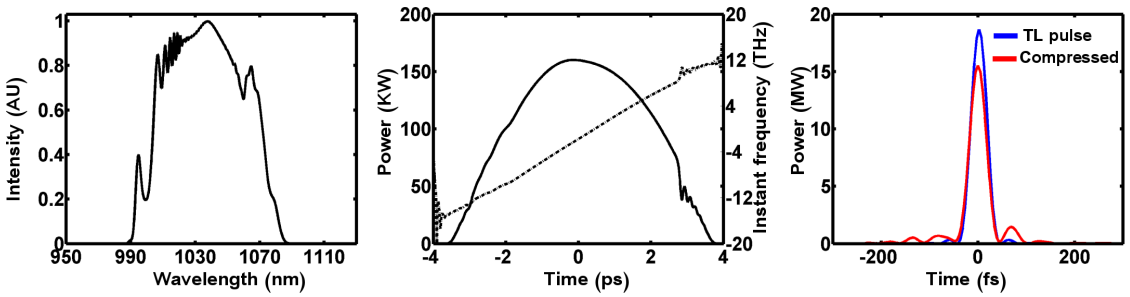

Figure 5.3: The simulated output of the above long cavity Mamyshev oscillator: (left) Spectrum, (middle) output pulse and its instantaneous frequency and (right) transform limited pulse and dechirped pulse.

(left)) and the chirp is almost linear (Fig. 5.3 (middle)). The compressed pulse (only GVD is compensated) is illustrated in Fig. 5.3 (right) and the peak power is $\sim 85\%$ of the transform-limited pulse, which demonstrates the good linearity of the chirp. This setup can eliminate the need for pulse picking.

5.1.3 Self-Starting Mamyshev

How to start the high-performance ring Mamyshev oscillator is still an important and interesting problem. Pump modulation has been demonstrated as a useful

approach to start the all-fiber ring Mamyshev cavity [1]. The pump was modulated with pulse train (microsecond duration) at tens of kilohertz. The pulse trains eventually evolve into the steady-state output pulses. So modulating the pump light for a Mamyshev oscillator with the formation of parabolic pulses is a promising experiment. This can be a significant result because it can both solve the starting problem and reach high performance output.

In addition, the self-starting oscillators without any auxiliary modulation have been demonstrated for linear cavities [2, 3]. By building two coupled cavities: the Mamyshev cavity with two spectral filters and a high-loss continuous-wave cavity, the self-starting can be achieved. A future experiment which should be taken into consideration is realizing the same idea in the ring Mamyshev cavity, which generates better performance than the linear design.

5.2 Understanding rogue waves in normal dispersion fiber lasers

In numerical simulation, stable dissipative solition and noise bursts were found. However, until now, the rogue-wave phenomenon in normal dispersion oscillator cannot be observed. The current numerical model includes Kerr nonlinearity, dispersion, stimulated Raman scattering, ideal saturable absorber, and filter.

From the experimental results, we know the filter plays a significant role. However, our simulation didn't include the phase profile of the filter. Therefore, the next step should be measuring the shape and the phase profile of the filter accurately and putting those measured values in the numerical model.

5.3 Multimode fiber oscillator

The pulse propagation in multimode fibers is studied experimentally and numerically in different dispersion regimes and significant progress has been achieved. In the future, devices based on multimode fibers should be a promising direction. Mode-locking mechanisms such as soliton, dissipative soliton, amplifier similariton, Mamyshev pulse shaping have been discovered in single-mode fiber oscillators. So, the next step of the study is finding all these solutions in multimode fiber lasers. The recent work on spatiotemporal mode-locking in multimode fiber lasers [4] proved mode-locking in multimode fiber has a bright future.

5.4 Interesting topics

In this section, questions on several different research topics are listed. These questions may or may not have a straightforward answers. More works are needed.

- Application of divided pulse technique: the incorporation of divided pulse technique within existing methods for pulse generation can offer a significant improvement. For example, new frequency generation by SPM, soliton self-frequency shift and four-wave mixing.
- Higher-order-mode mode-locking: By inserting a spatial light modulator into the laser cavity as a spatial filter, researchers have already demonstrated the on-demand selection of arbitrary laser modes (Fig. 5.4) [5]. Can this cavity generate the on-demand mode-locked output if a saturable absorber such as SESAM is placed in the cavity? Can we replace the Nd:YAG gain rod with a multimode fiber?

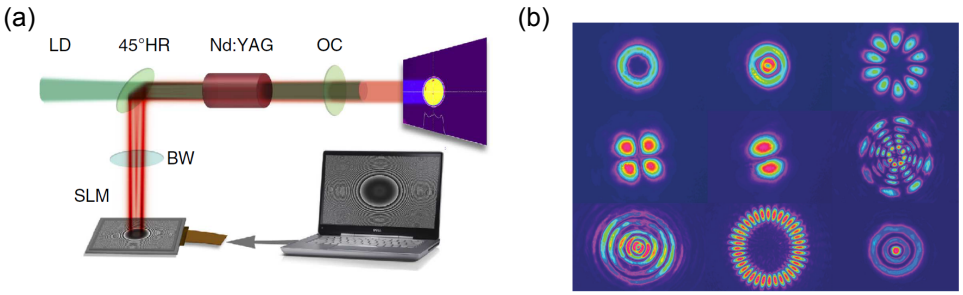

Figure 5.4: (a) Schematic of the digital laser concept showing the SLM, Brewster window (BW), high reflectivity (HR) mirror at an angle of 45 degree, Nd:YAG gain medium pumped by an external laser diode (LD) source and the output coupler (OC). (b) Higher-order LaguerreGaussian modes. An example range of modes created with the digital laser. Figure reproduced from Ref. [5]

BIBLIOGRAPHY

[1] I. Samartsev, A. Bordenyuk, and V. Gapontsev, Proc. SPIE **10085**, 100850S (2017).

[2] K. Regelskis and Želudevičius, WO2016020188 A1 .

[3] Z. Liu, Z. M. Ziegler, L. G. Wright, and F. W. Wise, Optica **4**, 649 (2017).

[4] L. G. Wright, D. N. Christodoulides, and F. W. Wise, ArXiv:1705.05050 (2017).

[5] S. Ngcobo, I. Litvin, L. Burger, and A. Forbes, Nature Communications **4**, 1 (2013).

APPENDIX A: MAMYSHEV REGENERATOR

The Mamyshev optical regenerator is an all-optical regenerator that relies on self-phase modulation induced spectrum broadening and the following offset spectral filtering. The schematic of a single-stage Mamyshev regenerator (MR) is shown in Fig. A.1. It is composed of a fiber amplifier, a normal dispersion fiber and a bandpass filter (the center wavelength is off from the center wavelength of the input pulse).

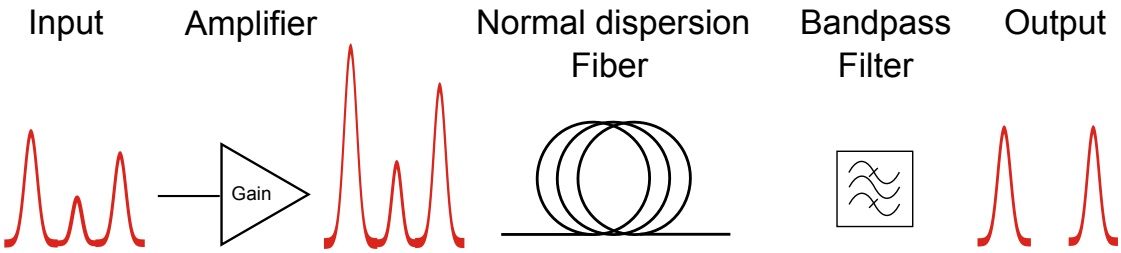

Figure A.1: Schematic of the single-stage Mamyshev regenerator setup.

Figure A.2 illustrates the principle of single-stage MR. The high energy pulse after the amplifier owns the strongest peak power and the spectrum is broadened significantly, and only a small portion of energy can pass the filter (upper figure). The low energy pulse, whose peak power is not high enough to broaden its spectrum, is completely blocked by the filter (middle figure). The spectrum of the medium energy pulse is broadened moderately and a medium percent of energy is able to transmit the filter (bottom figure).

Based on the similar principle, two-stages and multiple stages MR could be built and their transfer function are shown in Fig. A.3. The cutoff edge is becoming sharper as the increment of the number of stages. When the stage number is infinite, the transmittance is a step-like function.

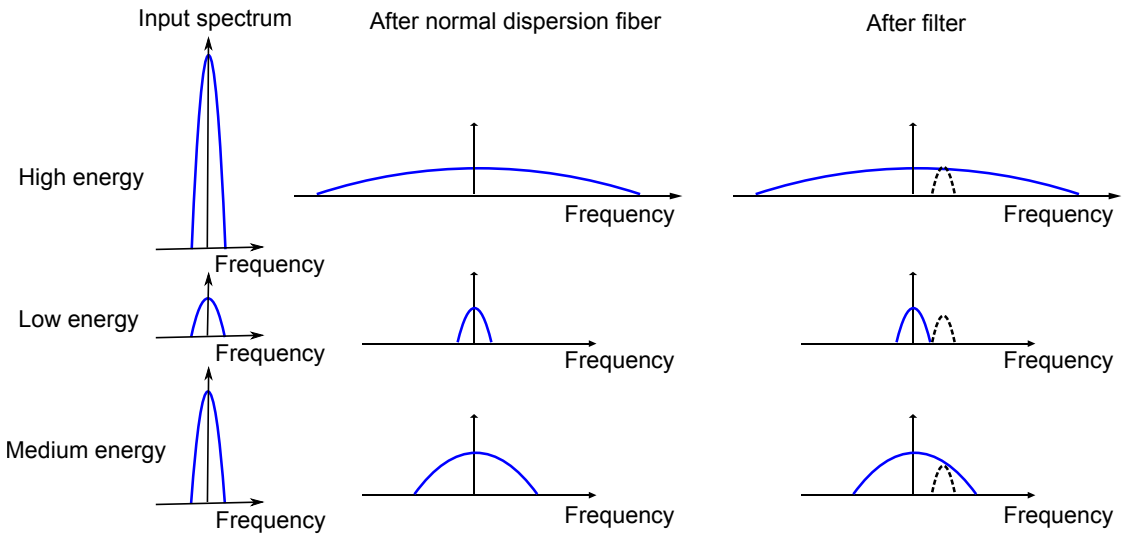

Figure A.2: Working principle of Mamyshev regenerator.

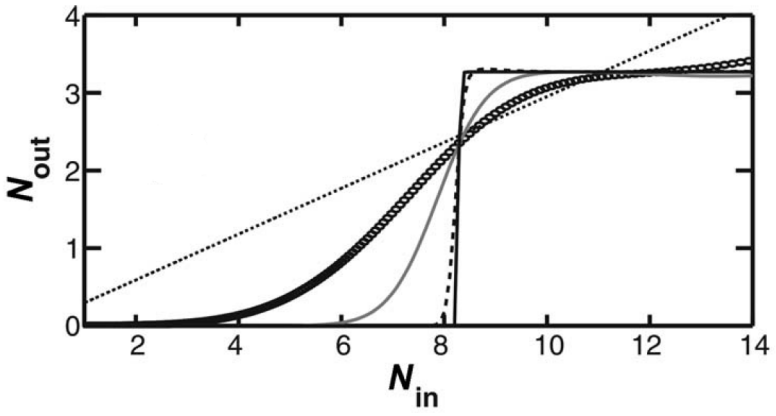

Figure A.3: Normalized TF after a single-stage MR (circles), a double-stage MR (gray solid curve), two regenerative blocks (dashed curve), and four double-stage MRs (solid black curve). Figure is from *Generation of localized pulses from incoherent wave in optical fiber lines made of concatenated Mamyshev regenerators*, JOSA B **25**, 1537-1547 (2008).